UNIVERSITEIT VAN PRETORIA
UNIVERSITY OF PRETORIA
YUNIBESITHI YA PRETORIA

Chemical and physical aspects of Lithium borate fusion

by

Magdeleen Loubser

Submitted in partial fulfilment of the requirements for the degree
Masters of Chemistry
In the Faculty of Natural & Agricultural Sciences
University of Pretoria
Pretoria

December 2009

Supervisor: Prof. P.H. van Rooyen
Co-Supervisor: Prof. J.P.R. de Villiers

SUMMARY

Fused glass beads as a sample preparation method for X-ray Fluorescence spectroscopy (XRF) were introduced in 1957 by Claisse; it soon became the preferred method to introduce oxide samples to the spectrometer, because heterogeneity, mineralogical and particle size effects are eliminated during the fusion process. Matrix effects are largely reduced by the resulting dilution. With the recent advances in XRF spectrometers, instruments with enhanced generator and temperature stability, improved sensitivity (even for light elements), and effective matrix correction software are available. Consequently, the largest proportion of analytical error results from the sample preparation step. Sampling error will always contribute the largest overall error but that is not the topic of this discussion.

After more than 50 years of fused bead use in XRF analysis, certain matrices remain problematic. Although many fusion methods for chromite-, sulphide- and cassiterite-rich materials have been published, easily reproduced, routine methods for these still elude analytical chemists. Lengthy fusions at temperatures higher than 1100ºC are often prescribed for refractory materials and ores, and until recently one of the biggest challenges was a metal-bearing sample e.g. contained in slags or certain refractory materials.

This study was conducted to identify and elucidate the reactions occurring in the formation of a lithium borate glass, but also between the lithium borate and oxides during glass formation. Different analytical techniques were used to investigate the reactions occurring during the fusion process based on theoretical glass-making principles.

As a starting point, Thermo Gravimetric Analysis (TGA) and Differential Thermal Analysis (DTA) were used jointly to evaluate the reactions occurring during the fusion of lithium borate glasses, and at a later stage, oxide/flux mixtures. When a different TGA instrument was used, Differential

Scanning Calorimetry (DSC) was used in conjunction with the TGA. Observed reactions were modelled in a muffle furnace to produce identical material in larger quantities, and this material was then investigated using X-ray Powder Diffractometry (XRD), Raman Spectroscopy and Electron Microprobe Analysis (EPMA).

The most enlightening result from the TGA/DSC results was the large mass loss above 1050 ºC. Literature often prescribes prolonged fusions at elevated temperatures for certain fusions, but it was proved beyond reasonable doubt that this practise causes volatilisation of the flux and leads to erroneous analytical results.

The next analytical technique applied to the flux and flux/oxide samples was XRD. Where pre-fused fluxes were investigated, the XRD data served as confirmation of the glassy state of the pre-fused flux as a broad humpy scan indicative of an amorphous material was seen in stead of a diffractogram with sharp, well defined peaks. After heating to above the temperature of re-crystallisation, the phases present could be identified from the diffractogram. Provisional results using the in-situ, high temperature stage point towards the possibility of using this technique to great effect to investigate the presence of different phases formed at high temperatures. Flux-oxide mixtures were measured on the high temperature stage and after cooling a new phase was observed indicating that new phases formed during a fusion reaction. As the heating stage is slow-cooled, the chance of crystallisation in the glass is good, providing the possibility for investigating this formation of new phases at elevated temperatures further with a more suitable heating element that will contain the material.

Raman spectroscopy was subsequently used to gain information about the bonds within the flux. Pure lithium tetraborate and lithium metaborate fluxes were analysed as well as flux oxide mixtures. The vibrations could not be predicted from first principles as band broadening occurs in glasses that makes theoretical predictions very difficult. The data obtained was compared to similar studies in literature and good agreement was found. In oxide-flux mixtures definite new

bands were observed that was not part of the flux or oxide spectrum.

EPMA results allowed calculation of the maximum solubilities of an oxide in a specific flux. It was done using Cr_2O_3 and ZrO_2 and compared well with experimental values obtained from literature. The microscope images revealed some new insights into the theory of XRF fusions. It could clearly be seen that dissociation of the minerals in the sample occurred, thus proving that no mineralogical effects exist in a fused glass bead, and it could be observed that the flux oxide mixture devitrify when over saturated.

Declaration

I, Magdeleen Loubser declare that the thesis/dissertation, which I hereby submit for the degree MSc Chemistry at the University of Pretoria, is my own work and has not previously been submitted by me for a degree at this or any other tertiary institution.

_____ _____

M. Loubser Date

This work is dedicated to Dr. Fernand Claisse, who in 1957 introduced fusions as method of sample preparation, and spent his subsequent years theorising the mechanisms. I am deeply aware of how fortunate I am to have the spectroscopic tools to investigate these mechanisms in an experimental manner, knowing that he yearned to do so for many years. Fernand is eighty six years old and still travels to the University of Western Ontario every year to teach fusions at the UWO XRF course. His enthusiasm about XRF and fusions is still an inspiration to many students from all over the world.

The important thing in science is not so much to obtain new facts as to discover new ways of thinking about them. -Sir William Bragg-

Table of contents

CHAPTER 1: INTRODUCTION

1.1 Historical background on the use of lithium borate glasses as fluxes in XRF sample preparation

Fused glass beads as a sample preparation method for X-ray Fluorescence (XRF) spectroscopy were introduced in 1957 by Claisse[1]. It soon became the preferred method to introduce oxide samples to the spectrometer, because heterogeneity, mineralogical and particle size effects are eliminated during the fusion process [2-7]. Matrix effects are also largely reduced by the resulting dilution [8-14]. Claisse[1] introduced borax, a di-sodium tetraborate with the formula $Na_2B_4O_7 \cdot 10H_2O$ as a flux, with a flux-to-sample ratio of 100:1. This was soon applied widely in industry for the analysis of various materials[15]. The main disadvantages of using this flux were its high loss on ignition and poor purity.

XRF spectroscopy technology improved to such an extent that the analyses of light elements like sodium became possible, resulting in the sodium content in borax prohibiting analysis. Rose et al. [9] introduced lithium tetraborate ($Li_2B_4O_7$) as a flux, and reduced the dilution to 4:1. Later, Hooper and Atkins[16] used a 2:1 flux-to-sample ratio with lithium tetraborate, but the resulting accuracy and precision were not satisfactory. Haukka and Thomas [17, 18] were the first to use lithium metaborate ($Li_2B_2O_4$), in a 2:1 flux-to-sample ratio. Although fusions reduced matrix effects,

these were not eliminated entirely. Norrish and Hutton[19] introduced the use of lanthanum oxide as a heavy absorber, to eliminate matrix effects, as part of the flux in a 5.4:1 flux-to-sample ratio. Rao and Govil[20] adapted this method by adding barium oxide instead of lanthanum oxide. This enabled the analysis of sodium using the same fused bead.

Over the years, many variations of fluxes based on borates were used with or without additives. Lithium tetraborate [21-24], lithium metaborate[17] sodium carbonate[3], sodium and potassium bisulphate[25], and ammonium metaphosphate[26] were some of the fluxes used previously. Soon laboratories started to develop custom-designed fluxes to fit specific purposes, such as Larson et al. [10], who prepared a flux from $6B_2O_3$:$2Na_2CO_3$:$1Li_2B_4O_7$, and Eddy and Balaes[27] who prepared a lithium borate flux with lanthanum oxide as heavy absorber. Barger[28] added cerium oxide as heavy absorber and glass-former. Jones and Wilson[29] designed a flux consisting of 57% lithium tetraborate and 43% lithium metaborate for magnesite, dolomite and related materials. Joslin and Salt[30] used lithium tetraborate with added germanium oxide as glass-forming agent to prepare fused glass beads from barites at a ratio of 0.5:0.05:2 for sample: GeO_2:flux. The commercial suppliers followed with a range of lithium borate fluxes consisting of varying ratios of lithium tetraborate and lithium metaborate (Table 1.1).

Table 1.1: Commercially available flux compositions

Flux	Composition	Melting Point/ºC	Supplier	Analytes suggested for
Lithium tetraborate	$Li_2O.2B_2O_3$	920	ICPH, Fluore-X ATL 100 Alfa Aesar, Spectroflux 100 Claisse	CaO, MgO, K_2O, Na_2O
Lithium metaborate	$Li_2O.B_2O_3$	845	ICPH, Fluore-X AML 100 Alfa Aesar, Spectroflux 100A Claisse	Al_2O_3, SiO_2, P_2O_5, sulphates
Sodium tetraborate	$Na_2O.2B_2O_3$	740	ICPH, Fluore-X ATS 100	
	$Li_2B_4O_7$: $LiBO_2$ (66:34)	875	ICPH, Fluore-X 65 Alfa Aesar, Spectroflux 110	Amphoteric characteristics
	$Li_2B_4O_7$:$LiBO_2$ (50:50)	870	ICPH, Fluore-X 50 Alfa Aesar, Spectroflux 110A	
	$Li_2B_4O_7$:$LiBO_2$ (35:65)		ICPH, Fluore-X 35 Alfa Aesar, Spectroflux 100D Sigma, 12:22	
	$Li_2B_4O_7$:$LiBO_2$ (20:80)	840	ICPH, Fluore-X 20 Alfa Aesar, Spectroflux 100B	Eutectic composition
	$Li_2B_4O_7$:$LiBO_2$ (80:20)		ICPH, Fluore-X 80	
Lithium metaphosphate	$(LiPO_3)n$	600		
Norrish Hutton flux	$Li_2B_4O_7$:$LiCO_3$:La_2O_3 (47:36.7:16.3)	700	ICPH, Fluore-X 119 Alfa Aesar, Spectroflux 105	

Fluxes like these have since been used routinely to fuse and analyse materials such as geological materials[31-35], various metal oxides[34], carbonate rocks[22,36], iron ores and slags[34, 37,38], raw materials for blast furnaces[39], rare earth concentrates[40], cement and allied materials[28,41-43], fly ash[44], glass and ceramics[45-47], pigments and paints[48], heavy mineral sands[49] and titanium slags, refractory materials[50] and soils[51].

An added advantage of using fused glass beads for XRF analysis is that it provides a simple method to prepare single- and multi-element standards from certified reference materials as well as from analytical reagent grade pure compounds.

Synthetic standards prepared in this manner [5,43,45,51-53], offer versatility regarding concentration range and composition.

One of the factors which has to be considered when using XRF spectroscopy, is that all matrix correction algorithms and fundamental parameter calculations assume a perfectly homogenous sample with a mirror surface, and that no mathematical correction can be used to rectify sample preparation deficiencies[2,5,6,42,54-56] that lead to inhomogeneous samples and surface effects. The chemical reactions during the fusion process involve breaking down the compounds, usually present in the sample as crystalline oxides, and mixing with the flux to form a homogenous solution. This mixture solidifies as a solid glass, which is the preferred sample to be introduced to the spectrometer.

1.2 Problems associated with the use of lithium borate fluxes

With the recent advances in XRF spectrometers, instruments with enhanced generator and temperature stability, high sensitivity (even for light elements), and effective matrix correction software are available reducing analytical errors, consequently, the largest proportion of analytical error results from the sample preparation step.

Even after 50 years of using fused beads for XRF analysis, certain matrices still prove to be problematic. Although quite a number of reports on fusion methods for

chromite-, sulphide- and cassiterite-rich materials have been published [34,45,53,57-61], routine methods for these materials still elude analytical chemists. Lengthy fusion steps at temperatures in excess of 1100 ºC are often stipulated [21,22,41,42,46,57,62] for refractory materials and ores, and until recently one of the biggest challenges facing a spectroscopist was samples containing metallic components, as in slags or certain refractory materials.

Lithium borate fluxes are well suited for most silicate rocks, refractories, ceramics and related materials, but often small changes in the sample composition can introduce various problems that manifest during the fusion reaction. Very few published papers report on these problems and often, when published methods are applied to similar materials, the results are not comparable due to small differences between the matrixes of the specific application and that for which the method was developed. Sulphide (S^{2-}) materials are not soluble in a lithium borate flux, although sulphate (SO_4^{2-}) materials do dissolve. Boron oxide (B_2O_3) has a high affinity for oxides, but does not dissolve sulphides. Sulphides need to be oxidised prior to fusion, because in addition to the solubility problem, sulphides react with the platinum crucibles used for fusion, forming a low melting alloy and destroy them. An additional complication is the fact that even when oxidation of the sulphide is successful, sulphur can be fully or partially lost as sulphur dioxide (SO_2). Neither does free sulphur dissolve in lithium borate.

Complex oxides like chromite ($FeO.Cr_2O_3$), with a spinel structure, and ilmenite

($FeO.TiO_2$) have structures that are very stable. A lot of energy is needed to dissociate the crystal structure in the process of solubilising the sample, and this is often attempted by increasing the temperature, with disastrous results such as volatilising the flux and loss of sample components[63].

In the case of halides and ionic compounds under glassy conditions, only the cationic part of the molecule is soluble in the flux and the anions remain solid, evaporates or melts, but do not dissolve into the glass phase[67].

In metals, the atoms form strong metallic bonds that cannot be broken by forming bonds with lithium borate flux as a solvent. These metals, similar to sulphides, react with the platinum reaction vessels. Pre-oxidation by roasting is often not sufficient, especially in the case of silicon carbide, as it has been shown that only a layer on the outer surface of the compound is oxidised, and this protects the rest of the particle against further oxidation. When the sample is then fused with flux, the oxidised outer layer is dissolved, leaving the un-oxidised metal in direct contact with the platinum crucible, which results in a platinum-metal eutectic forming, which causes destruction of the platinum crucible[64].

It appears that the reactions occurring in a sample/flux mixture during the fusion process have not been adequately addressed, as no references could be found in the literature.

1.3 Proposed mechanisms of fusion of analytical samples with lithium borate fluxes

Lithium borate fluxes rely on the glass-forming properties of boron oxide, B_2O_3, which is classified as a network-former in random network theory[65]. Boron oxide is obtained from dehydrated boric acid and cools down to a stable glass after melting. It consists of boron oxide rings joined together without any long-range order, hence the amorphous nature. Zachariasen[65] described boron glasses as a random arrangement of B_2O_3 building blocks following three rules: a) an oxygen atom is linked to no more than two boron atoms; b) the number of oxygen atoms surrounding each boron atom must be three or less and c) in the crystalline phase, the group of oxygen shares corners only, not edges or faces. The B-O bonds are covalent. The structure is open and atoms can easily enter these open spaces. Boron glass has the ability to form glasses with a mixture of alkaline, alkali-earth metals and oxides. Lithium oxide is an ideal network-modifier as Li is a small atom that does not distort the boron network. The lithium atoms occupy the interstitial spaces and the oxygen atoms the other binding sites. The B-O bonds are strong, but Li and O are free to move around. The viscosity of boron oxide is very high, which is detrimental in a flux, but the addition of lithium to the structure decreases the viscosity.

In the practical application of lithium borate fluxes, for the purpose of sample dissolution, a limited range of 17.7 – 31% Li_2O is used, the rest of the flux consists of B_2O_3. Figure 1.1 shows a phase diagram for the Li_2O-B_2O_3 system[66]. The most frequently used lithium borate flux is lithium tetraborate, $Li_2O.2B_2O_3$, the lower limit

of this range is at 17.7% Li_2O and 82.3% B_2O_3. This flux has a melting point of 920 ºC. It was one of the first fluxes to be used and is still the most widely used composition. Certain authors describe lithium tetraborate as an "acidic flux"[67] as is described in greater detail in the next paragraph. On the other limit of the specified range is lithium metaborate, $Li_2O.B_2O_3$, with 30% Li_2O and 70% B_2O_3. This flux has a melting point of 845 ºC and is sometimes referred to as an "alkaline flux". The third and often used composition is the eutectic mixture of 80% lithium metaborate and 20% lithium tetraborate with 27.54% Li_2O and 72.46% B_2O_3 (Figure 1.1). This flux has a melting point of 840 ºC.

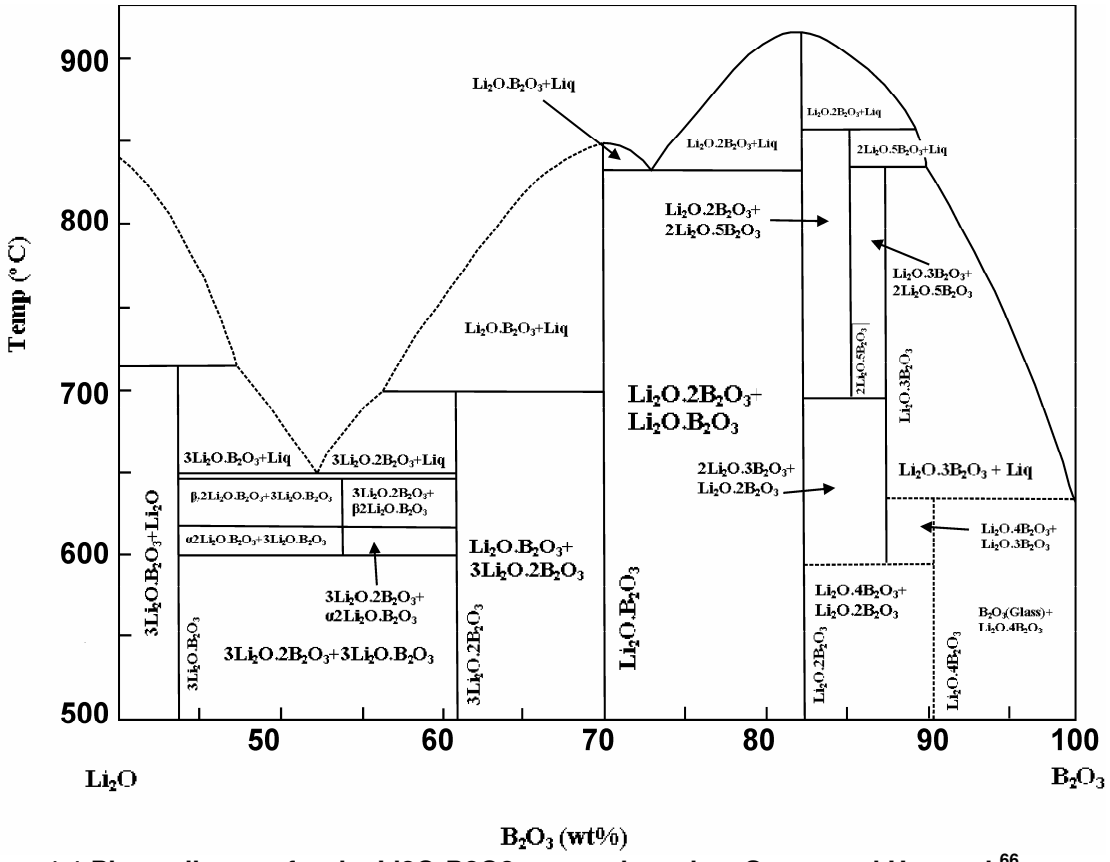

Figure 1.1 Phase diagram for the Li2O-B2O3 system based on Sastry and Hummel.[66]

Most oxides readily dissolve in lithium borate fluxes, but the solubility is always smaller than that of Li_2O in B_2O_3. Oxygen atoms are usually the largest atoms in a sample oxide, and it is likely that they are mostly responsible for limiting solubility of the oxide in flux.

Two main theories were postulated regarding the solubility of oxides in lithium borate fluxes. The first was that of Claisse[67] whose theory is based on the "acidity or basicity" of a flux. Claisse states that the acidity or alkalinity of oxides determines their solubility in a specific flux and the stability and mechanical properties of the resulting fused glass bead. His definition of the acidity of an oxide is based on the work of Smith[68], and expressed as the number of oxygen atoms in the oxide divided by the number of atoms. For example, the acidity index (AI) for P_2O_5 is calculated by dividing 5 by 2, resulting in an acidity index of 2.5, thus acidic. (All oxides with an acidity index greater than one are specified as acidic.) The AI is calculated for lithium tetraborate in the same manner, (AI = 1.17) and is thus slightly acidic. For lithium metaborate the corresponding value is 1.0, which classifies it as an alkaline oxide. Claisse prescribes that an acidic oxide should be dissolved using the more alkaline of the fluxes, thus lithium metaborate, and vice versa. He prescribes a lithium tetraborate-metaborate mixture for any oxide with an acidity index between 1.25 and 2. In practice this theory does not always hold as for example SiO_2 can effectively be dissolved in pure lithium tetraborate, thus some other theories were investigated.

Lang et al.[69] used the B_2O_3/Li_2O molar ratio to characterize the lithium borate flux system, reasoning that the polyborates are chemically neutral salts. They postulate that at a higher B_2O_3/Li_2O ratio, less LiO bonds per mass of flux are available to link the atoms of oxide between the various polyborate groupings, with resulting destabilisation of the glass structure. Their hypothesis is based on the random network theory proposed by Zachariasen[65] for the structure of oxide glasses.

They postulate that oxides bind to the borate chain by a covalent binding to a B-O group. These random links stabilise the glass structure on solidifying. Furthermore, they proposed that polyborates with a B_2O_3/Li_2O molar ratio of between 2 and 3, at elevated temperatures, will exist mostly in the biborate form, and for fluxes with a ratio of between 1.6 and 1, will be present in the melt as hexagonal rings formed by three molecules of metaborate (Figure 1.2).

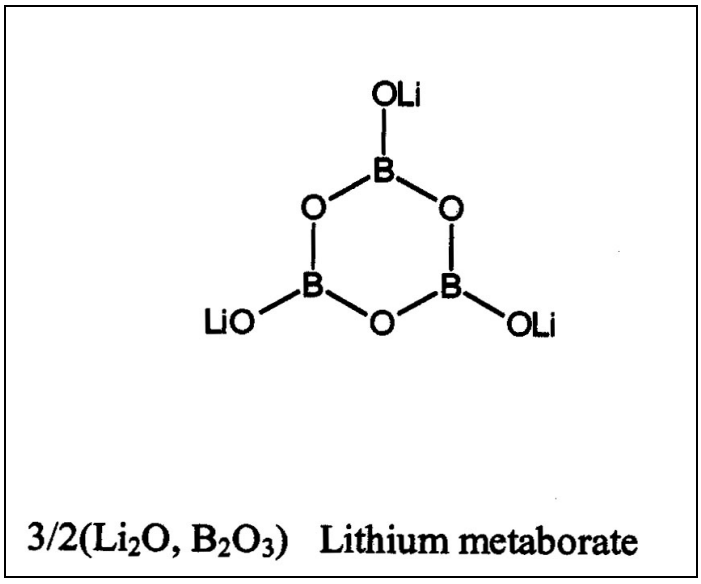

Figure 1.2: Structural drawing of lithium metaborate

Lithium tetraborate is present in the borate melt as a relatively large species and with a significant steric effect as confirmed by its high melting point 920-930 ºC. The fact that a 10 ºC melting range exists, is indicative of the co-existence of various structural forms: These forms include straight shaped (Figure 1.3), L-shaped, U-shaped and T-shaped forms. Lang et al.[69] proposed that close to the melting point, the tetraborate structure with four hexagonal rings linked by an oxygen atom and six LiO bonds are most probable (Figure 1.4). At higher temperature this form could break into two bi-borate groups. The B_2O_3/Li_2O molar ratio of 2 is much higher compared to lithium metaborate and indicates fewer Li-O bonds per volumetric mass, resulting in lower reactivity towards oxides in general. Divalent oxides and the –B-O- bonds link more easily and thus lithium tetraborate dissolves these better. The resulting glass produced is more stable.

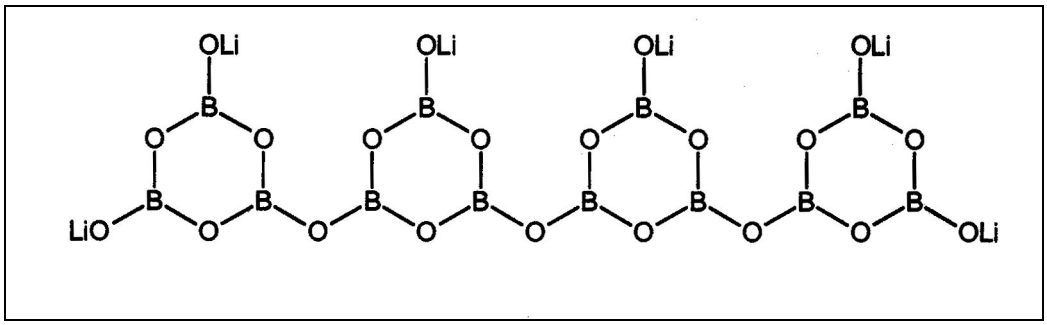

Figure 1.3: Structural drawing of lithium tetraborate (straight)

The B_2O_3/Li_2O molar ratio of lithium metaborate is one, with lower viscosity and more hydrophilic groups per mass unit, leading to higher hygroscopy. On cooling, metaborate glasses are less stable because of the high number of small identical groupings in the melt which can reorganise to clusters much faster, leading to

crystallisation[69]. In practice, mixtures of the above two end groups are made to maintain the lower viscosity and dissolving properties of the metaborate, while having a stable glass bead as a result.

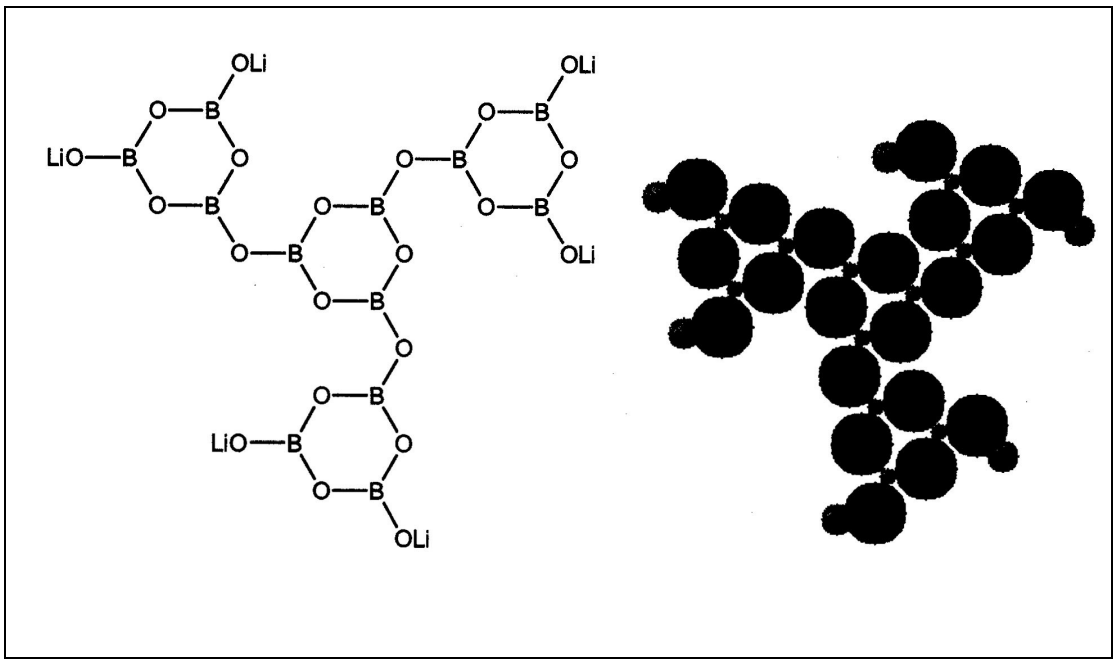

Figure 1.4: Structural drawing of lithium tetraborate (alternative structure)

Adding B_2O_3 or Li_2CO_3 to the flux system can change the B_2O_3/Li_2O molar ratio to move the flux towards lithium metaborate or tetraborate. Lang et al.[69] calculated the theoretical amount of various oxides which could be dissolved in a amount of flux based on the binding sites in the flux, i.e. the LiO- molecules in the flux that could be replaced by oxide molecules.

1.4 Study on the role of structure of lithium borate fluxes in the glass forming reaction

The objective of sample preparation is obtaining a homogenous glass bead with mirror surface, no crystallisation and no undissolved solids. Lithium borate fluxes have proved to be the most effective flux for glass bead preparation as the melting temperature is relatively low compared to that of a silicate rock (1700 ºC) and the resultant glass is stable. Lithium borate, as a light matrix has a low mass absorption coefficient so the sensitivity of the XRF is not reduced by the sample preparation method, and X-rays penetrate well into the bead increasing the analysed volume.

In this study different analytical techniques were used to investigate the reactions occurring during the fusion process and, based on this, attempted to postulate methods for the fusion and dissolution of different problematic materials, based on theoretical glass-making principles rather than the much used “hit and miss” technique. The aim was to prove or disprove the hypothetical mechanisms for fusion postulated in the literature.

As a starting point, Thermo Gravimetric Analysis (TGA) was used to evaluate the reactions occurring during the fusion of a lithium borate glass. TGA measures the percentage mass change as a function of increasing temperature, and thus provides an in situ measurement of what happens in a flux or a flux-sample mixture during heating, combined with Differential Scanning Calorimetry (DSC), where a

second reference crucible is present, and the heat flow in the samples measured by comparing the temperature change between an empty reference crucible and the crucible containing the sample, expressed as a potential in µV.

This indicates an endothermic or exothermic reaction occurring at a specific temperature during the heating cycle and is indicative of phase changes in the solid state, melting points and losses by evaporation. Observed reactions were scaled up in a muffle furnace to produce identical material in larger quantities, and these materials were investigated using X-ray Powder Diffractometry (XRD) and vibrational spectroscopy, specifically Raman Spectroscopy.

XRD was used to investigate the pure fluxes to confirm the structure and phases present in the solid state, as well as confirmation of amorphous nature in the case of glass fluxes. The material prepared in a muffle furnace was analysed by XRD to confirm the TGA/DSC results. Some sample/flux mixtures were also analysed using a temperature stage to evaluate the phase changes in situ and investigate if any phase changes can be observed below the melting point.

Raman Spectroscopy was used to investigate the amorphous glass phases where XRD cannot elucidate the structure. An attempt was made to identify the bonds in the glasses (pure flux and flux/sample mixtures), and in this way predict which bonds form in the glass and thus try to quantify the solution of oxides in the flux. If it was possible to identify the new bonds formed, this would elucidate the solution of

oxides in the flux. This data will confirm which hypothetical mechanism for fusion postulated in the literature regarding the formation of fused beads, was more feasible, whether Acidity Index or the available binding sites proves to be the best approach to design a fusion method. This would allow the prediction of the best flux systems and enable calculating the optimal sample to flux ratios for known sample composition.

A bright field Transmission Electron Microscopy (TEM) micrograph was used to investigate the presence of both amorphous and crystalline particles in the flux prototype, and characterise the structure.

Scanning Electron Microscopy (SEM) photos were taken to identify whether any physical changes occurred in the sample below the melting point to ascertain whether any changes in the XRD data could be expected.

To obtain an additional insight into the problem of identifying the mechanism and predicting the solubility of oxides in a flux electron microprobe analysis (EPMA) was done on two oxide/flux specimens prepared by fusion.

REFERENCES:

1. Claisse, F. Accurate X-ray Fluorescence analysis without internal standards. *Norelco Reporter*. **4**, 3-7 (1957).
2. Claisse, F. and Samson, C. Heterogeneity effects in X-Ray Analysis. *Adv. X-Ray Anal*. **5**, 335-354 (1961).
3. Campbell, W.J. and Thatcher, J.W. Determination of calcium in Wolframite concentrate by XRF. *Adv. X-Ray Anal*. **2**, 313-332 (1958).
4. Smithson, G.L., Eager, R.L. and Van Cleave, A.B. Determination of Uranium in Flotation Concentrates and in Leach Liquors by X-ray Fluorescence. *Adv. X-Ray Anal*. **2**, 175 (1960).
5. Bernstein, F. Application of X-ray Fluorescence Analysis to Process. *Adv. X-Ray Anal*. **5**, 486-499 (1961).
6. Bernstein, F. Particle Size and Mineralogical Effects in Mining. *Adv. X-Ray Anal*. **6**, 436-446 (1962).
7. LeHouillier, R. and Turmel, S. Bead homogeneity in fusion. *Anal Chem*. **46**, 734-736 (1974).
8. Townsend, J.E. X-Ray Spectrographic Analysis of Silica and Alumina Base Catalyst by a Fusion-Cast Disc Technique. *Appl. Spectr*. **17**, 37 (1963).
9. Rose, H.J., Adler, I. and Flanagan, F.J. X-Ray Fluorescence Analysis of the Light Elements in Rocks and Minerals. *Appl. Spectr*. **17**, 81 (1963).
10. Larson, J.O., Winkler, R.A. and Guffy, J.C. A Glass Fusion Method for X-ray Fluorescence. *Adv. X-Ray Anal*. **10**, 489-493 (1966).

11. Jenkins, R., Gould, R.W. and Gedcke, D.A. *Specimen Preparation. Quantitative Spectrometry*, Chapter 7. Marcel Dekker: New York (1981).

12. Tertian, R. and Claisse, F. *Principles of Quantitative X-Ray Fluorescence Analysis*. Wiley-Heyden: London (1982).

13. Bower, N.W. and Valentine, G. Critical comparison of sample preparation methods for major and trace element determination using XRF. *X-ray Spectrometry*.**15**, 73-87 (1986).

14. Buhrke, V.E., Jenkins, R. and Smith, D.K. *Preparations of Specimens for X-ray Fluorescence and Diffraction*. Chapter 2. Wiley-VCH: New York (1998).

15. Luke, C.L. Determination of Refractory Metals in Ferrous Alloys. *Anal. Chem.* **35**, 56-58 (1963).

16. Hooper, P.R. and Atkins, L. The preparation of fused samples in XRF. *Mineral Mag*. **37**, 409-413 (1969).

17. Haukka, M.T. and Thomas, I.L. Total X-ray Fluorescence analysis of Geological samples using a low -dilution lithium metaborate fusion method. *X-ray Spectrometry*. **6**, 204-211 (1977).

18. Thomas, I.L. and Haukka, M.T. XRF trace and major single fused disk. *Chemical Geology*. **21**, 39-50 (1978).

19. Norrish, K. and Hutton, J.T. An accurate XRS method for the analysis of wide range geological samples. *Geochim. Cosmochim. Acta*. **33**, 431-453 (1969).

20. Rao, T.G. and Govil, P.K. Merits of using Barium as a heavy absorber in major element analysis of rock samples by XRF. *Analyst*. **120**, 1279-1282 (1995).

21. Johnson, R.G. X-ray Fluorescence Analysis of Geological Materials Using Rousseau's Fundamental Algorithm. *Adv. X-Ray Anal*. **30**, 105-112 (1987).

22. King, B.S. and Vivit, D. Sample preparation Method for Major-Element Analyses of Carbonate rocks by XRF. *X-ray Spectrometry*. **17**, 85-87 (1988).

23. Couture, R.A., Smith, M.S. and Dymek, R.F. X-ray fluorescence analysis of silicate rocks using fused glass discs and a side-window Rh source tube: accuracy, precision and reproducibility. *Chemical Geology*. **110**, 315-328 (1993).

24. Couture, R.A. Improved fusion method for major element rock analysis by XRF. *Adv. X-Ray Anal*. **32**, 233-238 (1989).

25. Cullen, T.J. Potassium pyrosulphate fusion; determination of copper mattes and slags. *Anal. Chem*. **32**, 516-517 (1960).

26. Rinaldi, F. *Scientific and Analytical Bulletin*. Phillips: Eindhoven. **5**, (1966).

27. Eddy, B.T. and Balaes, A.M.E. A Flux for the Fusion of Samples in analysis by XRF. *X-ray Spectrometry*. **17**, 17-18 (1988).

28. Barger, G.S. A Fusion Method for the X-ray Fluorescence Analysis. *Adv. X-Ray Anal*. **29**, 581-585 (1985).

29. Jones, M.H. and Wilson, B.W. Rapid Method for the Determination of the Major Components of Magnesite, Dolomite and related materials by XRF. *Analyst*. **116**, 449-452 (1991).

30. Joslin, D. and Salt, P.D. Analyses of Barytes by XRF using fusion method. *X-ray Spectrometry*. **14(2)**, 69-73 (1985).

31. Bowling, G.D., Ailin-Pyzik, I.B. and Jones IV, D.R. A Rapid, Low Cost, Manual Fusion Sample. *Adv. X-Ray Anal*. **27**, 491-496 (1983).

32. Luedemann, G., Mann, D. and Hagan, R. Graphite Fusion of Geological Samples. *Adv. X-Ray Anal*. **34**, 213-216 (1990).

33. Johnson, D.M., Hooper, P.R. and Conrey, R.M. XRF Analysis of Rocks and Minerals for Major and Trace Elements on a Single Low dilution lithium tetraborate fusion. *Adv. X-Ray Anal*. **41**, 843-867 (1997).

34. Malmqvist, J. Semi-Low-Dilution Fusion Technique for Analysis. *X-ray Spectrometry*. **27**, 183-197 (1998).

35. Ingham, M.N. and Vrebos, B.A.R. High Productivity Geochemical XRF analysis. *Adv. X-Ray Anal*. **37**, 717-724 (1993).

36. Hettipthirana, T., Grey, N. and Naidu, R. Analysis of limestone using borate fusions. *Spectrochim Acta Part B*. **58**, 85-95 (2003).

37. Yamada, K. Kohno, H. and Arai, T. Measurements of Low Concentration Components in Iron Ores Using Fusion Method. *Adv. X-Ray Anal*. **35B**, 1147-1155 (1991).

38. Feret, F. Minimum flux fusion processing of Iron ores for XRF. *X-ray Spectrometry*. **11(3)**, 128-134 (1982).

39. Metz, J.G.H. and Davey, D.E. Statistical Comparison of Analytical Results Obtained by Pressed Powder and Borate Fusion XRF. *Adv. X-Ray Anal*. **35B**, 1189-1196 (1991).

40. Willis, J.P. and McNew, E.B. An evaluation of the analysis of Monazite and REE compounds. *Adv. X-Ray Anal*. **42**, 829-842 (1999

41. Watson, W., Parker, J. and Harding, A.R. Sample Preparation Optimization for EDXRF Analysis. *Adv. X-Ray Anal*. **32**, 221-226 (1988).

42. Andermann, G. and Allen, J.D. The Evaluation and Improvement of X-ray Emission. *Adv. X-Ray Anal*. **4**, 414-432 (1960).

43. Nettles, S.H. Effect of Specimen Preparation techniques on Calibration. *Adv. X-Ray Anal*. **43**, 424-428 (2000).

44. Schlorholtz, S. and Demirel, T. Comparison of Several Sample Preparation techniques. *Adv. X-Ray Anal*. **30**, 251-256 (1986).

45. Gazulla, M.F., Gomez, M.P., Barba, A. and Jarque, J.C. Characterization of ceramic oxide refractories. *X-ray Spectrometry*.**33**, 421-430 (2004).

46. Caballero, A.C., Valle, F.J. and Martin, Rubi, J.J. Determination of dopants in ZnO-based ceramic. *X-ray Spectrometry*. **30**, 273-279 (2001).

47. Bennett, H. and Oliver, G.J. Development of Fluxes for the Analysis of Ceramic Materials by XRFS. *Analyst*. **101**, 803-807 (1976).

48. Gazulla, M.F., Gomez, M.P., Barba, A. and Mestre, S. Characterisation of Chromite pigments by XRF and XRD. *X-ray Spectrometry*. **33**, 431-438 (2004).

49. Birch, S.L., Norrish, K. and Metz, J.G.H. Standard XRF methods for mineral processing and metallurgy industry. *Adv. X-Ray Anal*. **38**, 353-359 (1994).

50. Asakura, H., Ikegami, K., Murata, M. and Wakita, H. Determination of components in refractories. *X-ray Spectrometry*. **29**, 418–425 (2000).

51. Mahan, K.I. and Leyden, D.E. Simultaneous determination of sixteen major and minor elements in river sediments by EDXRF after LIT fusion. *Analitica Chimica Acta*. **147**, 123-131 (1983).

52. Mahan, K.I. and Leyden, D.E. Technique for preparation of lithium tetraborate fused single and multi-element standards. *Adv. X-Ray Anal*. **25**, 95-102 (1981).

53. Spangenberg, J. and Fontbote, L. XRF Analysis of Base metal Sulphide and Iron Manganese oxide ore samples in Fused Beads. *X-ray Spectrometry*. **23**, 83-90 (1994).

54. Vrebos, B.A.R. and Helsen, J.A. Ab Initio calculations of XRF intensities in non-homogeneous matrices. *Spectrochimica Acta*. **38B**, 835-842 (1983).

55. Gunn, E.L. The Effect of Particles and Surface Irregularities on the X-ray Fluorescent Intensity of Selected Substances. *Adv. X-Ray Anal*. **4**, 382-400 (1960).

56. Cloete, H.C.C. A Comparison of Software Packages for X-Ray Fluorescence Analysis of Silicates on Fusion Disks. *Adv. X-Ray Anal*. **41**, 743-752 (1997).

57. Sear, L.G. The Fusion of Difficult Materials Including Chromite, Cassiterite and Reduced Sulphur. *X-ray Spectrometry*. **26**, 105-110 (1997).

58. Merkle, R.K.W., Loubser, M. and Graser, P.P.H. Incongruent dissolution of chromite in lithium tetraborate flux. *X-ray Spectrometry*. **33**, 222-224 (2004).

59. Baker, J.W. Volatilization of Sulphur in Fusion Techniques for Preparation of Discs for X-ray Fluorescence Analysis. *Adv. X-Ray Anal*. **25**, 91-94 (1981).

60. Norman, M., Robinson, P. and Clark, D. Major and Trace analysis of Sulphide ores. *The Canadian Mineralogist*. **41**, 293-305 (2003).

61. Norrish, K. and Thompson, G.M. XRS Analysis of Sulphides by Fusion Methods. *X-ray Spectrometry*. **19**, 67-71 (1990).

62. Pella, P.A. Effect of gas burner conditions on lithium tetraborate fusion. *Anal. Chem*. **50**, 1380-1381 (1978).

63. Loubser, M., Strydom, C. and Potgieter, H. A thermogravimetric analysis study of volatilization of flux mixtures used in XRF sample preparation. *X-ray Spectrometry*. **33**, 212-215 (2004).

64. Lupon, D.F., Merker, J. and Scholz, F. The Correct use of Platinum in the XRF Laboratory. *X-ray Spectrometry*. **26**, 132-140 (1997).

65. Zachariasen, W.H. The Atomic Arrangement in Glass. *J Chem. Soc*. **54**, 3841 (1932).

66. Sastry, B.S.R., Hummel, F. A. Studies in lithium oxide systems: V, Li_2O-Li_20 B_2O_3 . *J Amer. Ceram. Soc*. **42,** 218 (1959).

67. Claisse, F. and Blanchette, J.S. *Physics and Chemistry of Borate Fusion - For XRF Spectroscopists*. Fernand Claisse Inc. Quebec, Canada. (2004).

68. Smith, D.W.J. An acidity scale for binary oxides. *Journal of Chemical Education*. **64(6)**, 480-481 (1987).

69. Lang, G. and Davidts, M. Contribution to the study of the glass Structure and Application to the X-Ray Analysis. *ICPH Chemicals Intl. S.A. Conference.* Nancy-France (1998).

CHAPTER 2: EXPERIMENTAL METHODS

A selection of commercially available lithium borate fluxes was chosen for this study. An attempt was made to include fluxes prepared using different manufacturing methods i.e. powdery calcined fluxes, pre-fused fluxes and different post preparation treatments. A newly developed experimental flux prototype was also included in the study (PR0301A and PR0301B). After initial investigation of the fluxes some sample flux mixtures were also evaluated, using PR0301A and PR0301B for the sample flux mixtures. Table 2.1 lists the fluxes and flux/sample mixtures used during this study.

2.1 Preparation of samples

TGA/DSC analyses were executed on the flux mixtures without prior drying to enable evaluation of the extent of moisture absorption from the atmosphere, as lithium borate mixtures are hygroscopic, which is one of the major problems encountered, in the use of these glass-forming materials as analytical fluxes. For the TGA analyses 20 to 40mg of flux were introduced in platinum crucibles.

Based on the TGA/DSC results that were obtained, larger volumes of selected fluxes were prepared in an Ultra Furn Muffle furnace with a TM-104 temperature controller and a range from 20 ºC – 1200 ºC, to reproduce phenomena observed in the DSC curves. 5±0.01g of flux was weighed into a platinum crucible using a five

decimal electronic balance. The flux was then heated to the selected temperature and kept at that temperature for 2 hours. After cooling in a desiccator, the flux was weighed again before heated to the next step.

Table 2.1 Materials investigated (LiT (Lithium tetraborate), LiM (Lithium metaborate))

Sample name:	**Composition:**	**Analysis method:**
FLUORE-X® ATL 100	$Li_2B_4O_7$	TGA, XRD, Raman
Spectroflux® 100	$Li_2B_4O_7$	TGA
Claisse Lithium tetraborate	$Li_2B_4O_7$	TGA
FLUORE-X® AML 100	$LiBO_2$	TGA, XRD, Raman
Spectroflux® 100A	$LiBO_2$	TGA
Claisse Lithium metaborate	$LiBO_2$	TGA
FLUORE-X® 20	20%$Li_2B_4O_7$.80%$LiBO_2$	TGA, XRD, Raman
FLUORE-X® 65	66%$Li_2B_4O_7$.34%$LiBO_2$	TGA
Claisse LiT/LiM	50% $Li_2B_4O_7$.50%$LiBO_2$	TGA
Sigma X-ray Flux 12-22	35% $Li_2B_4O_7$.65%$LiBO_2$	TGA
Sigma X-ray Flux 57-43	57% $Li_2B_4O_7$.43%$LiBO_2$	TGA
PR0301A	$Li_2B_4O_7$	TGA, XRD, Raman
PR0301B	$Li_4B_6O_{11}$	TGA, XRD, Raman
LiT with SiO_2	1g SiO_2 and 6g $Li_2B_4O_7$	TGA, XRD, Raman
PR0301B with SiO_2	1g SiO_2 and 6g $Li_4B_6O_{11}$	TGA
LiT with Fe_2O_3	1g Fe_2O_3 and 6g $Li_2B_4O_7$	TGA, XRD, Raman
PR0301B with Fe_2O_3	1g Fe_2O_3 and 6g $Li_4B_6O_{11}$	TGA
LiT with ZrO_2	1g ZrO_2 and 9g $Li_2B_4O_7$	TGA, XRD, Raman
PR0301B with ZrO_2	1g ZrO_2 and 9g $Li_4B_6O_{11}$	TGA

Sample name:	Composition:	Analysis method:
LiT with Cr_2O_3	0.5g Cr_2O_3 and 9g $Li_2B_4O_7$	XRD
LiT with UP1	1g granite and 6g $Li_2B_4O_7$	TGA, XRD, Raman

Loss on ignition was calculated as follows:

$$\%\ LOI = \frac{Weight1 - Weight2}{Weight1 - Weightcrucible} \text{x}100$$

Table 2.2 indicates the incremental LOI values and selected preparations at temperatures determined from the original TGA/DSC data. The lithium tetraborate that was reacted above the melting temperature produced a homogenous glass, but the lithium metaborate crystallised on cooling. A small amount of the prepared material, after homogenising in a mortar and pestle, where necessary, was placed on a microscopic glass plate and Raman spectra were obtained using a microscope to focus the laser on a selected particle. To confirm that observed reactions were not due to quenching, it was decided to introduce the original material on a temperature stage under the microscope and repeat analyses in situ. At a later stage when sample/flux mixtures were analysed using the temperature stage, problems were encountered, as results were dependent on the specific particle focused under the laser beam. To solve the problem, sample/flux mixtures were prepared at different temperatures, in a muffle furnace, as described before. After milling, these samples were introduced to the Raman spectrometer in a capillary tube, using the macro-operating mode, to ensure a large surface area exposed to the laser.

Table 2.2 **Preparation temperatures and incremental mass loss values for selected preparations**

Lithium metaborate	**320 ºC**	**440 ºC**	**520 ºC**	**720 ºC**	**920 ºC**	**1060 ºC**	**1150 ºC**
% mass loss		0.33	0.02	0.01	<0.01	1.7	3.9
Lithium tetraborate			**500 ºC**	**850 ºC**	**950 ºC**	**1050 ºC**	**1150 ºC**
% mass loss				<0.01	<0.01	0.50	2.3
80:20 mixture of lithium metaborate /tetraborate			**540 ºC**	**880 ºC**		**1040 ºC**	**1100 ºC**
% mass loss			1.18	<0.01		1.0	3.0

For XRD analysis, the prepared mixtures were directly introduced in a standard sample holder using the front-loading technique. Once again, to eliminate the possibility of observing quenching reactions, the XRD work was repeated on an instrument with an Anton Paar HTK16 heating chamber. Here, a small amount of the sample was introduced to the diffractometer by pipetting the sample, prepared by milling in ethanol, evenly onto a platinum heating strip.

2.2 Thermogravimetric analysis (TGA) and Differential Scanning Calorimetry (DSC)

For most silicate and oxide matrices, lithium tetraborate ($Li_2B_4O_7$), lithium metaborate ($LiBO_2$), or mixtures of different ratios are used as flux. A range of

different composition mixtures, from different commercial sources and thus manufacturing methods, were investigated by Thermogravimetric analysis (TGA) and Differential Scanning Calorimetry (DSC), using a NETZSCH Simultaneous Thermal Analyzer STA 409 EP. Between 20 and 40mg of the flux was analysed in a platinum crucible using a heating rate of 10 ºC/min over a range of 20 ºC – 1280 ºC, under air atmosphere. The TGA curve indicates percentage mass loss as a function of increasing temperature, and the DSC curve measures the heat flow in the samples, by comparing the temperature change between an empty reference crucible and the crucible containing the sample, expressed as a potential in µV. A positive signal indicates an exothermic reaction and a negative signal indicates an endothermic reaction. The results of the analysis using this instrument are shown in Figures 3.1 to 3.13.

A newly developed experimental flux prototype submitted to the laboratory was analysed using a METTLER TOLEDO STAR^{e} system with TGA and Differential Thermal Analysis (DTA) capacities, as the instrument used initially was not available. The TGA functions as described previously but in this technique (DTA) the temperature difference between a substance and an inert reference material (like an Al_2O_3 block with thermocouple) is measured as a function of temperature whilst the substance and reference material are subjected to a controlled temperature programme[1]. The DTA results were not as accurate as the DSC data, due to the limited mathematical algorithms used in this specific software, but as the temperature of reaction was more important than quantifying the reaction this had

no serious implications on the data obtained.

About 20mg of the flux was analysed in a platinum crucible using a heating rate of 10 ºC/min over a range of 30 ºC – 1200 ºC, under air atmosphere. Figures 3.15 and 3.16 were collected on this instrument.

For the sample flux mixtures, a TA Q600 TGA/DSC from TA Instruments was used. This instrument was selected for the higher accuracy of the DSC curves compared to the DTA obtained on the METTLER TOLEDO STAR^e system. About 20mg of the flux sample mixture was analysed in a platinum crucible using a heating rate of 10 ºC/min over a range of 50 ºC – 1200 ºC, under nitrogen atmosphere. Figures 3.17 – 3.24 were produced on this instrument.

2.3 X-ray Powder Diffraction (XRD)

The initial X-ray diffractograms were collected on a Siemens D-501, using Cu Kα (1.542 Å) radiation with a graphite monochromator. The analyses were executed at room temperature with a scintillation detector. The power settings were 40 kV, 40 mA, and the range 15<2θ<70º, with a 0.04 º2θ step width and 1.5s per step. Subsequent analyses were done on a PANalytical X'Pert Pro powder diffractometer with X'Celerator detector and variable divergence- and receiving slits with Fe filtered CoKα radiation and an Anton Paar HTK16 heating chamber.

The phases were identified using X-Pert Highscore plus software.

2.4 RAMAN Spectroscopy

Raman Spectroscopy relies on inelastic scattering, of monochromatic light, usually from a laser in the visible, near infrared, or near ultraviolet range. The laser light interacts with photons in the system, resulting in the energy of the laser photons being shifted to higher or lower energy. The shift in energy gives information about the bonds present in the system. Raman spectroscopy lends itself ideally to the study of lithium borate fluxes, as it can be used to analyse the amorphous glass phase where XRD fails. The Raman bands in the spectra of glasses are generally broader than in comparable crystals. This is caused by the deformation of the vibrating groups in the vitreous state, consequently leading to a broader density of states, (Brawer[2]). For the above-mentioned reasons it is difficult to give a sound theoretical interpretation of the Raman spectra of the lithium borate glasses. However, by comparison with Raman spectra of the appropriate compounds whose crystal structure is known, it is possible to obtain qualitative information on the presence of certain structural units in the glasses.

The first Raman spectra of glasses were published shortly after the discovery of the effect (1923-1928), by Kujumzelis[3], but only with the introduction of ion-gas lasers did it become a valuable tool. The first articles on laser Raman spectroscopy of glasses appeared during 1970-1971 [4-7]. The properties of these spectra were characterised by a limited number of well-defined bands. The spectra were relatively simple compared to infrared spectra, and there were changes as a function of

composition[8].

Raman spectra were recorded with a XY Raman spectrometer from Dilor®, using the λ=514.5 nm laser line of a Coherent Innova®90 Ar^+-laser, with a resolution of at least 2 cm^{-1}, as excitation source. The samples were recorded in a backscattering configuration under the Olympus microscope attached to the instrument, using a 50x objective. A liquid nitrogen cooled CCD detector was used with the laser power 200 mW at the laser exit, resulting in a laser power <20 mW at the sample. The spectra were baseline corrected, using the Labspec software program supplied by Dilor®. For the in situ heating experiments, a TMS93 Linkam® heating cell was introduced on the stage of the Olympus confocal microscope. An operational range between 20 °C and 600 °C was used. For selected tests, a macro set-up was used where a powdered sample was introduced into a glass capillary, which was illuminated by the laser beam. These measurements were recorded at room temperature.

2.5 Transmission Electron Microscopy

In Chapter 4 a bright field TEM micrograph is shown (Figure 4.10). The purpose of the TEM micrograph was used to investigate the presence of both amorphous and crystalline particles in the flux prototype, and characterise the structure. This was photographed on a Philips CM200 TEM bright field at 200kV. The sample

was prepared by suspending the finest particles of the flux prototype in methanol, placing a drop of the suspension on a holey carbon film and allowing it to dry.

2.6 Scanning Electron Microscopy

In Chapter 4 some SEM photos are shown (Figures 4.3 and 4.4). A Jeol 5800 was used at 25kV and a secondary electron image collected. As XRD could only be used successfully on crystalline samples, SEM photos were taken to identify whether any physical changes occurred in the sample below the melting point to ascertain whether any changes in the XRD data could be expected.

2.7 Electron Probe Micro Analysis

In Chapter 6, Electron Probe Micro Analysis was executed on polished sections prepared of fused beads. Specimens of an excess pure oxide (low solubility) were prepared in lithium borate flux: 0.25g chromite ($Fe^{2+}Cr_2O_4$), with 6g $Li_2B_4O_7$ was fused for an hour at 1050 ºC while mixing continuously to homogenise the fused glass. After the prepared glass bead was annealed, a cross section was cut using a diamond saw and mounted and carbon coated for EPMA analysis. A second specimen consisting of 1g Zircon ($ZrSiO_4$), with 6g $Li_2B_4O_7$ was prepared according to the same method.

The specimens were mapped with the CAMECA SX 100 Electron Probe Micro Analyser (EPMA). This state of the art instrument, equipped with four wavelength dispersive spectrometers as well as the latest energy dispersive system from Röntec, facilitates analysis of major and trace elements on a microscopic scale. The analytical conditions were as follows: 20KV and 20 nA for the beam. Al, Ti, Cr, Fe analysed for 10 seconds on the peak position with equal time on symmetrical backgrounds all using Kα lines, Zr was analysed using the Lα line. As standards the following minerals were used: Corundum, Magnetite, Rutile, Cr2O3 and Zircon.

REFERENCES:

1. Mackenzie, R.C. Nomenclature for Thermal Analysis IV. *Pure & Appl. Chem*. **570(11),** 1737-1740 (1985).
2. Brawer, S. Theory of the vibrational spectra of some network and molecular glasses. *Phys. Rev*. **B11**, 3173 (1975).
3. Kujumzelis, J. The Raman Effect and Its Chemical Applications. *Z. Phys*. **100**, 221 (1939).
4. Etchepare, J. Raman scattering spectra of vitreous silica and binary glasses of alkaline silicates. *J Chim.Physicochim.biol.* **67**, 890 (1970).
5. Etchepare, J. Interpretation des Spectres de diffusion Raman de verres de silice binaires. *Spectrochim.Acta*. **26A**, 2147 (1970).
6. White, W.B., McCarthy, G.J. and McKay, *J. Amer. Ceram. Soc. Bull*. **50**, 411 (1971).
7. Tobin, H.C. and Brook, T. *J Opt. Soc. Amer*. **60**, 368 (1970).
8. Brill, T.W. Raman Spectroscopy of Crystalline and Vitreous Borates. *Philips Res. Rep. Suppl.* No.2. (1976).

CHAPTER 3: THERMOGRAVIMETRIC AND DIFFERENTIAL SCANNING CALORIMETRY STUDY OF LITHIUM BORATE FLUX MIXTURES

As part of a systematic program to evaluate the reactions occurring during the fusion process of a lithium borate glass, Thermogravimetric analysis (TGA) and Differential Scanning Calorimetric (DSC) analysis were used. In this study, the conditions prevailing in a crucible with a flux mixture were simulated with a thermogravimetric analyser and pure flux mixtures were used to provide baseline results.

3.1 Experimental results

Fluxes from different manufacturers were compared, namely; ICPH FLUORE-X®, Spectroflux®, Claisse and Sigma X-ray Flux. This led to the evaluation of volatilisation of commercial fluxes. Subsequently mixtures of pure oxides and flux were prepared, as for a routine fusion, and analysed in the same manner as the pure fluxes to investigate the interaction between flux and sample. Pure quartz, SiO_2, pure hematite, Fe_2O_3 and zirconium oxide, ZrO_2, were used for this exercise as they are difficult oxides to dissolve in a flux. A typical mixed oxide, a granite sample (UP1), was also investigated.

3.1.1 Pure fluxes

Three commercially available pure lithium tetraborate samples were evaluated (Figures 3.1, 3.2, 3.3). They were selected because the manufacturing methods of the three differed. Below the melting point for lithium tetraborate (920 ºC), the TGA curve is constant around 0%. Some initial mass losses around 200 ºC can be ascribed to the loss of adsorbed water. Lithium borates are known to be hygroscopic. The content of adsorbed water was lowest in the flux from ICPH FLUORE-X® ATL 100, which is a pre-fused flux, thus melted after preparation by a calcination reaction. The advantages of a fusion step in the manufacturing process are the elimination of residual volatiles and an increase in density and particle size, resulting in a decrease of surface area exposed to the atmosphere. The endothermic peak on the DSC curve at 920 ºC corresponds to the melting range of lithium tetraborate (920 – 930 ºC). Another small endothermic peak is seen around 830 to 840 ºC on all three lithium tetraborate spectra (Figures 3.1-3.3). The endotherm was most marked for the FLUORE-X® ATL 100 and Claisse lithium tetraborate, but could not be associated with any described thermal event. At approximately 1020 ºC, a sudden decrease in the TGA curve is observed, corresponding to a small exothermic peak on the DSC curve in FLUORE-X® ATL 100 (Figure 3.1), and Claisse lithium tetraborate (Figure 3.3). In the FLUORE-X® ATL 100 (Figure 3.1), a rate change is observed in the mass loss, with an accompanying endotherm in the DSC curve. During the 18 minutes heating from

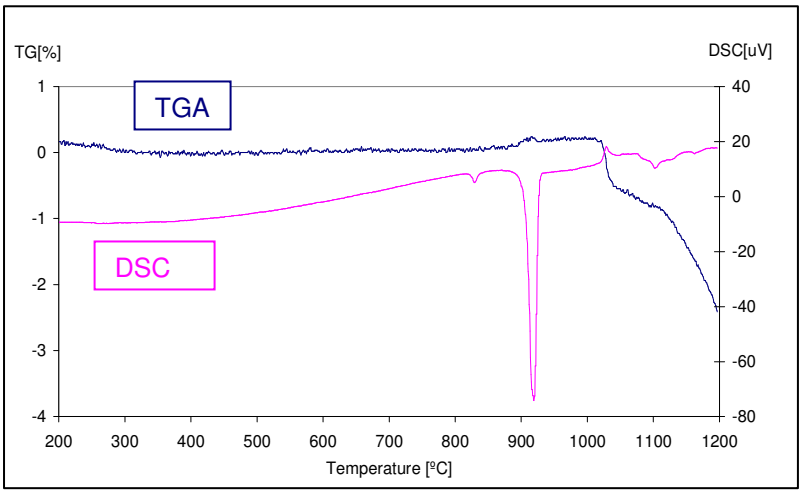

Figure 3.1 TGA and DSC curves: Lithium tetraborate: FLUORE-X ATL 100

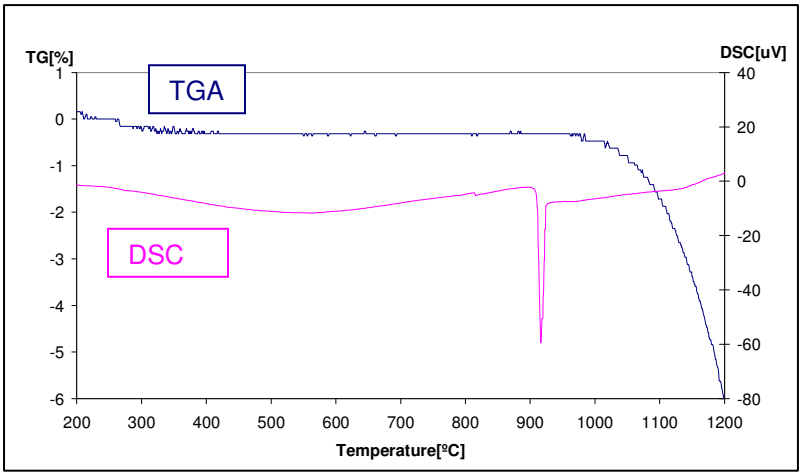

Figure 3.2 TGA and DSC curves: Lithium tetraborate: Spectroflux 100

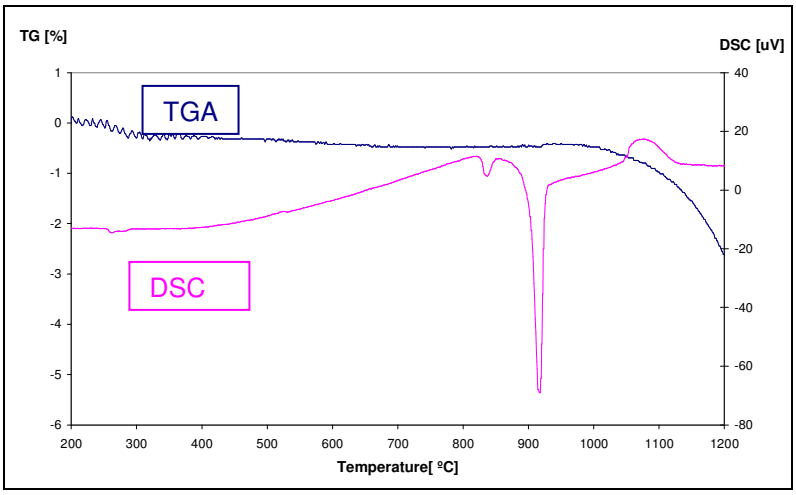

Figure 3.3 TGA and DSC curves: Lithium tetraborate: Claisse lithium tetraborate

1020 ºC to 1200 ºC, between 2 and 6% mass loss was observed in the samples. The largest mass loss was in Spectroflux® 100 (Figure 3.2), which was not pre-fused during the manufacturing process. This loss of flux is described in more detail later.

Three pure lithium metaborate samples (FLUORE-X® AML 100, Spectroflux® 100A and Claisse lithium metaborate), were evaluated (Figures 3.4, 3.5, 3.6). The comparatively large mass loss below 500 ºC, in two of the three samples, can be ascribed to the hygroscopic nature of lithium metaborate. This is one of the reasons why lithium metaborate is seldom used on its own as a flux for XRF sample preparation, although the melting point is lower than that of lithium tetraborate. This latter characteristic is advantageous when preparing a sample solution for analysis by Inductively Coupled Plasma and Atomic Absorption Analysis. From 500 ºC to the melting point around 845 ºC, the TG curve is stable and, as in the case of lithium tetraborate, a 2 to 6% mass loss was observed between 1020 ºC to 1200 ºC. ICPH FLUORE-X® AML 100 (Figure 3.4) was the only sample in which the TG loss corresponded to a clear small exothermic event on the DSC curve, and as with the FLUORE-X® ATL 100, a rate change was observed for the mass loss marked by another small peak on the DSC curve. The manufacturing process of this sample included a pre-fusion step. Looking at ICPH FLUORE-X® AML 100 (Figure 3.4) in more detail, the DSC curve has additional features, apart from the large endotherm at 845 ºC indicating the melting point. Small exothermic peaks are observed at

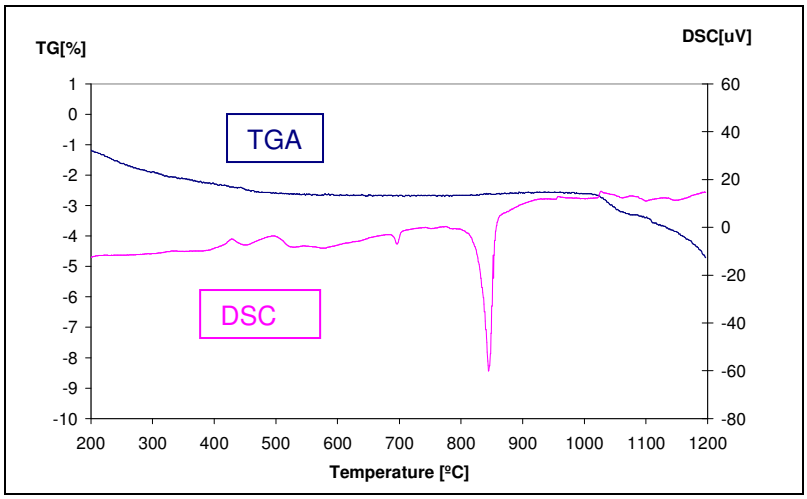

Figure 3.4 TGA and DSC curves: Lithium metaborate: FLUORE-X AML 100

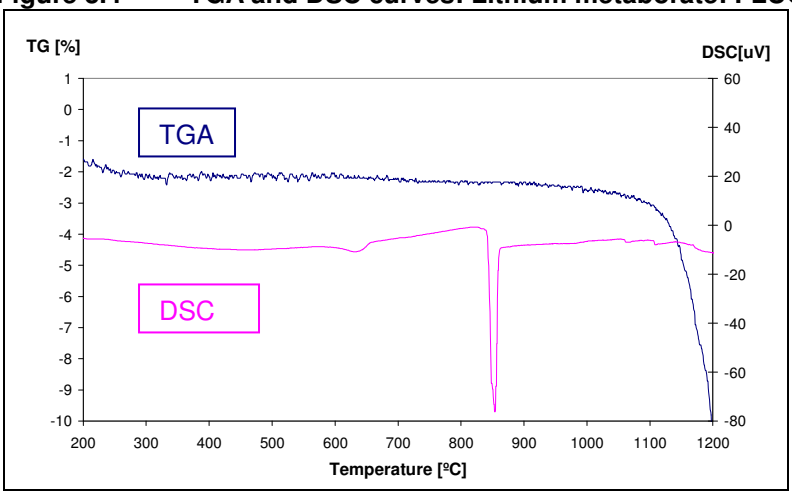

Figure 3.5 TGA and DSC curves: Lithium metaborate: Spectroflux 100A

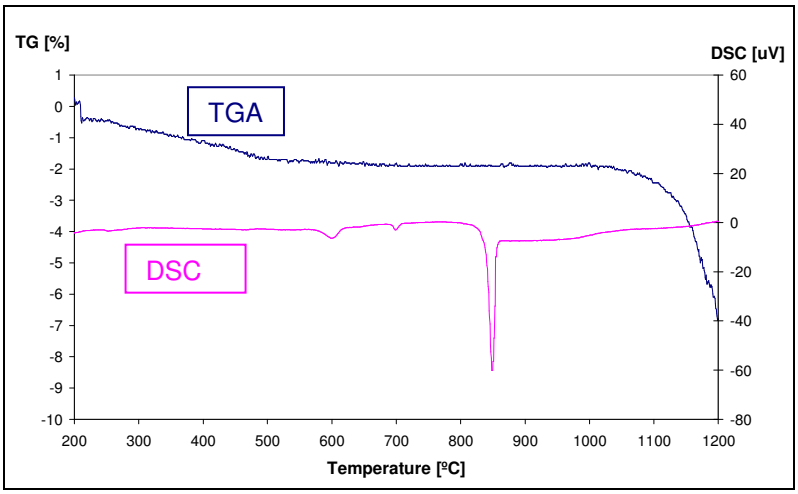

Figure 3.6 TGA and DSC curves: Lithium metaborate: Claisse lithium metaborate

435 ºC and 500 ºC and a small endotherm at 700 ºC, apart from the very small exotherm at 1033 ºC and very small endotherm at 1082 ºC described under the mass loss. For the Spectroflux® 100A sample (Figure 3.5), apart from the melting point endotherm at 855 ºC, another small endotherm is seen at 639 ºC, and around 1117 ºC, some irregularities are observed in the DSC curve corresponding to the TG mass loss. For the Claisse lithium metaborate (Figure 3.6), two additional endotherms are observed at 605 ºC and 703 ºC, apart form the melting point endotherm at 850 ºC. Just as all three lithium tetraborate samples demonstrated endotherms around 830 ºC, two of the lithium metaborate samples have an endotherm around 700 ºC and the remaining Spectroflux metaborate has one at 639 ºC. Spectroflux 100A is also prepared without a pre-fusion step in the manufacturing process.

Five commercially available mixtures of lithium tetraborate and lithium metaborate, from three different manufacturers, were evaluated, (Figures 3.7, 3.8, 3.9, 3.10, 3.11 and 3.13). Melting points for the individual mixtures are easy to identify by the large endothermic peak on the DSC curves. For compositions with more than 50% lithium metaborate, the melting temperatures are in the same range as for pure lithium metaborate (Figures 3.7, 3.8 and 3.13), around 840 ºC. For compositions with more lithium tetraborate than lithium metaborate, dual melting points were observed; one at 840 ºC and a smaller one at 900 ºC (Figures 3.10, 3.11 and 3.13). Both these flux mixtures were pre-fused during the manufacturing process, which

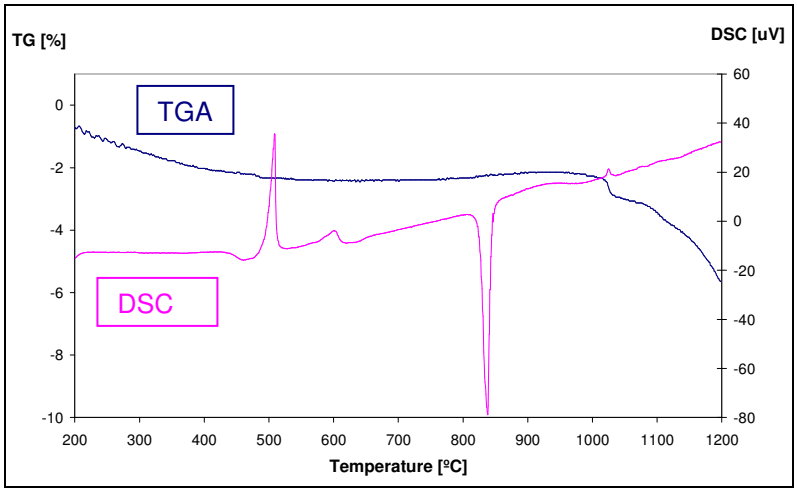

Figure 3.7 TGA and DSC curves: 20%$Li_2B_4O_7$:80%$LiBO_2$: FLUORE-X 20

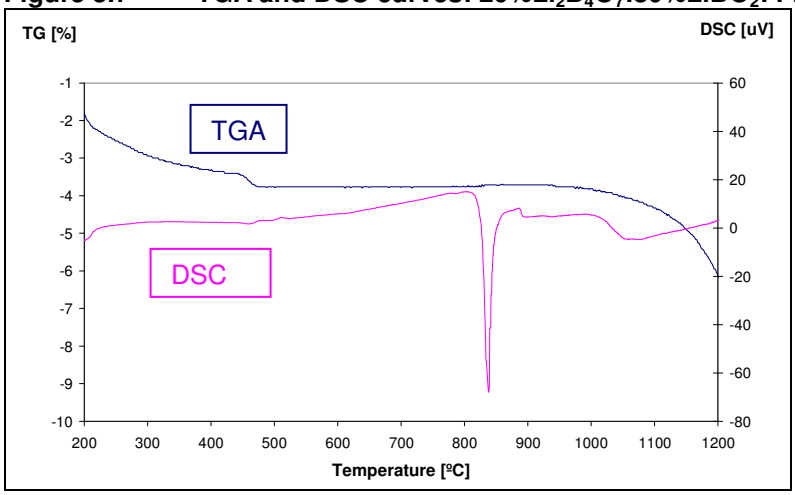

Figure 3.8 TGA and DSC curves: 35%$Li_2B_4O_7$:65%$LiBO_2$: Sigma X-ray Flux 12-22

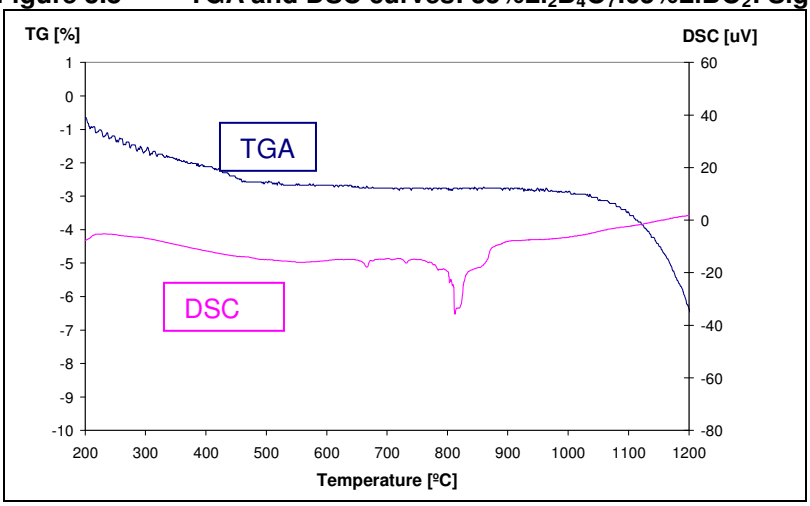

Figure 3.9 TGA and DSC curves: 50%$Li_2B_4O_7$:50%$LiBO_2$: Claisse LiT/LiM

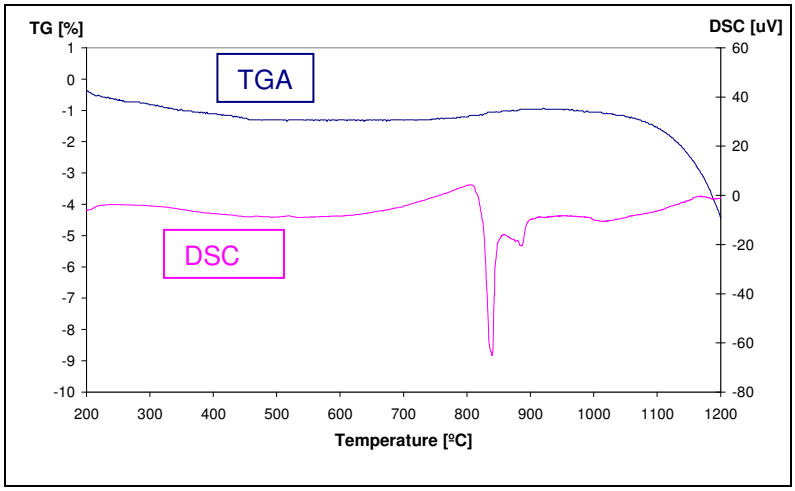

Figure 3.10 TGA and DSC curves: 57%$Li_2B_4O_7$:43%$LiBO_2$: Sigma X-ray Flux 57-43

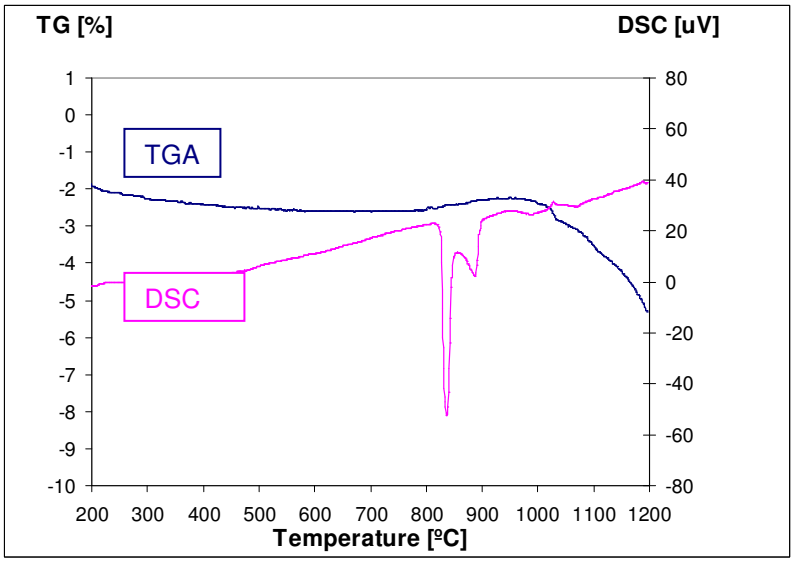

Figure 3.11 TGA and DSC curves: 66%$Li_2B_4O_7$:34%$LiBO_2$: FLUORE-X 65

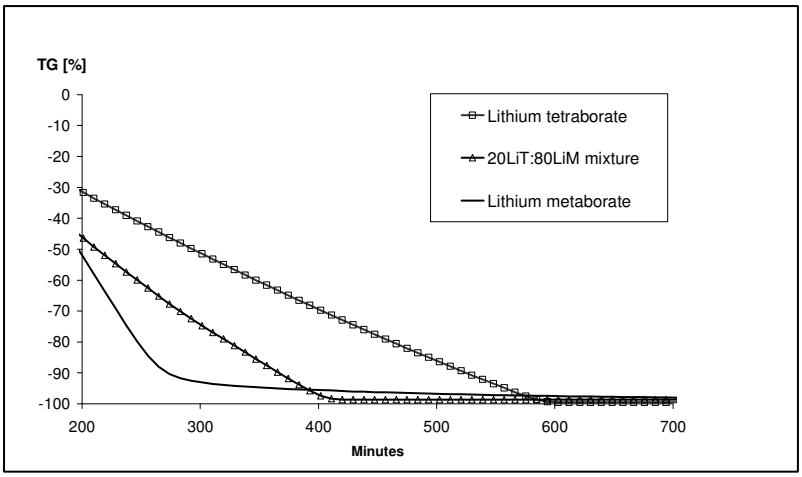

Figure 3.12 TGA curves for 900 minutes at 1230 ºC

indicates that different lithium borate species might co-exist even after fusion, although not pure lithium tetraborate and lithium metaborate. It was only for the 50:50 mixtures (Figure 3.9 and 3.13) that a single, different melting temperature, an eutectic around 820 ºC, was observed. Above 1020 ºC, a mass loss of more than 2% was observed for all the compositions. To evaluate the DSC curves in greater detail, Figure 3.13 represents a comparison of all five the lithium tetraborate - metaborate mixtures in order of increasing lithium tetraborate content. From this figure the previously discussed melting points are clearly seen, as well as some additional features. All the mixtures displayed endotherms around 150 ºC and 200 ºC, related to initial water loss from the flux mixtures. At 510 ºC the FLUORE-X® 20 sample showed an exotherm corresponding to the re-crystallisation temperature of a lithium borate glass, which indicates that this sample was the only one that was an amorphous glass when investigated. The idea of a pre-fused flux is that the material exists as an amorphous glass which increases the density, decreases the surface area and result in less hygroscopic reactions. Although many of the fluxes investigated were supposedly pre-fused, only this sample showed the exothermic DSC reaction confirming its glassy nature. This does pose questions regarding the stability of the pre-fused material and whether, over time it could crystallise at room temperature. The same sample also showed another exothermic peak at 605 ºC that could not be ascribed to any known reaction. The 50:50 Claisse sample displayed various small endothermic peaks at 670, 735 and 773 ºC apart from the melting point endotherm at 800 ºC. Both the FLUORE-X® 20 and FLUORE-X® 65 mixtures displayed an exotherm at 1030 ºC, corresponding to the TGA mass loss,

and the DSC curve for Sigma X-ray Flux 12-22 showed an irregularity at the same temperature.

For practical routine application it is important to know whether this observed mass loss reaches equilibrium during the time required for fusing. Portions of lithium tetraborate, lithium metaborate and a 20:80 LiT: LiM mixture were heated to 1230 ºC and monitored by TGA analysis under isothermal conditions (Figure 3.12). For previous TGA work, the heating curve was programmed from 20 ºC to 1280 ºC, but measurements were only recorded between 200 ºC and 1200 ºC because the accuracy of measurements decrease as the heating curve's upper limit is approached. For the isothermic measurements, 1280 ºC was also set as the upper limit, but recordings were done at 1230 ºC for the same reason. It was found that all flux had evaporated after a period varying from 350 minutes for lithium metaborate, 400 minutes for the mixture and 600 minutes for the lithium tetraborate (Figure 3.12).

Gradual loss of flux could imply that the flux was evaporating, or dissociating to more volatile components, i.e. components were lost preferentially. To investigate this aspect further, 5g portions of lithium tetraborate, lithium metaborate and a 20:80 LiT: LiM mixture were dried and tempered in a muffle furnace at 1000 ºC for 12 hours. A second portion of each was heated at 1150 ºC for 12 hours. The samples were subsequently dissolved in a 25% HCl acid solution and analysed on a Varian Liberty 220 ICP analyser for lithium and boron.

Neither boron nor lithium analyses agreed with the theoretical compositions listed (Table 3.1). This is probably more indicative of the limitation of the analytical technique for the stated elements than the sample purity since certified, ultra pure fluxes were used in the investigation. When considering the boron/lithium mass ratios, 3.6 for lithium tetraborate, (theoretical 3.1), 1.7 for lithium metaborate (theoretical 1.6), and 2.0 for the 20:80 LIT: LIM mixture (theoretical 1.8), it was found that the lithium and boron levels decreased at a constant rate, which indicates that the loss on ignition (LOI) is a volatilisation reaction rather than a dissociation of one or the other constituent that is more volatile.

Table 3.1: ICP analysis on Flux mixtures:

FLUX:		**12 hours @1000 ºC**		**12 hours @1150 ºC**		**% LOI gravimetrically determined**
		% B	**% Li**	**% B**	**% Li**	
Lithium tetraborate	analysed concentration	25.0	6.9	24.4	6.7	2.17
	theoretical value	**25.57**	**8.21**			
Lithium metaborate	analysed concentration	21.5	12.4	20.6	12.0	2.19
	theoretical value	**21.73**	**13.95**			
20:80 LiT:LiM Mixture	analysed concentration	22.3	11.2	22.0	11.0	1.60
	theoretical value	**22.50**	**12.80**			

3.1.2 New flux prototype

One of the commercial flux manufacturers; ICPH, approached the laboratory with a new prototype and requested the inclusion of two samples in the study. The samples were submitted as a pure lithium tetraborate (labelled PR0301A) and a “bi-borate” (labelled PR0301B), as termed by the manufacturer, with a molar ratio B_2O_3/Li_2O of 1.5 and a presumed structure of two metaborate units joined by

bridging oxygen (Figure 3.14). These fluxes were prepared with the inclusion of a pre-fusion step, resulting in the fluxes being amorphous glass with microcrystalline inclusion particles.

Figures 3.15 and 3.16 present the TGA/DTA curves for these. As in previous lithium tetraborate samples, The DTA curve for PR0301A (Figure 3.15) shows an endothermic peak around 920 ºC that corresponds to the melting temperature of pure lithium tetraborate. Also observed is an exothermic peak around 520 ºC, corresponding to the re-crystallisation reaction of the amorphous glass back to its crystalline state. This was previously only observed in the 20% lithium tetraborate – 80% lithium metaborate mixture from the same manufacturer (Figure 3.7). Also apparent in the TGA curve is the absence of an initial mass loss due to absorbed water. This is remarkable if taken into consideration that these fluxes were not stored with any special precautions (plastic screw top jar on a laboratory bench for five months before analysis).

The DTA curve for PR0301B (Figure 3.16), assumed to be bi-borate, shows the same exothermic peak around 520 ºC, corresponding to the re-crystallisation reaction. The absence of any significant mass loss on the TGA curve below 200 ºC is remarkable when compared to the previous lithium metaborate curves (Figures 3.4, 3.5 and 3.6). An interesting observation is made around the endotherm on the DTA curve associated with the melting point. Instead of one sharp melting point at 845 ºC, as observed in Figures 3.4-3.6, two distinct melting points are observed,

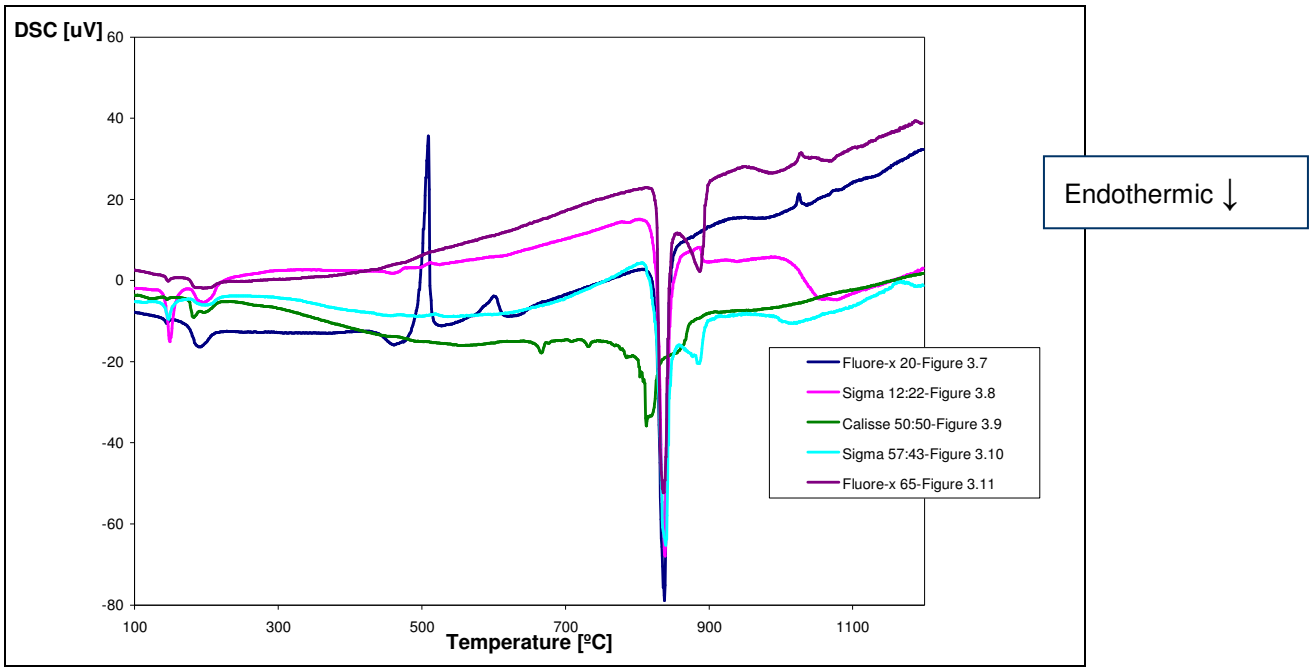

Figure 3.13 DSC curves of comparison of all LiT/LiM mixtures

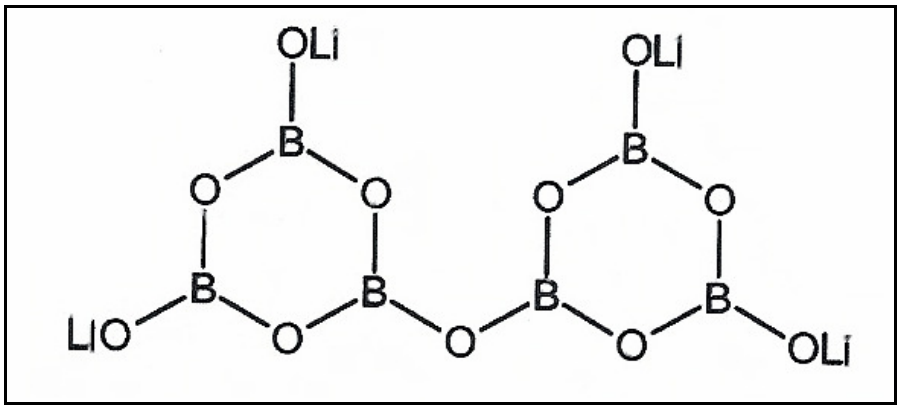

Figure 3.14 Structural drawing of $2Li_2O$-$3B_2O_3$ Lithium bi-borate

one at 845 ºC, and a smaller one at 902 ºC. This is similar to what was observed in Figures 3.10 and 3.11 where mixtures with more lithium tetraborate than metaborate were presented, and yet again it is noted that the manufacturing process of these fluxes includes a pre-fusion step. Consequently, it can be deduced that even after fusion at 1100 ºC, distinct species co-exist.

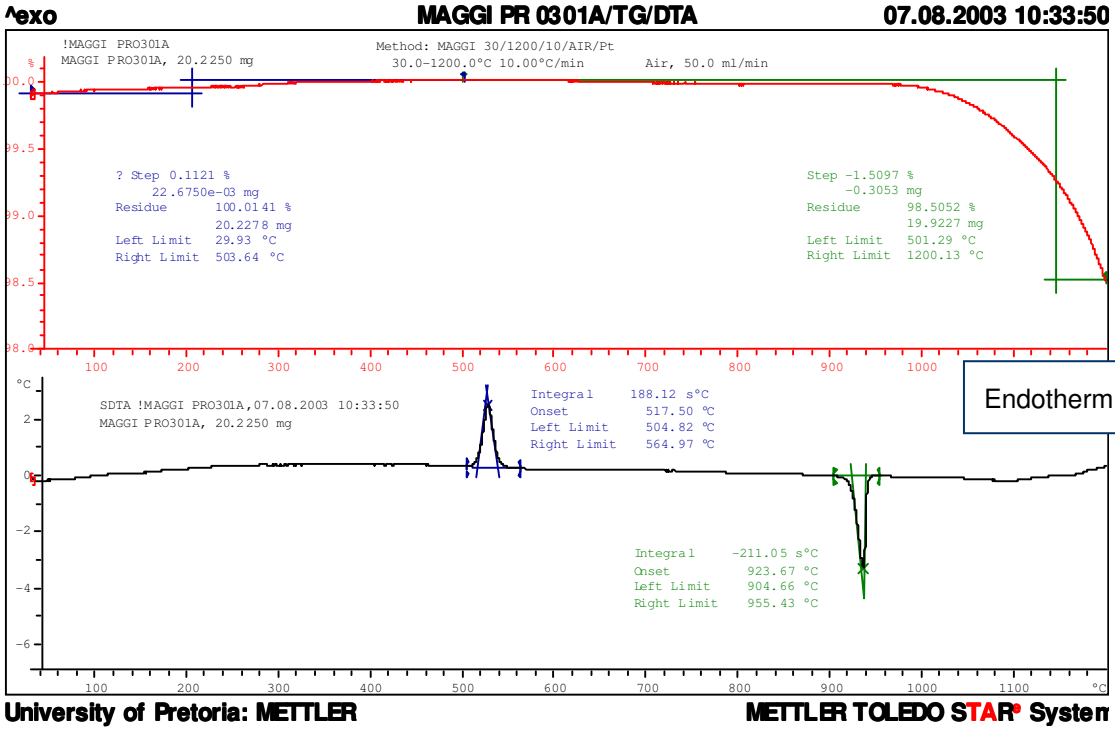

Figure 3.15 TGA/DTA curve for lithium tetraborate prototype

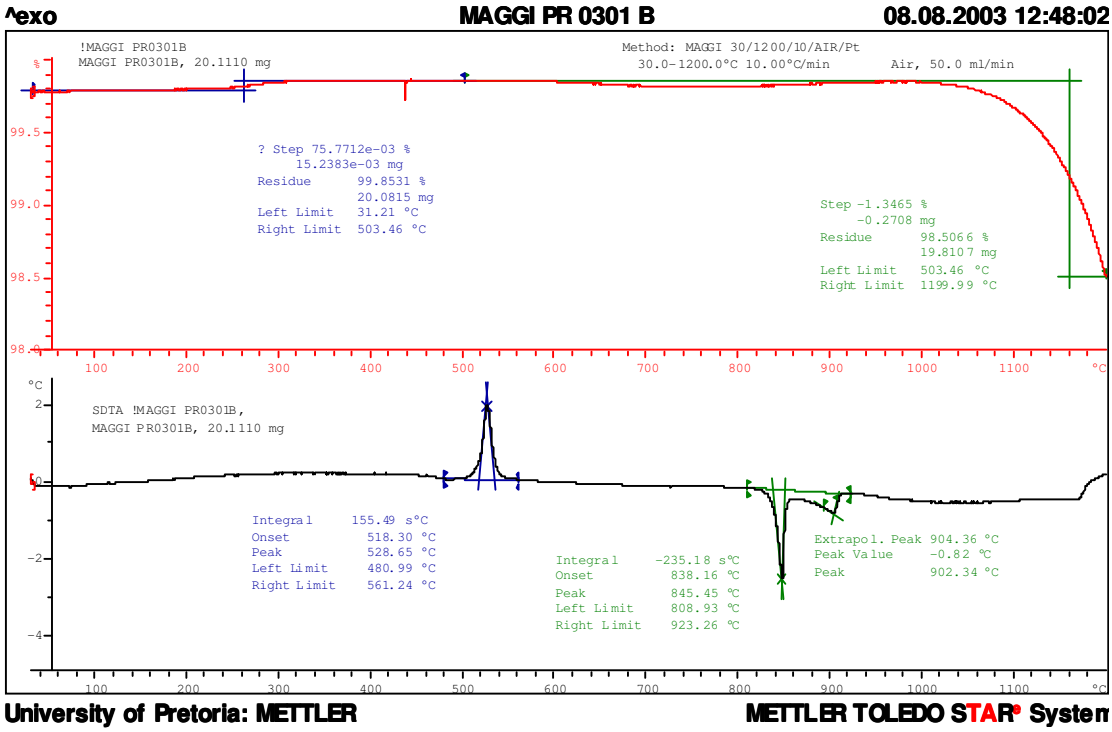

Figure3.16 TGA/DTA curve for lithium bi-borate prototype

3.1.3 Sample and flux mixtures

As adequate amounts of both of these ICPH prototype fluxes were available, and the stability and performance of these fluxes proved it to be a good choice, they were used in the sample flux experiments executed with some pure oxides. The samples were prepared according to routine laboratory methods as follows;

1g pure oxide sample was added to 6g of flux and homogenised.

20mg of the homogenised mixture were analysed with the TGA method. The samples were heated at a rate of 20 ºC per minute from 25 – 1200 ºC.

3.1.3.1 SiO_2 as sample

The first sample was pure SiO_2 fused with the pure lithium tetraborate PR0301A (Figure 3.17). The TGA curve is similar to the pure flux curves with a stable signal up to 1100 ºC where a weight loss is observed. It is interesting to observe that the volatilisation reaction proposed under the pure flux experiments still occurred, even when sample is present. The DSC curve shows the same exothermic peak due to re-crystallisation at 524 ºC as was observed in the pure flux. Where a single endotherm around 920 ºC was observed for the pure flux's melting point (Figure 3.15), double peaks were now observed in the flux/sample mixture at a temperature well below the melting point of the pure flux, indicative of the presence of two different phases. The observed melting points were at 874 ºC and 890 ºC.

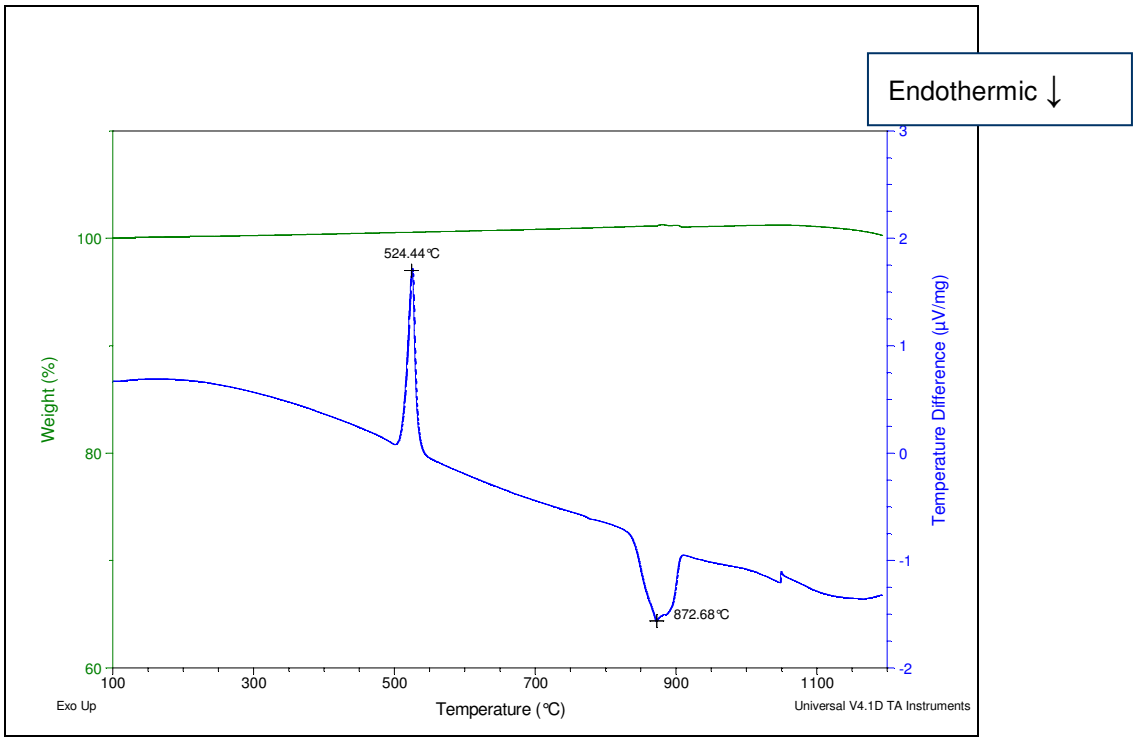

Figure 3.17 DSC-TGA curves for lithium tetraborate with SiO_2

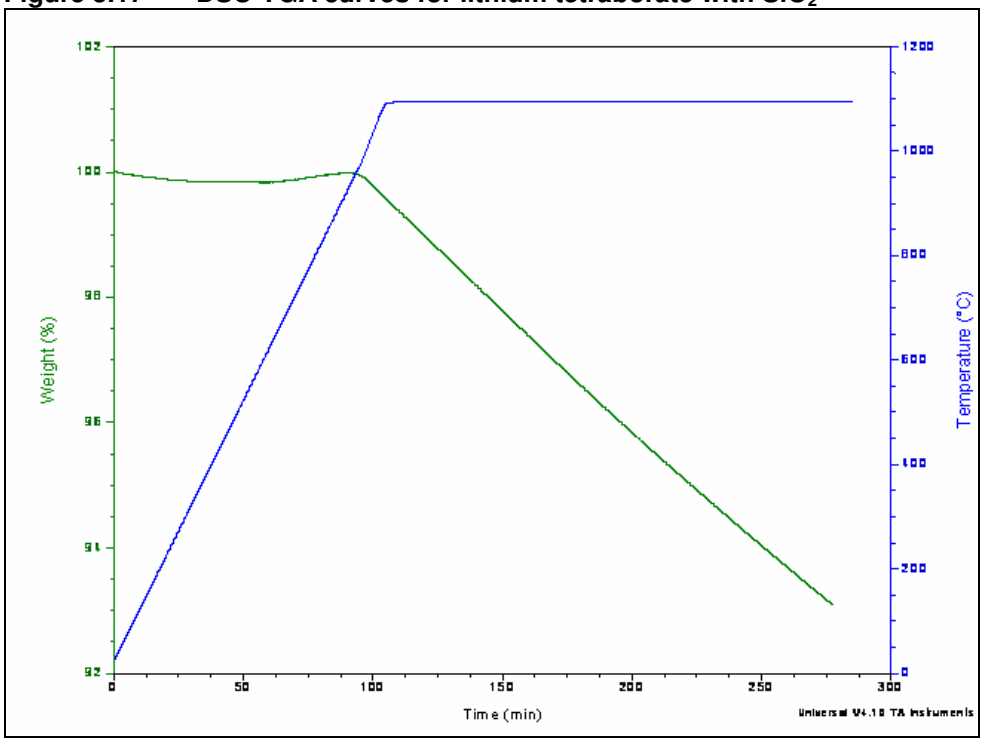

Figure 3.18 SiO_2 and lithium tetraborate: Isothermal TGA curves for 300 minutes at 1100 ℃

To evaluate the nature of the weight loss above 1000 ºC where sample is present in the flux, an isothermal TGA run was done above 1000 ºC (Figure 3.18). After 300 minutes a 6% weight loss was observed with no indication that the rate of weight loss was levelling off. This is consistent with the observations for pure flux. (Refer to 3.1.1).

The same SiO_2 sample was also fused with the bi-borate PR0301B (Figure 3.19). The re-crystallisation peak is observed at 525 ºC and, as with the pure flux, two distinct melting points at temperatures lower than that of the pure flux are seen at 821 ºC and 874 ºC. Identical volatilisation of the flux is observed above 1050 ºC.

3.1.3.2 Fe_2O_3 as sample

The next sample was pure Fe_2O_3 fused with the pure lithium tetraborate PR0301A (Figure 3.20). The TGA curve was stable with the exception of mass loss above 1050 ºC. The exotherm due to the re-crystallisation reaction, as observed in the pure flux, was observed at 526 ºC. An endotherm, due to the melting point of the flux/Fe_2O_3 mixture was observed as a double peak with the first peak at 882 ºC and a second peak on the shoulder. The same Fe_2O_3 sample was also fused with the bi-borate PR0301B (Figure 3.21). Again the re-crystallisation peak is observed at 522 ºC and, as with the pure flux, two distinct melting points at temperatures lower than that of the pure flux are seen i.e. 810 ºC and 872 ºC. Identical volatilisation of the flux is observed above 1050 ºC.

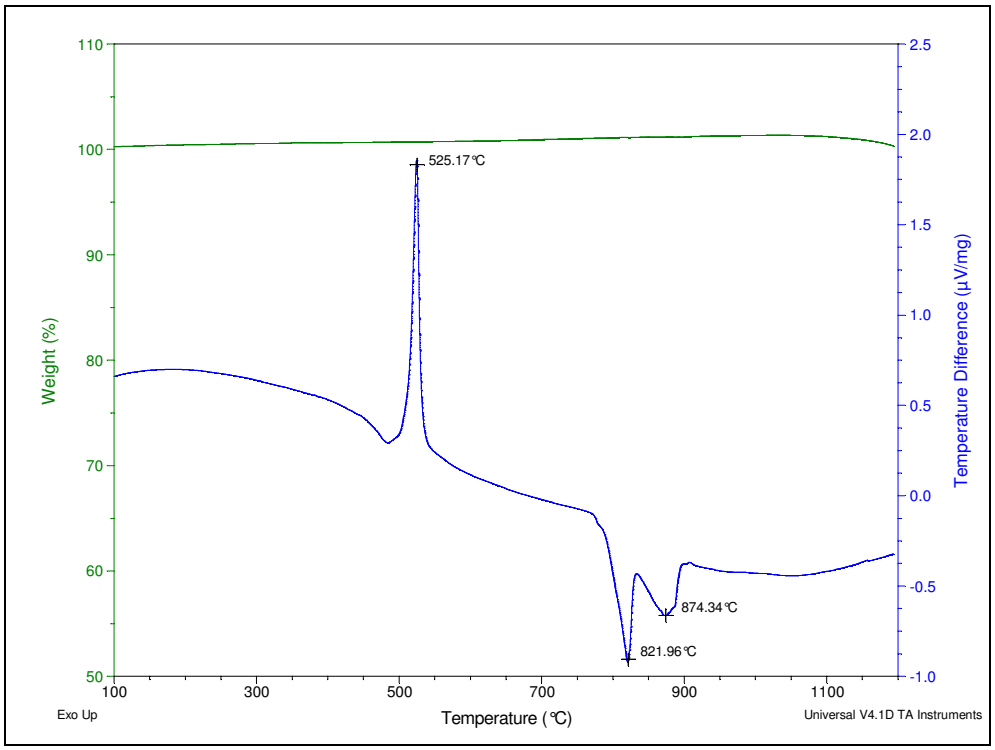

Figure 3.19 DSC-TGA curves for lithium bi-borate with SiO_2

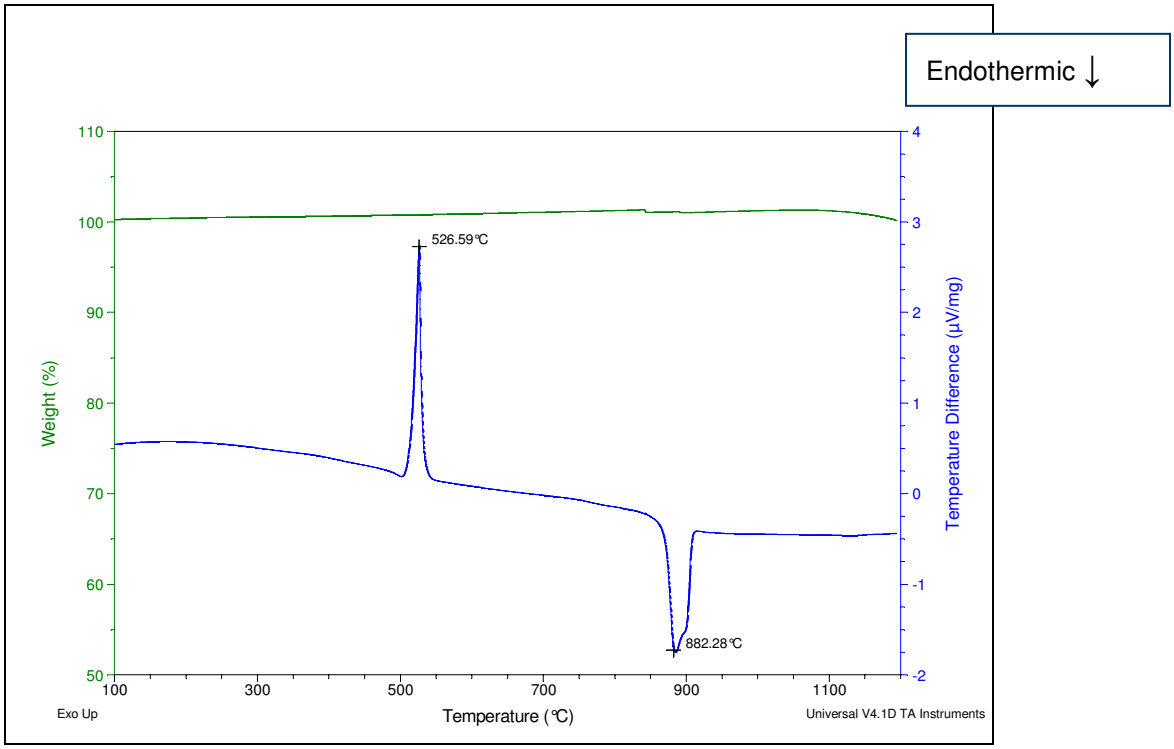

Figure 3.20 DSC-TGA curves for lithium tetraborate with Fe_2O_3

3.1.3.3 ZrO_2 as sample

The TGA curve for ZrO_2 fused with the lithium tetraborate PR0301A is shown in Figure 3.22. As in the previous instances, the exotherm at 526 ºC is indicative of the re-crystallisation reaction and the melting point is seen at 906 ºC. For the bi-borate PR0301B (Figure 3.23), the exothermic re-crystallisation is observed at 526 ºC and the dual melting points at 824 and 880 ºC. A mass loss above 1050 ºC was observed as in the pure flux and previous mixtures implying volatilisation.

3.1.3.4 UP1 as sample

The last example was a mixture of 1g of an in-house reference material UP1, mixed with 6g lithium tetraborate PR0301A (Figure 3.24). The exothermic re-crystallisation peak at 524 ºC is identical to the previous cases, but here a shoulder on the lower temperature side accompanies the melting point endotherm at 884 ºC. This could be interpreted if viewed in the context of the composition of UP1, a granite sample containing quartz (SiO_2), orthoclase ($KAlSi_3O_8$), plagioclase ((Ca, Na) Al $_{1-2}$ Si $_{2-3}$ O_8), orthopyroxene ((Mg, Fe) SiO_3), ilmenite ($FeTiO_3$) and apatite ($Ca_5(PO_4)_3$(F, Cl, OH)) with some hornblende (Ca_2(Mg, Fe, Al)$_5$ (Al, Si)$_8O_{22}(OH)_2$) and biotite (K(Mg,Fe)3AlSi3O10(F,OH)2) present that melts incongruently in the presence of quartz at lower temperatures.

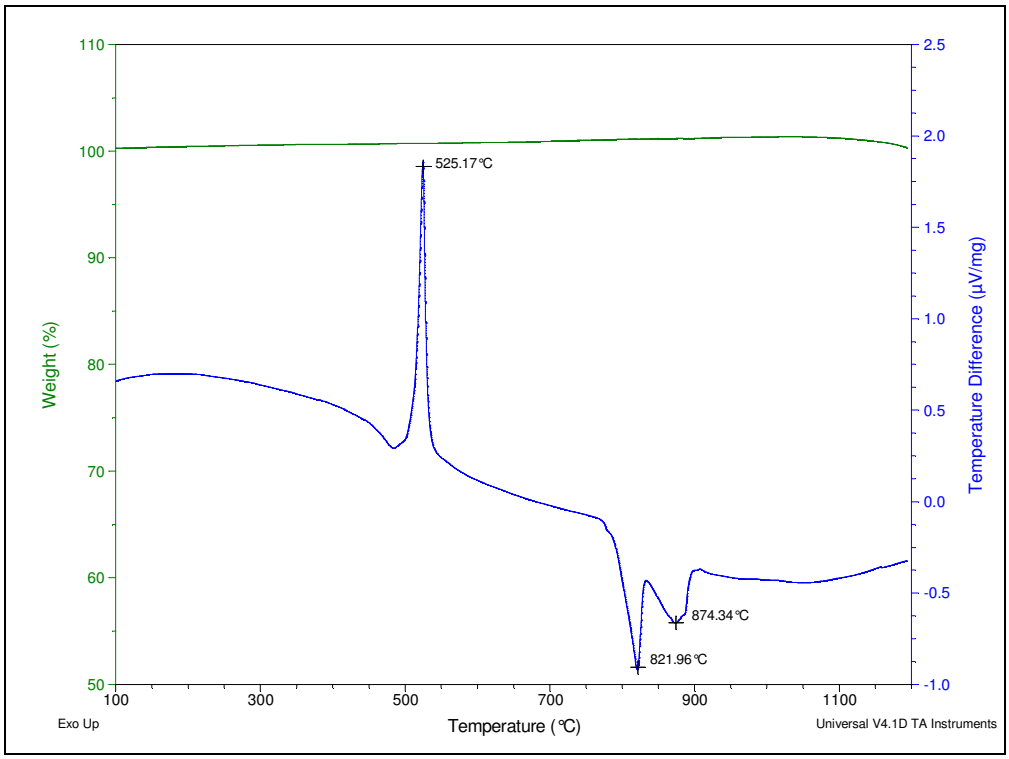

Figure 3.21 DSC-TGA curves for lithium bi-borate with Fe_2O_3

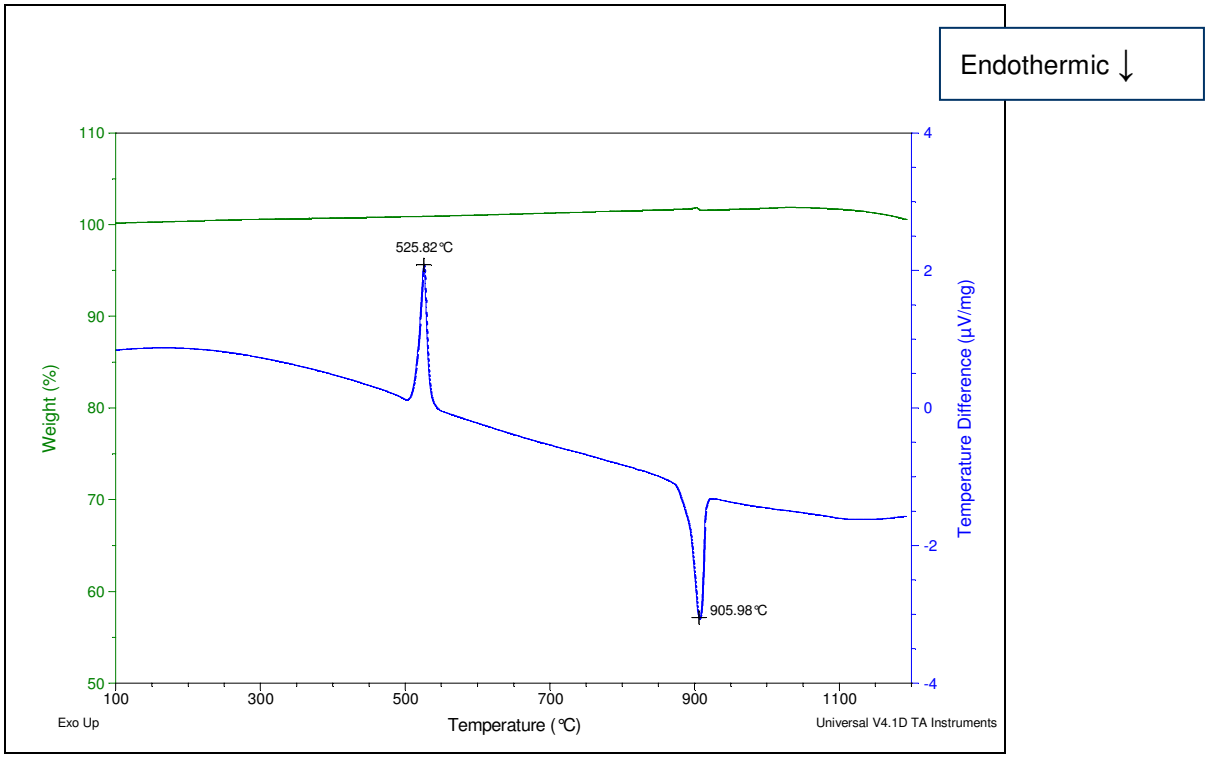

Figure 3.22 DSC-TGA curves for lithium tetraborate with ZrO_2

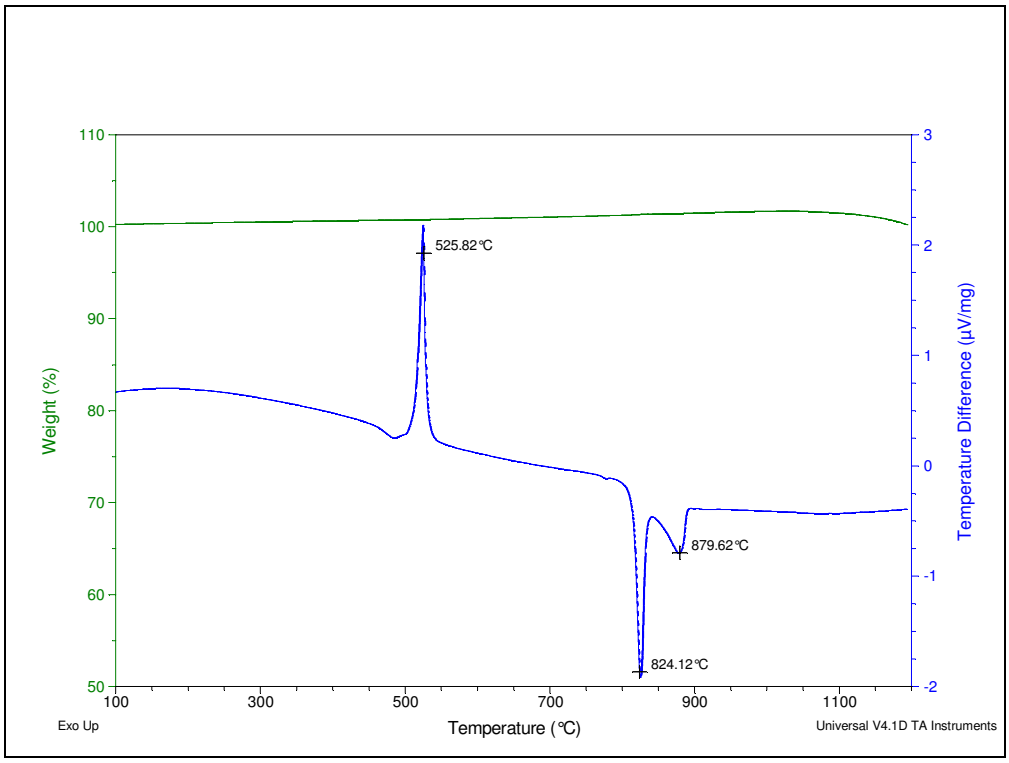

Figure 3.23 DSC-TGA curves for lithium bi-borate with ZrO_2

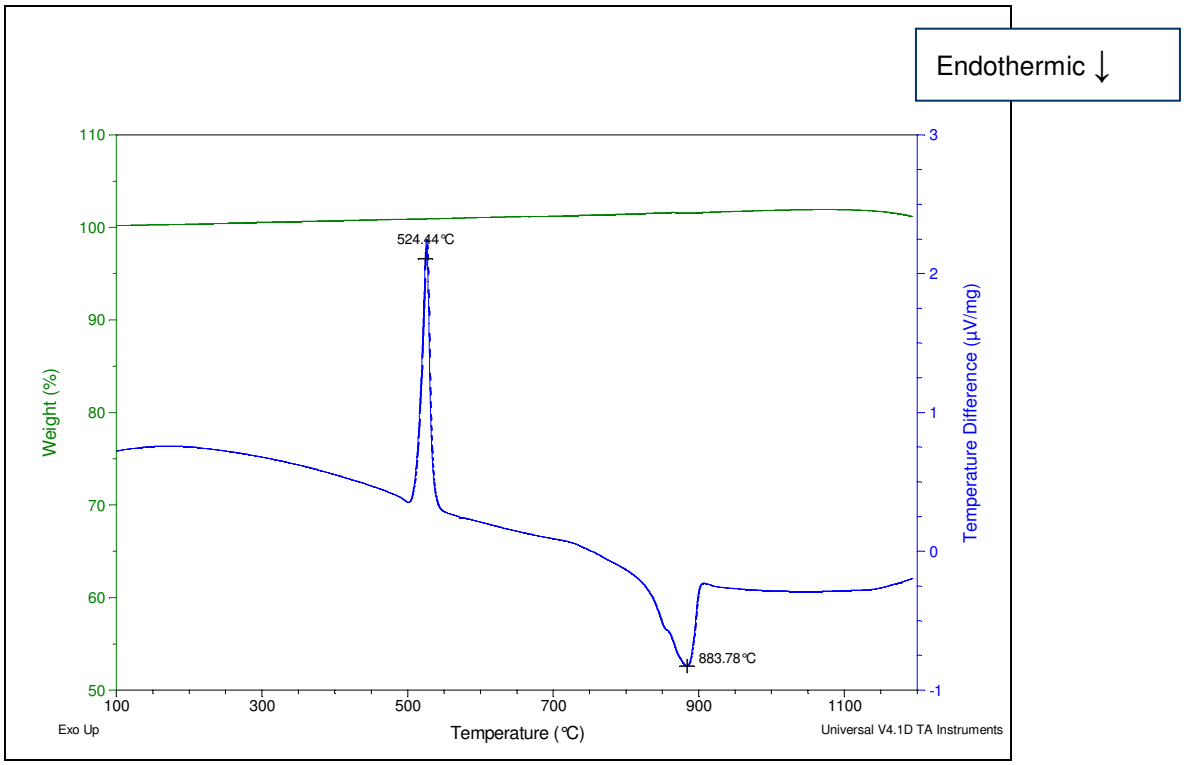

Figure 3.24 DSC-TGA curves for lithium tetraborate with UP1

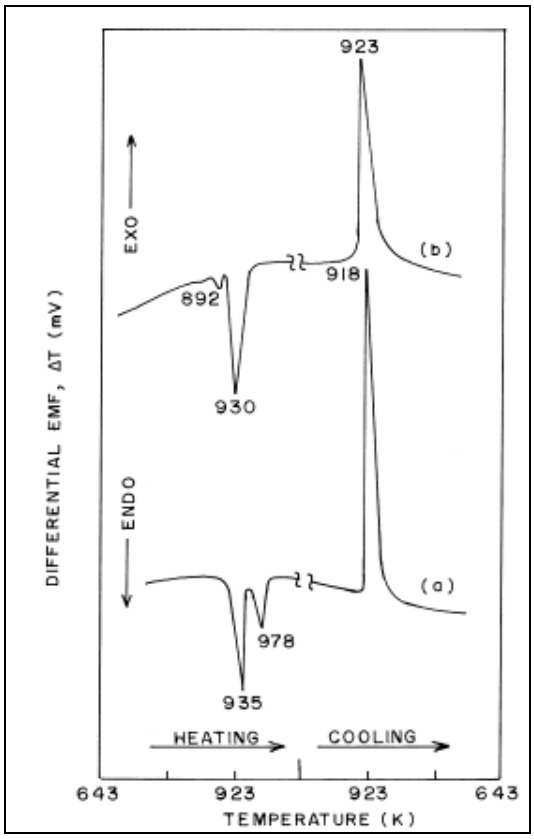

Figure 3.25 DTA curves of (a) $LiBO_2$ and $Li_2B_4O_7$ from Mathews et al.[1]

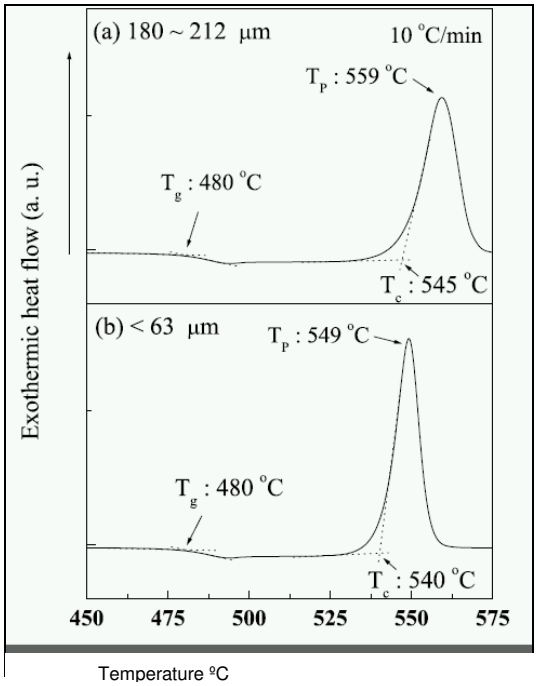

Figure 3.26 DSC curves for heat flow in various sized $Li_2B_4O_7$ particles from Kim et al.[3]

3.2 Discussion of results with relation to published literature

The references found in the literature regarding the use of TGA in the study of lithium borates focussed mostly on the study of these materials for application in surface acoustic wave substrates and non-linear optical devices for frequency conversions in the UV region. Lithium borate glass and glass ceramics are also investigated for use in solid-state battery applications. Mathews et al. published a paper in two parts[1, 2] on the high-temperature behaviour of lithium borates. They reported the stable, ambient temperature, binary Li_2O-B_2O_3 systems as Li_3BO_3, α-$Li_4B_2O_5$, β-$Li_4B_2O_5$, $Li_6B_4O_9$, α-$LiBO_2$, $Li_2B_4O_7$, $Li_3B_7O_{12}$, LiB_3O_5 and $Li_2B_8O_{13}$, of which only α-$LiBO_2$ and $Li_2B_4O_7$ retain their original symmetry up to the liquidus temperatures in air, i.e. they melt congruently. This dispels the claims of the manufacturer of the prototype sample PR0301B, that the sample was a “bi-borate”, consisting of two metaborate units, bound by a bridging oxygen ($Li_4B_6O_{11}$). According to Mathews et al.[1, 2], no such stable phase exists, and in the TGA (Figure 3.16), two distinct melting points were observed, one at 845 ºC, and a smaller one at 902 ºC, implying two distinct phases. This aspect will be further investigated using XRD. The DTA curves obtained in this paper (Figure 3.25), correlated with the congruent melting endotherms observed in all the pure flux samples examined, namely the lithium metaborate congruent melting endotherm at 848 º C and the lithium tetraborate congruent melting endotherm at 915 ºC.

The third paper published citing DSC curves on lithium borates, was that of Kim et

al.[3] who investigated the kinetics of the crystallization process in $Li_2B_4O_7$ glasses (figure 3.26). The glass transition temperature (Tg), crystallisation temperature (Tc), and temperature where the crystallisation rate is at a maximum (Tp), are shown. In the DSC curve of ICPH FLUORE-X® AML 100 (Figure 3.4), two small peaks corresponding to possible exothermic reactions were observed at 434 and 500 ºC. From Kim et al.[157], these could be interpreted as the glass transition temperature at 434 ºC and the re-crystallisation reaction at 500 ºC. The same for the FLUORE-X® 20 sample (Figure 3.7), where a strong re-crystallisation peak was observed at 510 ºC, the slight elevation before the peak could be interpreted as the glass transition temperature. In the present study, the re-crystallisation temperature for pure $Li_2B_4O_7$ was observed around 520 ºC (Figure 3.14) compared to the 550 ºC reported by Kim et al. [3]. It is also evident from Kim et al. that particle size plays a role in the crystallisation temperature, but so does the heating rate. As the experiments in this study were all performed using the same heating rate, though on different instruments, particle size effect differences best explain the slightly different crystallisation temperatures observed (Figures 3.7, 3.13, 3.15 – 3.17, 3.19 - 3.24).

3.3 Conclusion

The most important conclusions drawn from the TGA/DSC study of pure fluxes and flux sample mixtures are that fluxes that were pre-fused during the manufacturing process can be identified using DSC by the exothermic re-crystallisation peak shown around 520 ºC. The very small mass loss shown by these fluxes below

200 ºC in the TGA curves confirms the manufacturers' claim of their reduced hygroscopic nature. This confirms their preferred use in sample preparation as large errors can be introduced by weighing moist flux. The lithium tetraborate and lithium metaborate melting points were in the theoretical ranges, but interestingly, the mixtures with more than 50% lithium tetraborate showed dual melting points, one around 845 ºC and another at 900 ºC, implying the co-existence of species, even after a pre-fusion step. Only the 50:50 lithium tetraborate, lithium metaborate mixture showed an eutectic just above
800 ºC. The proposed "bi-borate" also showed a dual melting point (Figure 3.16) and would thus seem to be a mixture of species rather than a single species. This corresponds to the Li_2O - B_2O_3 phase diagram (Figure 1.1)

From the sample flux mixtures it was observed that the melting point differs from oxide to oxide, but is always lower than the original flux melting point. Where the "bi-borate" was used (Figures 3.19, 3.21 and 3.23), dual melting points were found, but always at lower temperatures than the original flux. From this we can conclude that normal melting point suppression due to mixing occurs.

Probably the most important result was the volatilisation of flux above 1050 ºC. From these results it is strongly recommended that fusion temperatures for lithium borate fluxes do not exceed 1050 ºC. Higher temperatures (e.g. 1230 ºC) inevitably lead to the loss of flux. Depending on the flux type, such volatilisation was found to vary from 2% to 6% per hour (Figure 3.12). The effect of network formers like SiO_2

or network modifiers like Mg, Na and K on this volatilisation will have to be evaluated as the presence of more network formers will likely stabilise the melt structure, increase the viscosity and decrease volatilisation. This could not be confirmed in this study though, as even in the case of ZrO_2 and lithium borate flux (Figure 3.22), a mass loss was observed. The danger lies particularly in fusing relatively insoluble materials, for long times at elevated temperatures in an attempt to achieve complete dissolution. But even so, the presence of network formers and/or network modifiers might still affect the rate of volatilisation.

Constant rates of volatilisation, which have to be evaluated for every flux type, can be accommodated in laboratory sample preparation techniques if time schemes for the fusion steps are strictly adhered to and temperatures of fusion are rigorously controlled.

REFERENCES:

1. Mathews, M.D., Tyagi, A.K. and Moorthy, P.N. High-temperature behaviour of lithium borates: Part I: Characterization and thermal stability. *Thermochimica Acta*. **320,** 89-95 (1998).
2. Mathews, M.D., Tyagi, A.K. and Moorthy, P.N. High-temperature behaviour of lithium borates: Part II: High-temperature X-ray diffractometric and dilatometric studies. *Thermochimica Acta*. **319,** 113-121 (1998).
3. Kim, S.J., Kim, J.E., Rim, Y.H. and Yang, Y.S. Kinetics of non-isothermal crystallization process in various sized Li2B4O7 glasses. *Solid State Communications*. **131**, 129-133 (2004).

CHAPTER 4: X-RAY POWDER DIFFRACTOMETRY STUDY OF LITHIUM BORATE FLUX MIXTURES

After analysing the TGA/DSC data it is necessary to try to understand the transitions or reactions observed in the DSC scans. To accomplish this, X-ray powder diffraction (XRD) techniques were used to study the crystalline materials and to investigate any possible phase transitions below the melting point of the fluxes.

4.1 Experimental results

The fluxes were dried at 110 ºC to remove any absorbed moisture and analysed by XRD between 3 and 70 degrees 2θ.

4.1.1 Pure fluxes

As a starting point three of the ICPH fluxes were analysed: FLUORE-X®ATL 100 (lithium tetraborate), FLUORE-X®AML 100 (lithium metaborate) and FLUORE-X®20 (20% lithium tetraborate with 80% lithium metaborate). Figure 4.1 shows the diffractograms. All three fluxes were supposedly pre-fused during the manufacturing process. Only the 80:20 mixture showed an amorphous diffractogram with the other two being clearly crystalline as reflected by the identification of tetragonal lithium

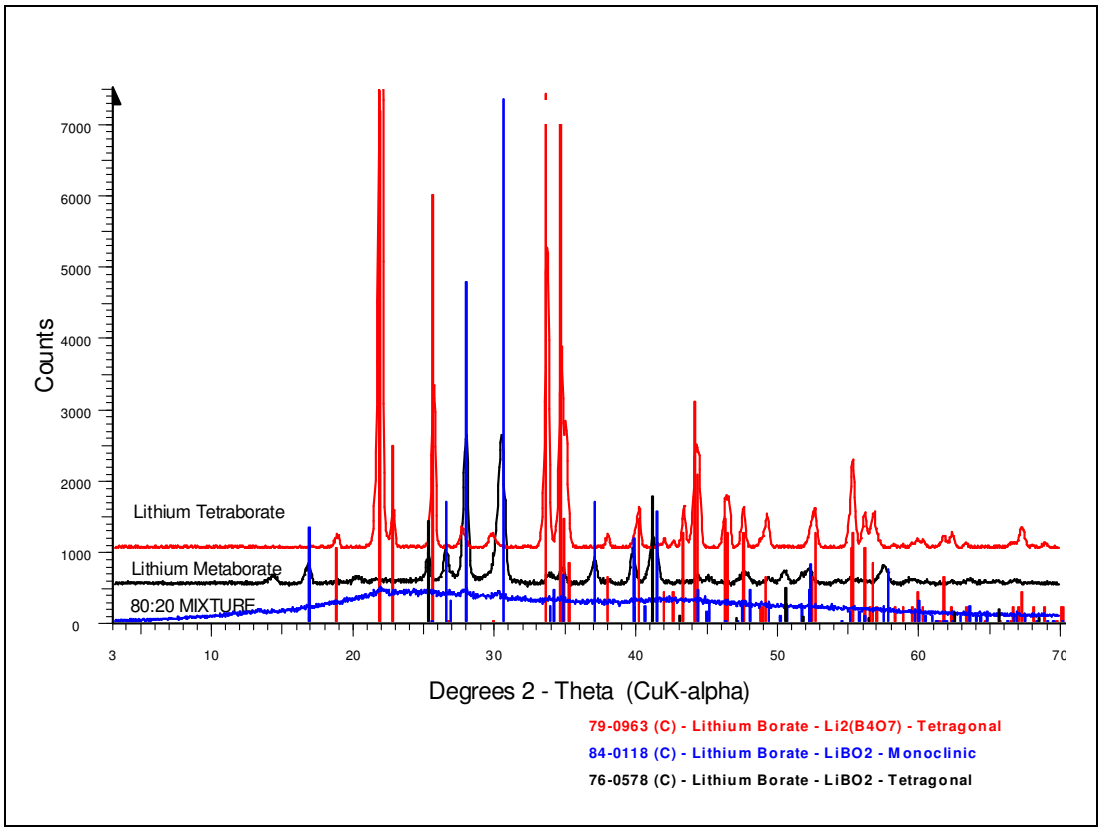

Figure 4.1 X-ray diffraction patterns of three flux compositions investigated

tetraborate (79-0963(C)) [1] in the ATL100 and both monoclinic (84-0118(C)) [1] and tetragonal (76-0578(C)) [1] lithium metaborate in the AML100. This corresponded with the TGA/DSC results where, only in the case of the FLUORE-X®20 (Figure 3.7), an exothermic re-crystallisation reaction was observed around 520 ºC.

The heat-treated samples described in Table 2.2 were also analysed. For the lithium tetraborate (FLUORE-X®ATL 100), the samples reacted above 920 ºC were clearly stable glasses and consequently were not analysed. Two samples were analysed namely those that were reacted at 500 and 850 ºC (Figure 4.2). Tetragonal lithium

tetraborate (79-0963 (C))[1] was observed in both, with the exception of a peak at d=3.221Å that could not be identified and was not evident at the higher temperature. The peak positions for lithium metaborate (84-0118(C))[1] were indicated in the figure to test the possibility of the d=3.221Å peak being lithium metaborate. Scanning Electron Microscopy photographs were taken (Figures 4.3 and 4.4), and from these it can be seen that some physical changes occurred in the flux as the melting point was approached, which may be indicative that atoms start to re-arrange before the melting point is reached.

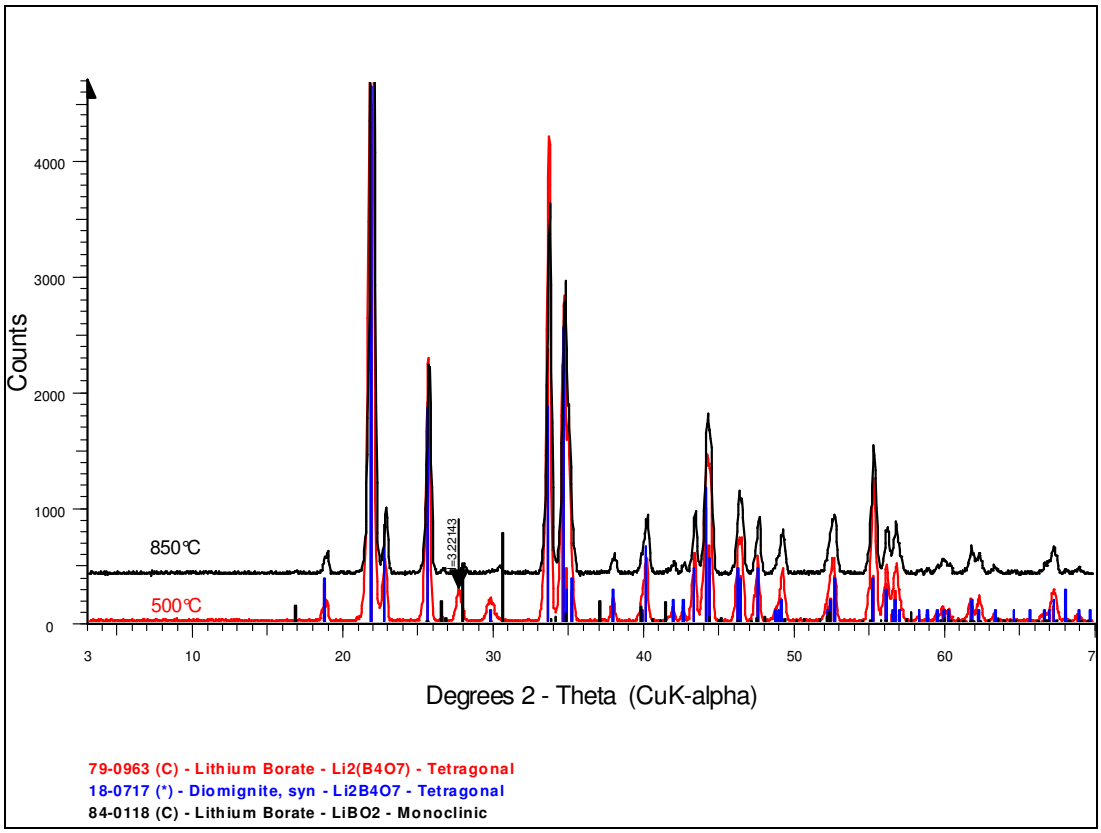

Figure 4.2 X-ray diffraction patterns of lithium tetraborate

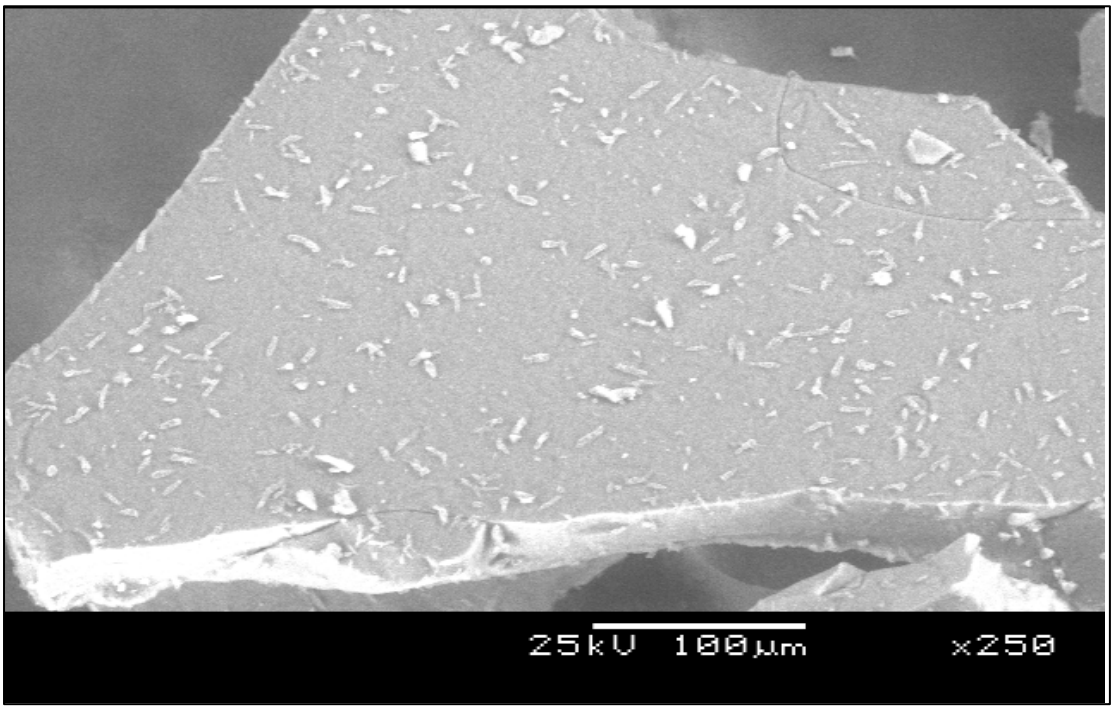

Figure 4.3 Scanning electron micrograph photo of lithium tetraborate treated at 500 ℃

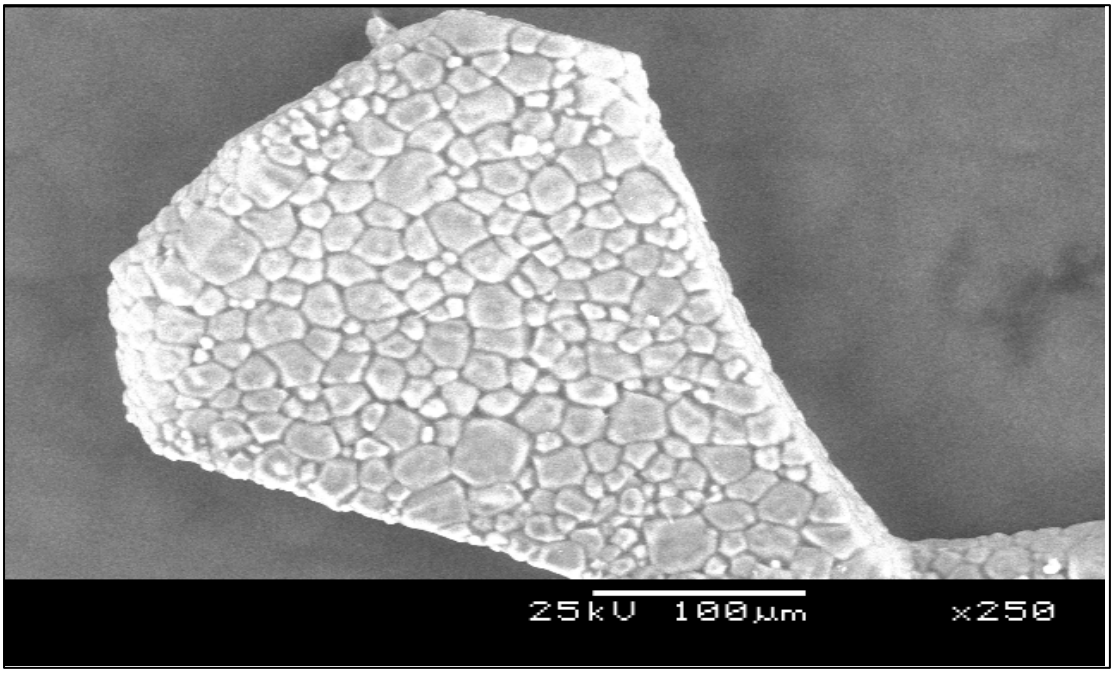

Figure 4.4 Scanning electron micrograph photo of lithium tetraborate treated at 850 ℃

For the lithium metaborate (FLUORE-X®AML 100), the TGA/DSC curves showed more features that could be indicative of endothermic reactions. Consequently more samples were prepared at different temperatures before analysing using XRD. These are represented in Figure 4.5. The phases identified were monoclinic lithium metaborate (84-0118(C))[1] recognised at all temperatures and tetragonal lithium metaborate (76-0578 (C))[1], whose peaks disappeared above 720 ºC. Even samples prepared above the melting temperature of the flux, crystallised on cooling so powder diffraction was possible. The material treated above the melting temperature crystallised only the monoclinic phase. In the low temperature diffractograms, 320 ºC, 440 ºC and 520 ºC, additional peaks were observed at 14 º2θ and 20.5 º2θ. These peaks disappeared at higher temperatures and could not be identified. Their disappearance above 700 ºC corresponds with the small endothermic reaction that was observed in the DSC curve (Figure 3.4).

The third flux investigated was the 20% lithium tetraborate with 80% lithium metaborate mixture (FLUORE-X®20), represented in Figure 4.6. Although all these fluxes were supposedly pre-fused during the manufacturing process, only this one showed an amorphous diffractogram after drying. After heat treatment at 540 ºC the sample was crystalline and the diffractogram corresponded to the exothermic crystallisation product observed in the DSC curve (Figure 3.7). Tetragonal lithium tetraborate (79-0963 (C))[1] was observed as well as tetragonal lithium metaborate (76-0578(C))[1]. Another phase was present inferred to be monoclinic lithium

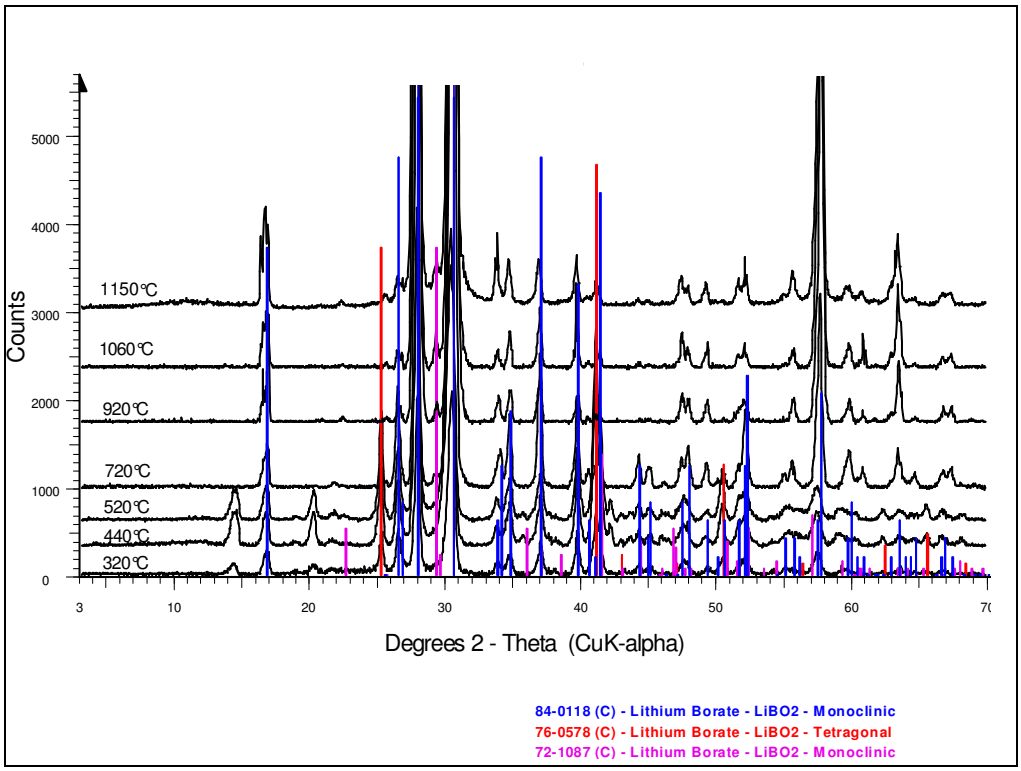

Figure 4.5 **X-ray diffraction patterns of lithium metaborate**

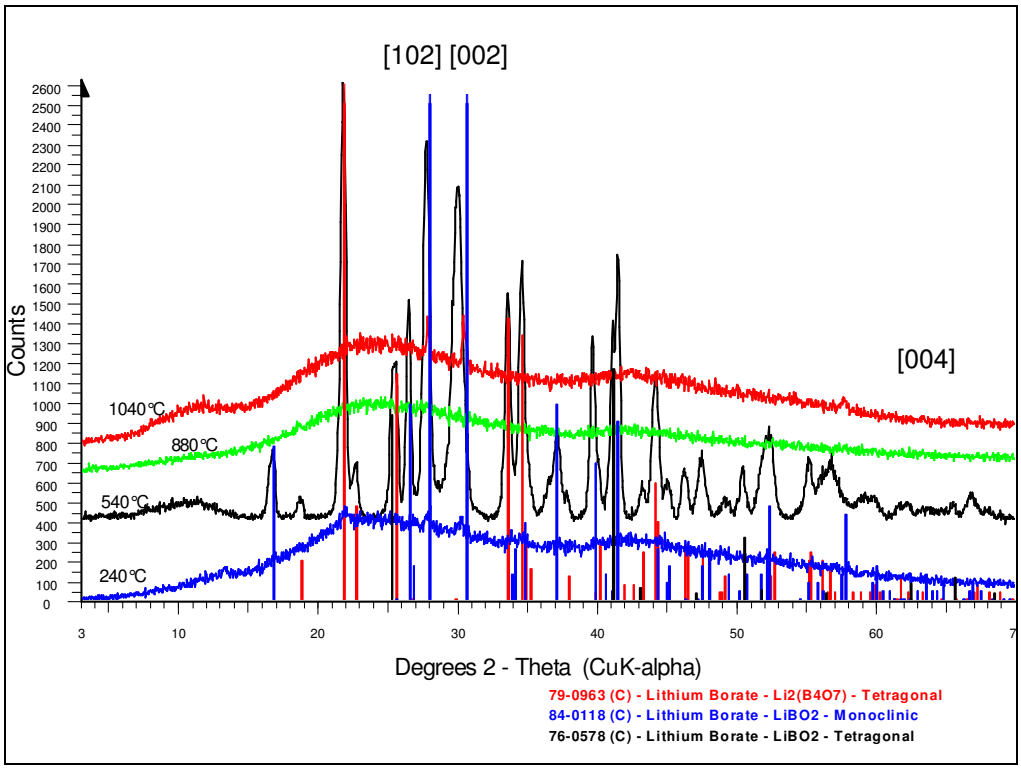

Figure 4.6 **X-ray diffraction patterns of 20% lithium tetraborate with 80% lithium metaborate**

metaborate (84-0118(C))[1], (peak positions indicated on the figure) although the peaks did not fit exactly. Some definite peak shifts were observed. Bragg peaks for the Miller indices (102) and (002) shifted towards high angle, but the intensity of the (004) peak was too low to confirm possible shift of this peak as well. Above the melting point at 838 ºC according to DSC curve, the sample quenched to an amorphous glass.

4.1.2 New flux prototype

The inclusion of a new flux prototype in this study was discussed in section 3.1.2. The advantage of pre-fused fluxes was previously discussed in section 3.1.1. Extensive use of pre-fused fluxes has permitted the recognition that with sudden temperature increases during fusions, the flux can “explode” out of the platinum crucibles with resultant loss of flux and sample material, leading to erroneous results. A postulated reason for this is that residual strains in the pre-fused flux have resulted in the explosive reaction on fast heating. ICPH came up with a solution for the problem in that they included microcrystalline particles into the flux mixture, which served to block the propagation of the micro fissures and prevent the explosive reaction.

The first submitted prototype PR0301A was reported to be amorphous lithium tetraborate glass with microcrystalline particles included, represented in Figure 4.7.

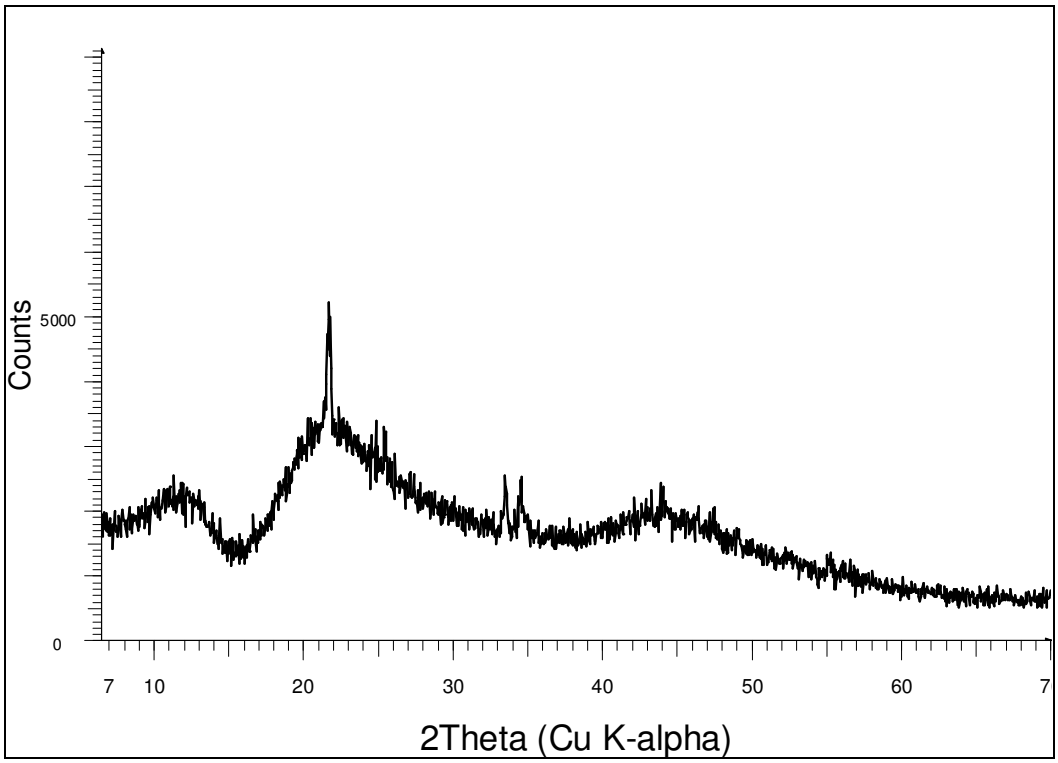

Figure 4.7 X-ray diffraction pattern of lithium tetraborate prototype (PR0301A)

After heating to 600 ºC, the re-crystallisation reaction occurred as seen in the DSC curves (Figure 3.15), and a crystalline structure is revealed. Tetragonal lithium tetraborate (79-0963 (C))[1], is the only phase present (Figure 4.8). Figure 4.9 shows X-ray diffraction patterns at room temperature of lithium tetraborate for the glass state and crystalline phase with a few Miller indices of some large Bragg peaks indexed from a paper by Kim et al.[3]. Comparison of these with Figure 4.8, they are almost identical. The XRD analysis verifies the claim of the manufacturer regarding the included crystalline particles as well as the pre-fusion step. Figure 4.10 shows a Transmission Electron Microscope picture also confirming the amorphous and crystalline nature of the flux.

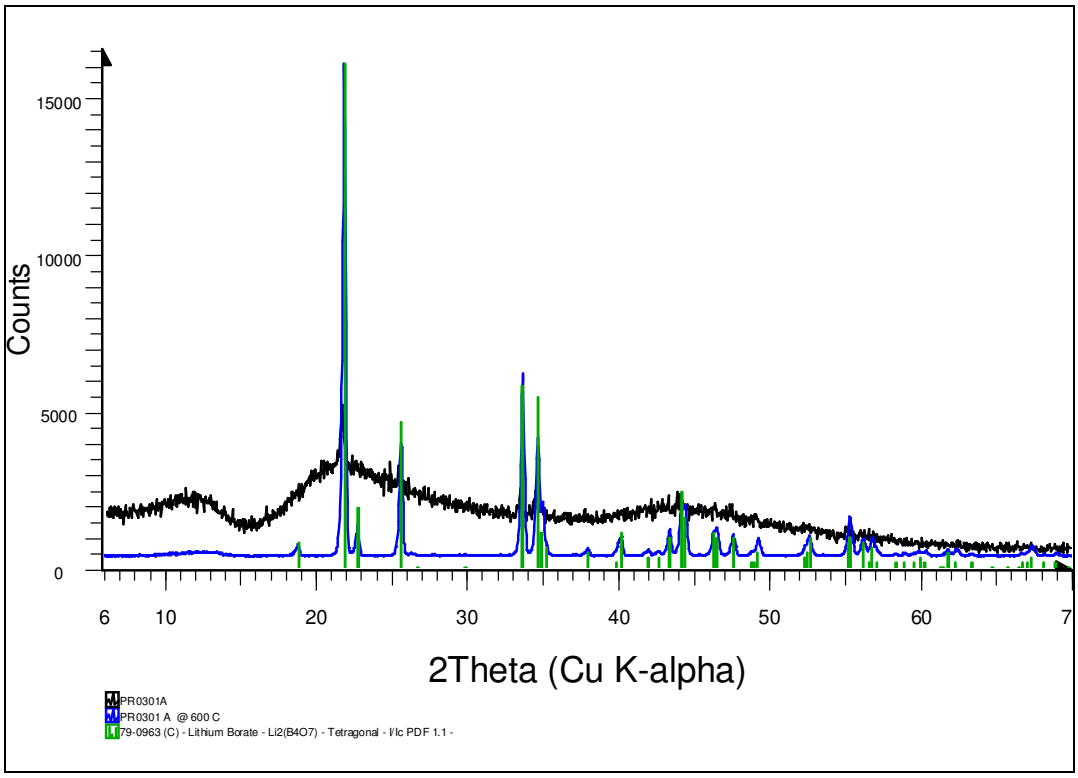

Figure 4.8 **X-ray diffraction patterns of PR0301A after heating to 600 ºC**

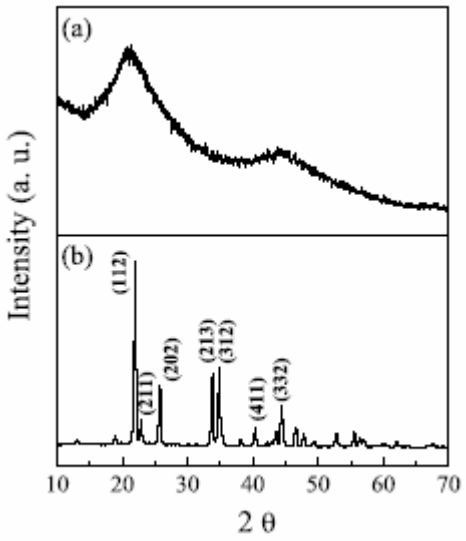

Figure 4.9 **X-ray diffraction patterns of $Li_2B_4O_7$ for (a) the glass phase and (b) the crystalline phase[3]**

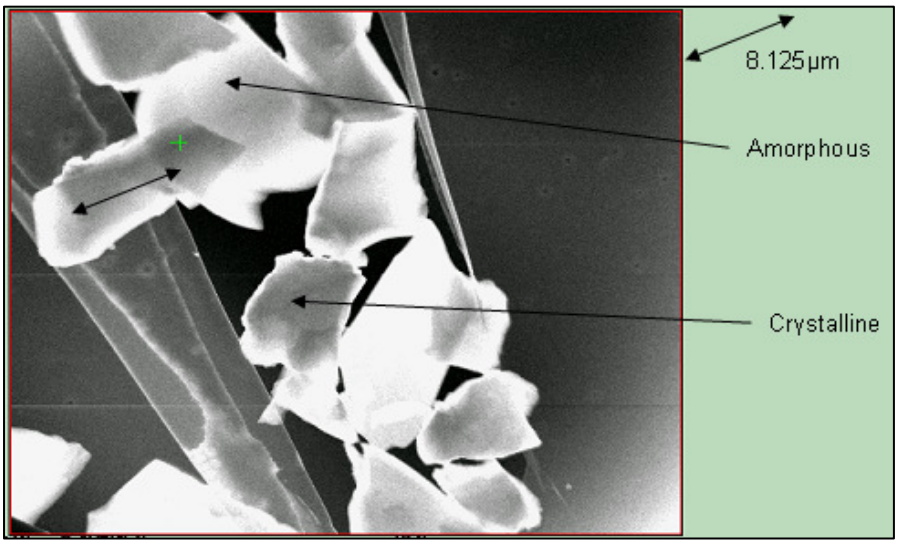

Figure 4.10 Transmission electron microscope picture of lithium tetraborate prototype PR0301A

PR0301B was reported to be a biborate with B_2O_3/LiO ratio 1.5, presented in Figure 3.14. The XRD confirms that the flux is amorphous with crystalline particles, Figure 4.11, but after heating to 600 ºC the phases revealed are lithium tetraborate (79-0963 (C))[1] with additional "shifted" monoclinic lithium metaborate peaks (84-0118(C))[1], see Figure 4.12. Again, as with the lithium metaborate, the tetragonal phase is not present. This is additional evidence that it is a low-temperature phase. In this case there was no corresponding reaction on the DSC curve (Figure 3.16) The shifted peaks could be explained by change in the dimensions of the unit cell. The two distinct phases present correspond with the dual melting point observed in the TGA Figure 3.16

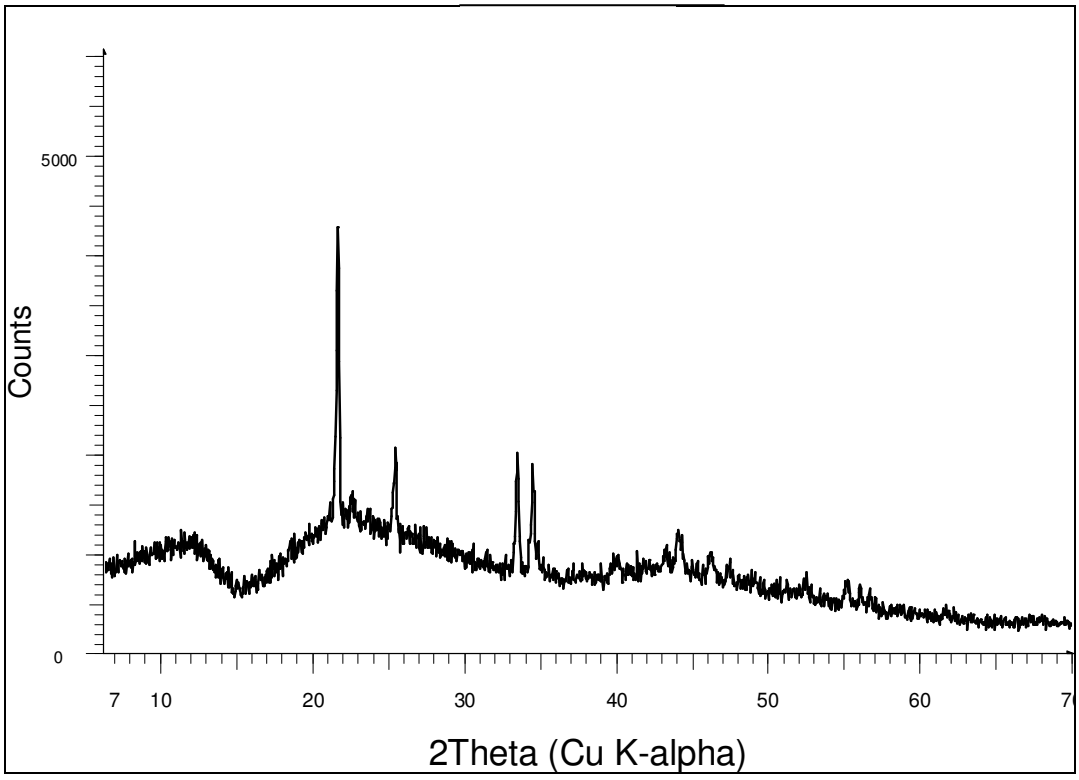

Figure 4.11 X-ray diffractogram of lithium bi-borate prototype (PR0301B)

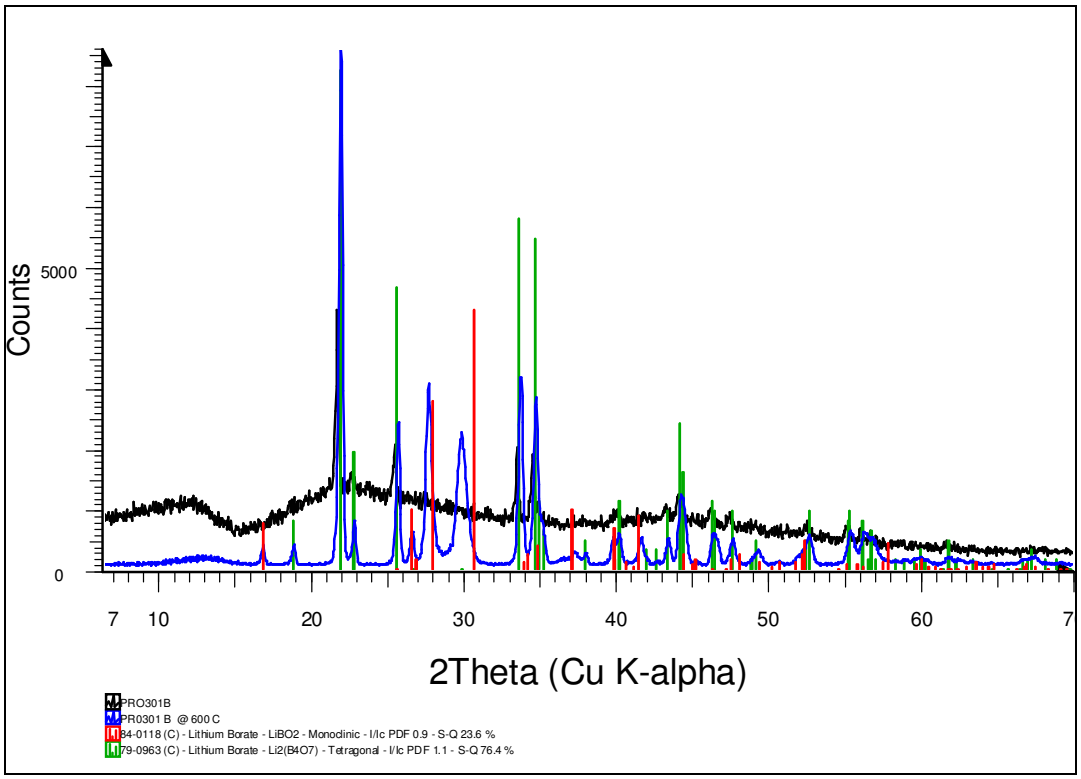

Figure 4.12 X-ray diffractogram of PR0301B after heating

4.1.3 In situ measurements

It is important to keep in mind that the purpose of this study is the investigation of reactions occurring in a flux during the fusion process. Concern exists regarding the legitimacy of data collected on samples prepared in a muffle furnace and then annealed. To validate the previous results for in situ applications some samples were analysed using a heating chamber to collect diffractograms at temperature.

Figures 4.13 to 4.16 represents diffractograms of pure lithium borate fluxes heated from 25 ºC to melting point and with data recorded at selected temperatures. Data was collected in the range 15<2θ<70º, but only that collected in the range 15<2θ<40º is represented here because the platinum peaks from the sample holder obscures detail above 40 º2θ that falls in the vicinity of the Pt peaks.

Figure 4.13 represents diffractograms of a pure lithium tetraborate flux FLUORE-X®ATL 100, heated from 25 ºC to 960 ºC, with data recorded at 60, 140, 260, 380, 560, 680, 740 and 960 ºC and again at 25 ºC after cooling. For the steps below the melting point (<920 ºC) the only phase observed was tetragonal lithium tetraborate (79-0963 (C)) [1], as in Figure 4.2. No additional, unidentifiable peaks were observed in the in situ experiment. The dataset collected at 960 ºC shows an amorphous glass. The dataset recorded after cooling, show small peaks at 19, 22.5, 30, 34.5 and 34.5 º2θ that are not characteristic of lithium tetraborate or lithium metaborate patterns, tetragonal or monoclinic. These could not be identified at this stage and

further work will have to be done including quench experiments.

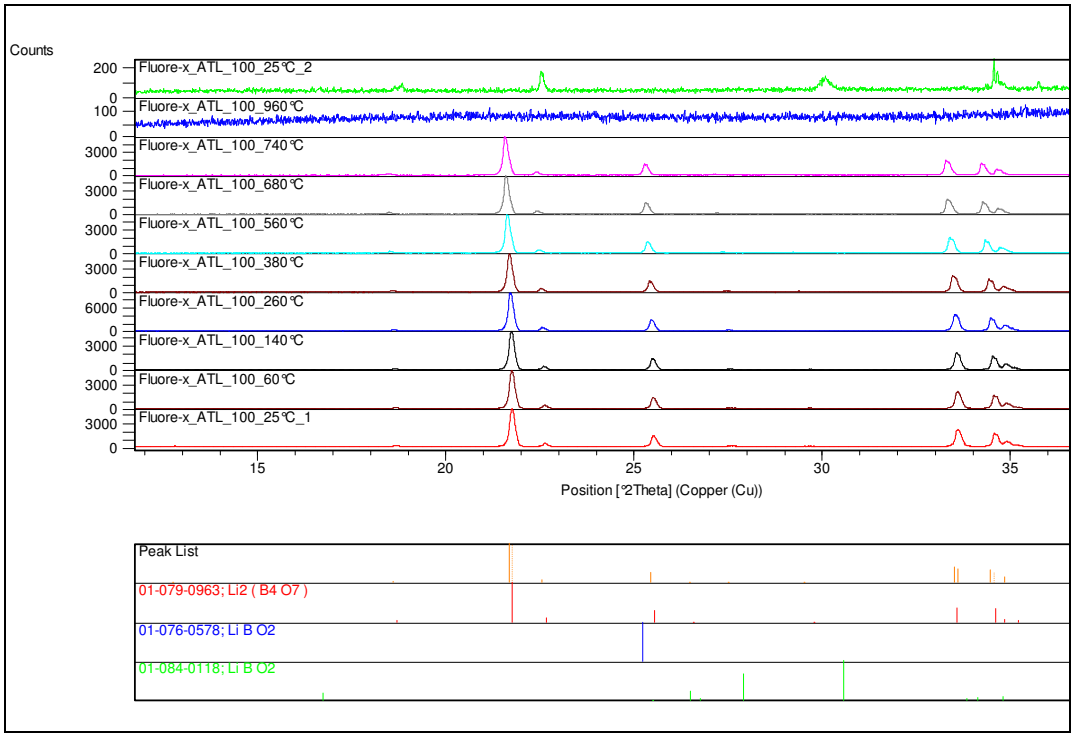

Figure 4.13 X-ray diffractograms collected using a heating chamber of lithium tetraborate

When doing this run, the flux melted over the Pt strip and electrodes causing damage, so future experiments were executed to temperatures below the melting range.

Figure 4.14 represents diffractograms of the reacted and quenched specimen of the 20% lithium tetraborate with 80% lithium metaborate mixture (FLUORE-X®20) as presented in Figure 4.6. The material was heated from 25 ºC to 800 ºC, collecting data at 25, 97, 187, 287, 389, 489, 589 and 689 ºC. After an equilibrium period a second spectrum was obtained at 689 ºC. An amorphous diffractogram was observed below the temperature of re-crystallisation. At 489 ºC, slightly lower than

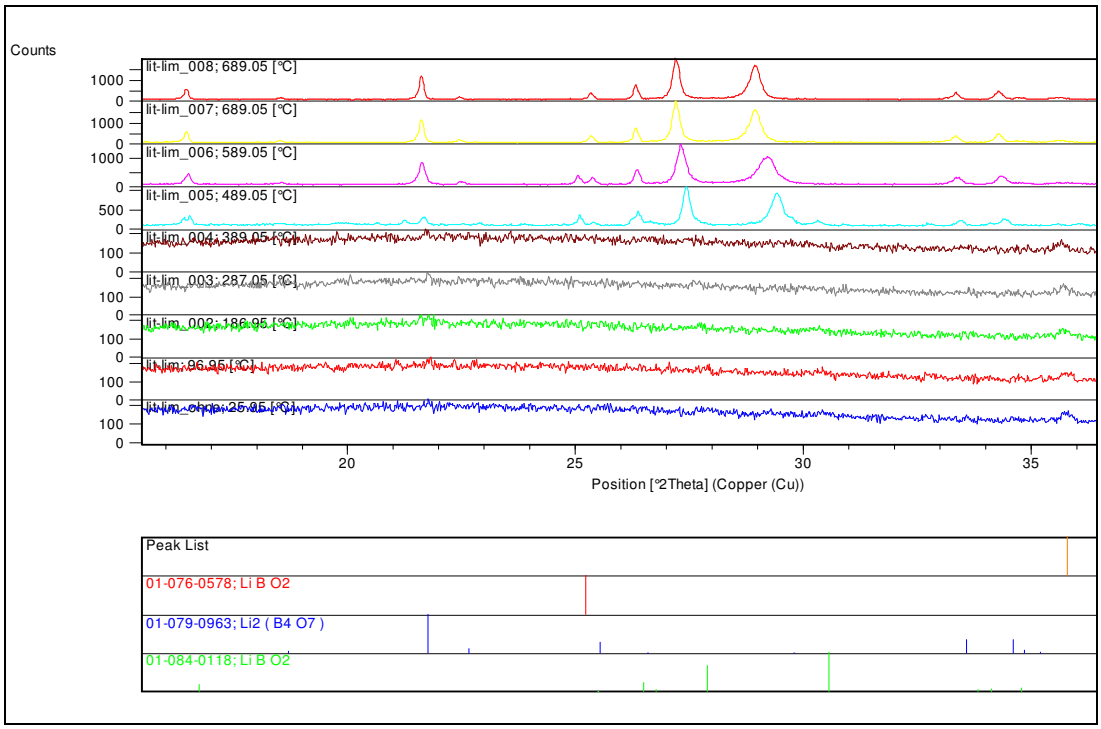

Figure 4.14 **X-ray diffractograms collected using a heating chamber of 20% lithium tetraborate with 80% lithium metaborate mixture (FLUORE-X®20)**

the 540 ºC previously used, a crystalline structure was recognised – corresponding to the exothermic re-crystallisation reaction observed in the DSC curve (Figure 3.7). Tetragonal lithium tetraborate (79-0963 (C))[1] was observed as well as tetragonal lithium metaborate (76-0578(C))[1]. As in Figure 4.6, two peaks observed at 27.5 and 29 º2θ, did not fit the monoclinic lithium metaborate (84-0118(C))[1] pattern exactly, but showed slight displacement. This serves as confirmation that the displaced peaks observed in Figure 4.6 were not quenching phenomena, but a property inherent to the flux and indicative of a change in the unit cell parameters.

The two prototype samples discussed in section 4.1.2 were also reanalysed in situ; See Figures 4.15 and 4.16. The samples were heated from 25 ºC to 800 ºC,

collecting data at temperature intervals. The lithium tetraborate (PR0301A) spectra were collected at 25, 96, 188, 289, 389, 490, 591, 691, and 794 ºC. The diffraction patterns were identical to the original sample in Figure 4.8 with the exception that this sample was pre-heated and did not start off as an amorphous glass. The peaks all fitted lithium tetraborate (79-0963 (C))[1]. Data for PR0301B, the reported bi-borate with B_2O_3/LiO ratio 1.5, see Figure 3.14, was recorded at 97, 187, 288, 389, 490, 591 and 690 ºC and showed an amorphous pattern with small crystalline particles, as in Figure 4.11. After heating to 490 ºC lithium tetraborate (79-0963 (C))[1], numerous phases are revealed, but fewer than observed in Figure 4.12. The peaks at 19 º2θ, 22 º2θ and 23 º2θ are missing (Figure 4.12). These peaks were previously ascribed to tetragonal lithium tetraborate (79-0963 (C))[1], and did not appear when re-crystallised in situ. Peaks at 27 º2θ and 29 º2θ resemble the displaced lithium metaborate peaks (84-0118(C))[1].

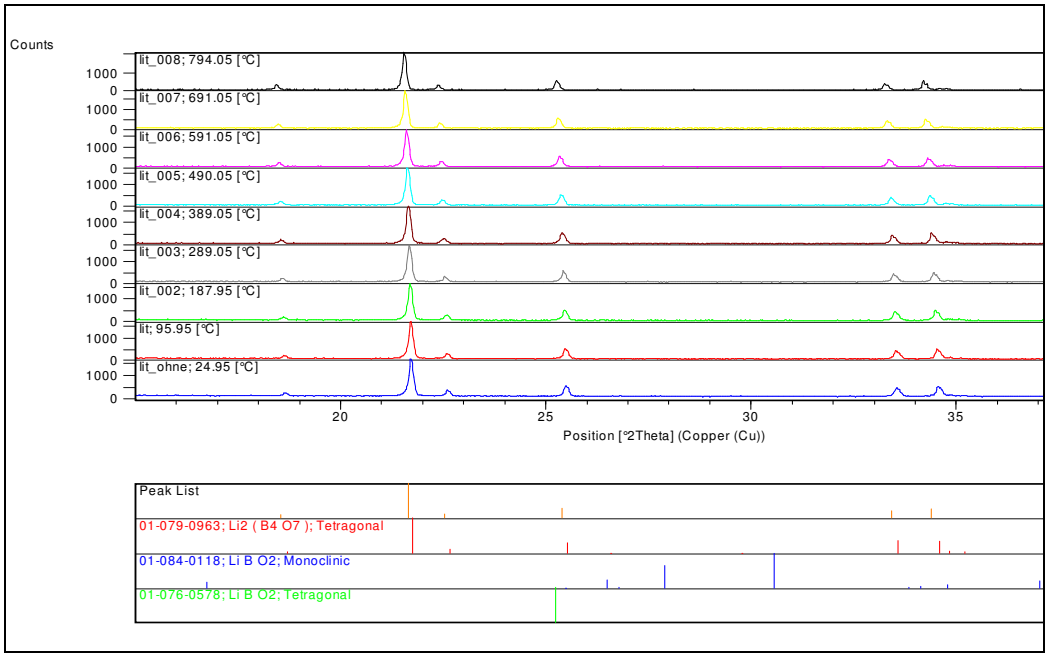

Figure 4.15 X-ray diffractograms collected using a heating chamber of lithium tetraborate prototype (PR0301A)

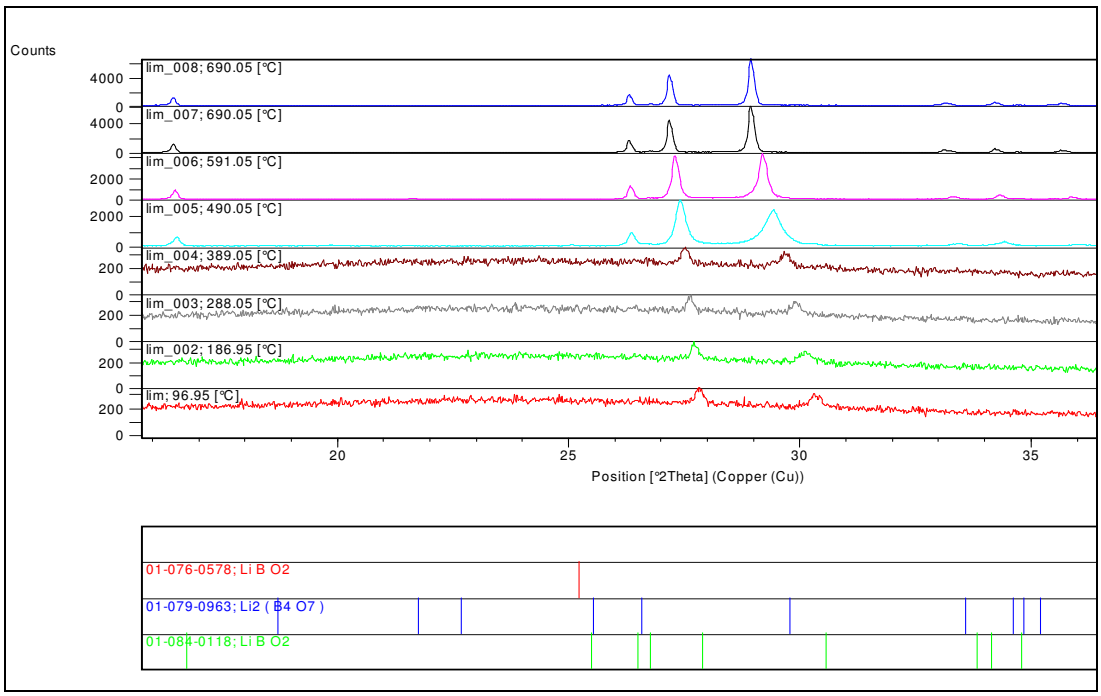

Figure 4.16 **X-ray diffractograms collected using a heating chamber of lithium bi-borate prototype (PR0301B)**

4.1.4 Sample/flux mixtures

As the purpose of this study is ultimately the study of the production of fused glass beads of sample flux mixtures, some pure oxide/flux mixtures were investigated using the in situ heating stage to see whether the diffraction patterns could elucidate any possible phase changes around the melting temperature and provide information regarding the method in which flux and sample interact. The samples were prepared using pure oxides mixed with lithium tetraborate in the same ratio used in routine fusions, i.e.1g sample and 6g flux for most oxides but 1g sample and 9g flux for ZrO_2 and 0.5g sample and 9g flux for Cr_2O_3. After milling together to ensure thorough mixing, a small amount was placed by pipette onto the platinum

strip and heated on the heating stage from 25 to 825 ºC with data collected every 100 ºC. Care was taken to remain below the melting temperature of the flux to protect the electrodes from damage by molten flux flowing off the platinum strip and over the electrodes.

4.1.4.1 SiO_2

The first experiment was performed using pure quartz (SiO_2) mixed with lithium tetraborate. Data was collected at 25, 200, 400, 500, 600, 800, 825 ºC and again, once cooled down to 25 ºC. Figure 4.17 represents the results. Two phases are clearly distinguished, lithium tetraborate (79-0963 (C))[1] and quartz (01-083-0539)[1], which is seen throughout the temperature gradient with the only change being the relative intensities of certain lithium borate versus quartz peaks, particularly the two peaks at 29.5 º2θ and 31 º2θ. The cooled spectrum is identical to the original apart from the abovementioned intensity ratios.

4.1.4.2 Fe_2O_3

For a hematite (Fe_2O_3) flux mixture, data was also collected at 25, 200, 400, 500, 600, 800 and 825 ºC. The phases identified in Figure 4.18 are hematite (01-08900598)[1] and lithium tetraborate (79-0963 (C))[1], with no changes occurring over the heating gradient, which, as for quartz, ends below the melting temperature of the flux.

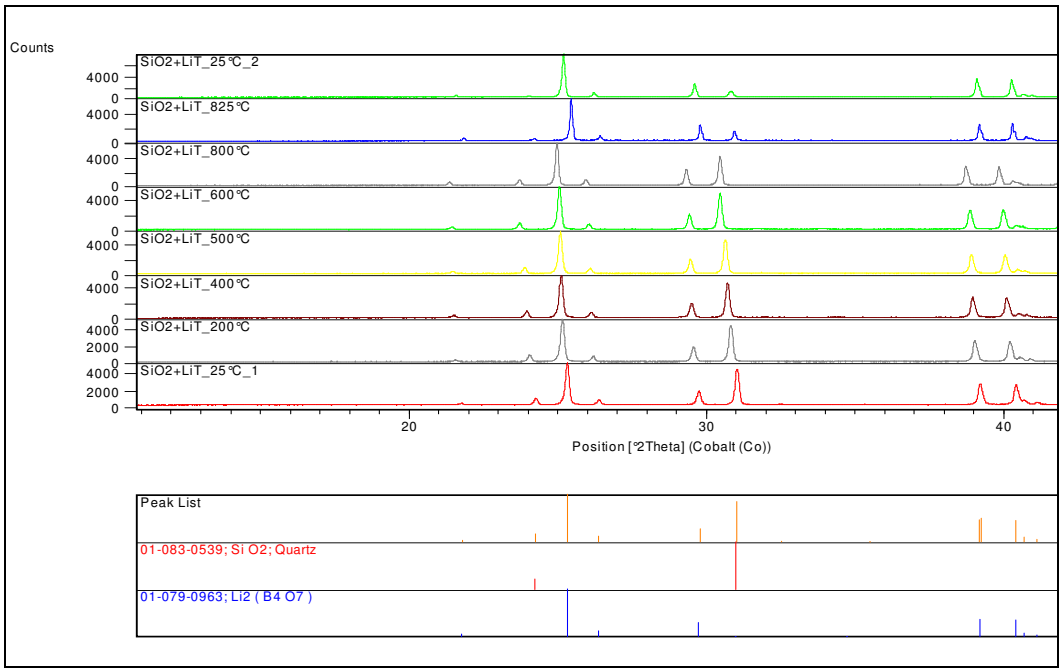

Figure 4.17 **X-ray diffractograms collected using a heating chamber of SiO_2 and flux mixture**

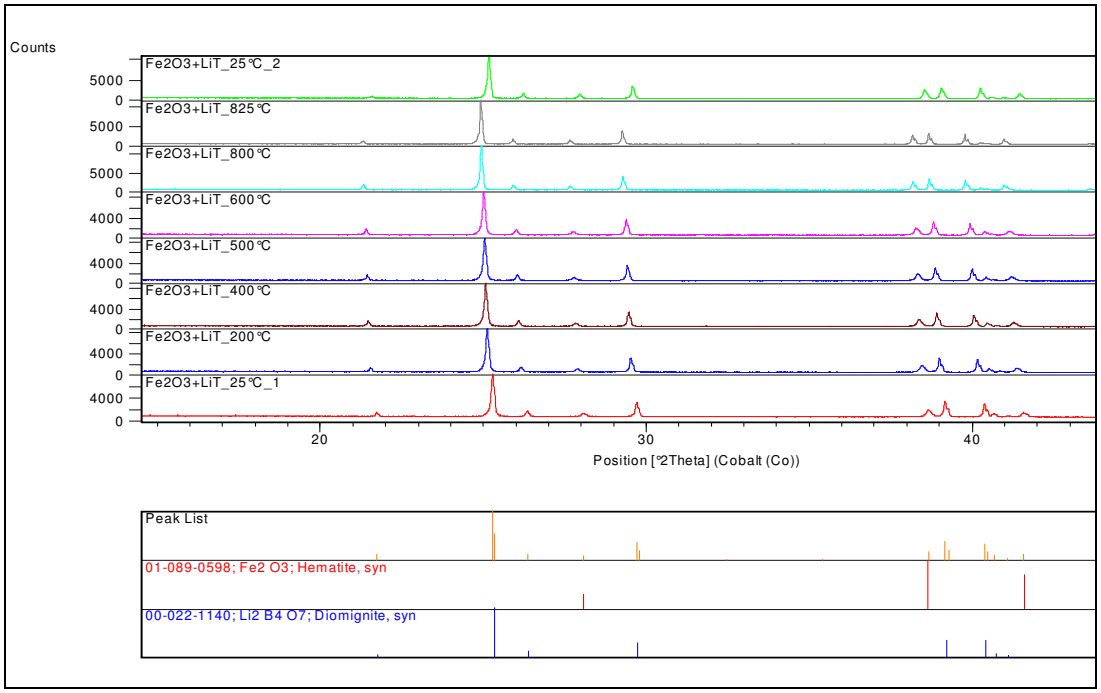

Figure 4.18 **X-ray diffractograms collected using a heating chamber of Fe_2O_3 and flux mixture**

4.1.4.3 ZrO_2

Figure 4.19 represents data collected at 25, 200, 400, 500, 600, 800 and 825 ºC on a mixture of 1g ZrO_2 and 9g lithium tetraborate. A higher sample/flux ratio is used for ZrO_2 as it is difficult to dissolve in flux. The phases identified were Baddeleyite (00-037-1484)[1] and lithium tetraborate (79-0963 (C))[1], with no changes occurring over the heating gradient, which, as for SiO_2, ends below the melting temperature of the flux.

4.1.4.4 Cr_2O_3

The last in this series was a mixture of 0.5g Cr_2O_3 and 9g lithium tetraborate, with data collected at 25, 200, 400, 500, 600, 800 and 825 ºC (Figure 4.20). The phases identified were Cr_2O_3 (00-006-0504)[1], lithium tetraborate (79-0963 (C))[1] and a peak that could be ascribed to $LiCrO_2$ at the higher temperature data collections.

4.2 Discussion of results

Lithium tetraborate is tetragonal, space group P4mm with lattice parameters a = b = 9.477 Å and c = 10.286 Å[3, 4]. Lithium metaborate is monoclinic, space group $P2_1/c$ with four molecules in a cell of dimensions a = 5.838, b = 4.348, c = 6.449 Å, β = 115.12º, and all atoms in general positions[2, 5]. The structure consists of endless chains of BO_2 triangles with Li-O bonds between the chains. Tetragonal lithium

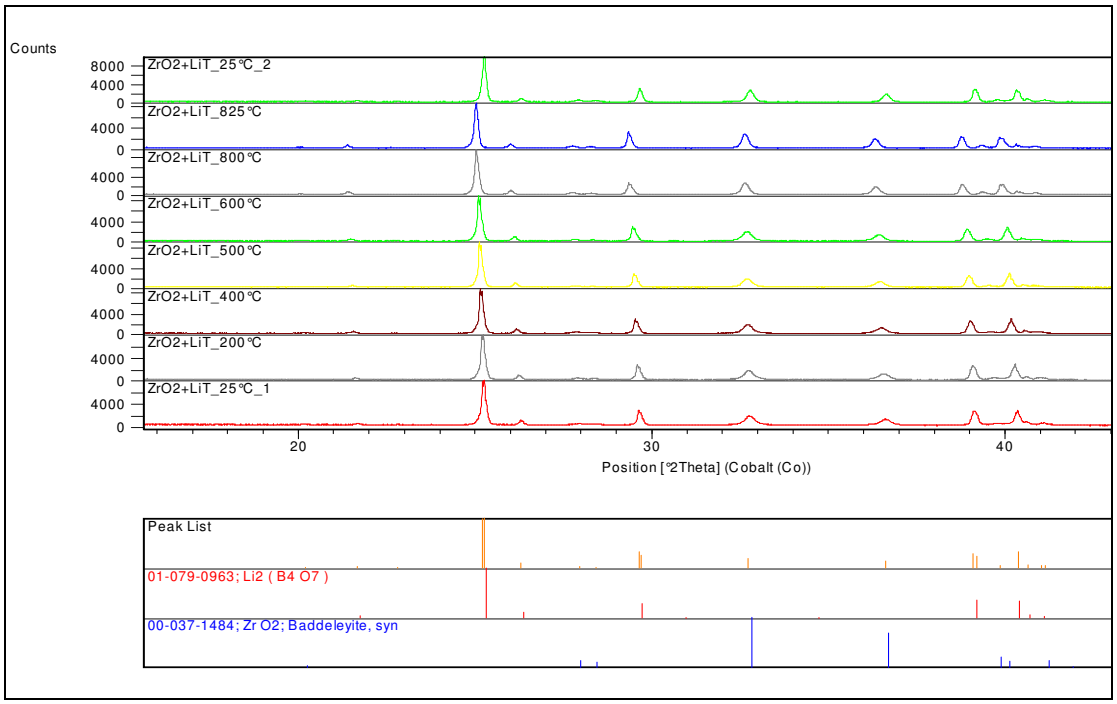

Figure 4.19 **X-ray diffractograms collected using a heating chamber of ZrO_2 and flux mixture**

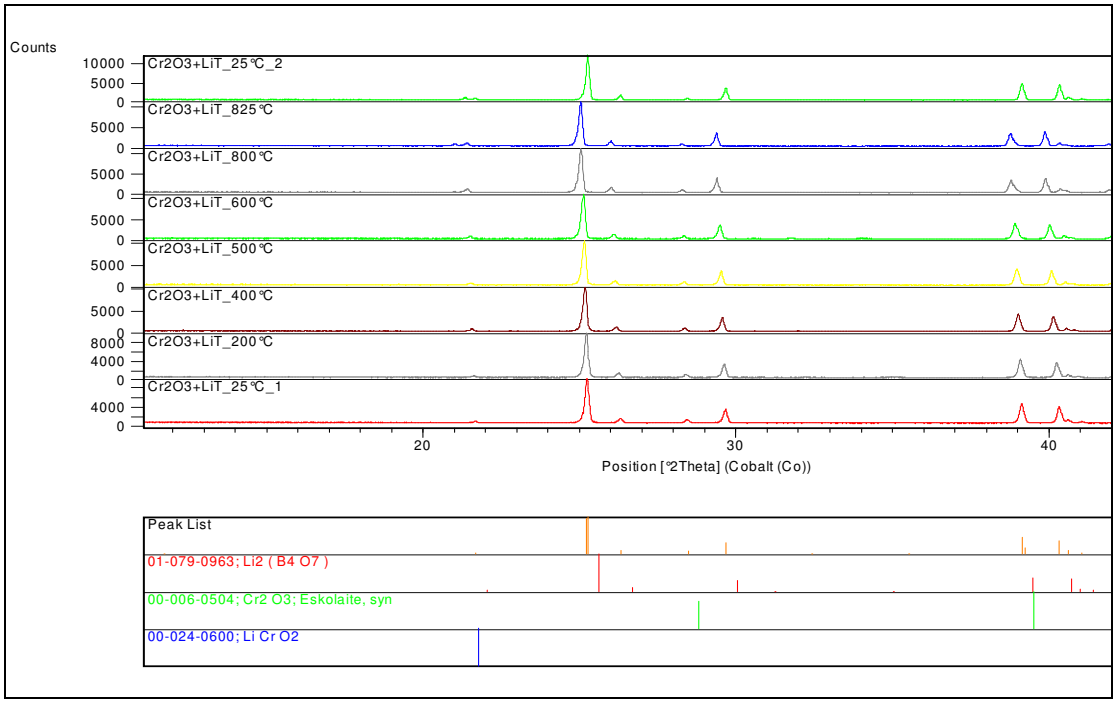

Figure 4.20 **X-ray diffractograms collected using a heating chamber of Cr_2O_3 and flux mixture**

metaborate was observed in the low temperature samples in Figures 4.1, 4.5 and 4.6. These Miller indices disappeared at higher temperatures implying that tetragonal lithium metaborate is a low temperature polymorph.

XRD was used to elucidate the events seen in the DSC scans. The exothermic reaction observed in the DSC scans of some pre-fused fluxes; the FLUORE-X®20, and two prototype samples PR0301A and PR0301B (Figures 3.7, 3.15 and 3.16 respectively), were confirmed by their respective X-ray diffractograms (Figures 4.6,4.8, 4.12, 4.14 and 4.16).

The dual melting points observed in the DSC scans for the “bi-borate” PR0301B (Figure 3.16), was confirmed by the two different phases observed in the X-ray diffractogram in Figure 4.12.

When Figures 4.2 and 4.13 are compared, the unidentifiable peak at d=3.221Å is not present in the in situ experiment which is indicative that it was either a quenching phenomenon or due to contamination.

In Figure 4.13 where the flux was heated above the melting point and cooled down again, the dataset collected at 960 ºC shows an amorphous glass. The last dataset after cooling, shows a mostly amorphous diffractogram as well as small peaks at 19, 22.5 and 34.5 º2θ that correspond to some of the lithium tetraborate (79-0963 (C))[1] peaks. Additional new peaks at 30 and 36 º2θ are not characteristic of lithium

tetraborate or of the lithium metaborate patterns, tetragonal or monoclinic. When these are compared to the published glass spectrum (Figure 4.9) and the pre-fused glassy lithium tetraborate flux PR0301A (Figure 4.7), the same peaks are observed, some corresponding to strong peaks in the crystalline pattern and some new peaks. These peaks may provide a clue to the structure of the fused glass.

The possible $LiCrO_2$ peak in Figure 4.20 was the only indication of the kind of result that could be anticipated. It would be a good idea to repeat this experiment but with a different platinum heating strip that is grooved to prevent molten flux from flowing from the strip over the electrodes of the heating chamber. With the current instrument setup this was not possible.

The temperature could be increased on such a setup to the melting temperature of the flux to evaluate whether any new phases start to form close to the melting temperature and also which phases remain on cooling. Very slow cooling may prevent glass formation and would retain the actual phases present in the melt in a crystalline form so that XRD can be used to investigate them. Information regarding the phases that form in the melt can elucidate the role of different flux mixtures and consequently the role that different structures play in the binding of sample to the flux.

4.3 Conclusion

In the analysis of the three ICPH fluxes, FLUORE-X®ATL 100 (lithium tetraborate), FLUORE-X®AML 100 (lithium metaborate) and the FLUORE-X®20 (20% lithium tetraborate with 80% lithium metaborate), it was observed that only the 80:20 mixture showed an amorphous diffractogram, although all three fluxes were pre-fused during the manufacturing process. This raises concerns regarding the stability of fused lithium borate glasses and whether the advantages of a pre-fusion step i.e. lower LOI, higher density and a lower hygroscopic nature is lasting.

Regarding the experimental flux prototype; the XRD analysis verifies the claim of the manufacturer regarding the included crystalline particles as well as the pre-fusion step. PR0301A was confirmed to be pure lithium tetraborate as stated by the manufacturer, but the composition of PR0301B is not clear. From the diffractograms (Figure 4.12 and 4.16) there is definitely lithium tetraborate present, but also another phase that does not fit the calculated lithium metaborate peaks. The presence of two phases corresponds to the TGA/DSC curve (Figure 3.16) where a dual melting point was observed. Raman spectroscopy may help to elucidate the true composition.

REFERENCES:

1. ICDD (2003) “Powder Diffraction File” *International Centre for Diffraction Data*, edited by Frank McClune, 12 Campus Boulevard, Newton Square, PA 19073-3272.
2. Zachariasen, W.H. The Crystal Structure of Lithium Metaborate. *Acta Crystallogr.* **17.** 749-751 (1964).
3. Kim, S.J., Kim, J.E., Rim, Y.H. and Yang, Y.S. Kinetics of non-isothermal crystallization process in various sized $Li_2B_4O_7$ glasses. *Solid State Communications.* **131**, 129–133 (2004).
4. Mathews, M.D., Tyagi, A.K. and Moorthy, P.N. High-temperature behaviour of lithium borates: Part I: Characterization and thermal stability. *Thermochimica Acta*. **320,** 89-95 (1998).
5. Mathews, M.D., Tyagi, A.K. and Moorthy, P.N. High-temperature behaviour of lithium borates Part II: High-temperature X-ray diffractometric and dilatometric studies. *Thermochimica Acta*. **319,** 113-121 (1998).

CHAPTER 5: RAMAN SPECTROSCOPY STUDY OF LITHIUM BORATE FLUX MIXTURES

The TGA/DSC analysis (Chapter 3) showed reactions occurring during the fusion process as endothermic or exothermic reactions on the DSC curve. XRD was subsequently used (Chapter 4) to identify the phases present and to determine whether new phases formed during the fusion process could be identified. This failed on two accounts, firstly, when the fluxes and flux/oxide mixtures were prepared above the melting temperatures, homogenous glasses were formed that could not be investigated with XRD. Secondly, when in situ reactions were prepared on a heating stage it was found that heating above the melting point caused damage to the equipment and therefore this line of action could not be successfully completed.

Raman spectroscopy as an analytical tool was selected as it gives information regarding bonding between atoms, and this would be a way to identify possible new bonds formed as well as the presence of existing bonds, and thus the structural units, present. Raman spectroscopy could also be used to distinguish between glass and crystalline phases and fingerprinting could be used to identify the composition of a sample where published spectra are available.

5.1 Experimental results

For the Raman work, the FLUORE-X® fluxes from ICPH were selected because of their inherent stability due to the manufacturing method used (section 3.1.2). These fluxes are pre-fused during manufacturing and are therefore expected to show amorphous nature up to 500 ºC where re-crystallisation occurs. The Raman spectra of a number of pure lithium borate fluxes, reacted at different temperatures in a muffle furnace as selected from TGA data, (Table 2.2), are shown in Figures 5.1, 5.3 and 5.5. Some concern existed regarding the possibility that the bands seen in the Raman spectra could be due to quenching phenomena, and would not be formed in a normal heating process of the flux. Consequently the data was re-collected using a heating stage, thus doing the experiment in situ. The measurements presented in Figures 5.2, 5.4 and 5.6 are a repetition of Figures 5.1, 5.3 and 5.5, but executed in situ. The Linkam® heating cell has an operational range between 20 °C and 600 °C and the temperatures were selected in this range to reflect possible changes observed in the pre-reacted samples.

Table 5.1 is a summation of the observed Raman bands of pure lithium borate flux samples investigated in this study, with indication of the structural units present in the compounds, causing the bands, and references to the literature where these units were previously published. In Figures 5.10, 5.11, 5.13 and 5.15, the Raman spectra of mixtures of lithium borate fluxes and oxides are presented to evaluate the

Table 5.1 Observed Raman frequencies for lithium borate fluxes

Wavenumber cm^{-1}	Signal character	Flux composition	Crystalline Glass	Description	Literature reference
167	s	LiT	C		
237-413	w	LiM	C	lattice modes	15,3,5
500	w	LiT	C/G	diborate groups/BO_4	3,14
550	w,b	LiM	G	diborate groups/ tetracoordinated B atoms	14,5
610-630	s	Absence LiM	C	endless chain structure	1
630	ms	LiM	C	chain deformation modes	3,5,6
635	w	LiM	G	metaborate chains	14
660	w	Absence LiT	G	pentaborate groups absent	
670	sh	LiT	G		4
670	w	LiM	C	chain deformation modes	3,5,6
720	s	LiM	C	chain deformation modes chain metaborate groups ($B\O_2O^-$)	3,5,6
730	s	LiT	C	symmetric vibration	3
765	b	LiM	G	network triborate, diborate groups	14
765	sh	LiM	G	metaborate chains, BO_4^-	14
750-770	b	LiT	G	Six membered rings, $B\O_2O^-$ triangles	14
770	ms	LiT	C	vibrations 6-membered rings of borate groups, BO_4 units	1,2
806	s	absence	G	B_2O_3 groups	1,2
950		LiT	C	BO_4^-	3,14
955	w, b	LiM	G	diborate groups/ tetracoordinated B atoms	14,5
1035		LiT	C	vibration of diborate groups	4
1115	b	LiT	G	vibration of diborate groups	4
1150		LiT	G	BO_4^-	3
1150		LiM	G	diborate groups	14
1170		LiT	C	vibration of diborate groups	4
1300-1600		LiT	G		14
1464	b	LiM	C	Symmetric stretch B-O bonds	5,6
1495	b	LiM	C	Symmetric stretch B-O bonds	5,6
1500	b	LiM	C	Symmetric vibrations of three non-bridging oxygens	1,3

s = sharp sh = shoulder G = glass Ø = bridging oxygen
ms = medium strong b = broad LiM = lithium metaborate
w = weak C = crystal LiT = lithium tetraborate

reactions occurring between a sample and flux, as during fusions for XRF/ICP sample preparation. This is discussed under section 5.1.3.

5.1.1 Pure Fluxes

5.1.1.1 Lithium tetraborate

Consider the spectra of lithium tetraborate, ($Li_2O.2B_2O_3$) as presented in Figures 5.1 and 5.2. For the spectra in Figure 5.1, samples of the ICPH FLUORE-X®ATL100 (Li-tetraborate), were reacted in a muffle furnace at 500, 850, 950, 1050 and 1150 ºC. The spectra below the melting temperature of lithium tetraborate, 920 ºC, appear crystalline with strong characteristic bands at 167, 515, 723, 783, 1034 and 1174 cm^{-1}. Some weaker bands were observed between 167 and 723 cm^{-1}, but are difficult to identify as the weak bands barely protrude above the background and are weakly resolved. In the in situ heating spectrum, Figure 5.2, where the sample was heated from 20 ºC to 600 ºC, and spectra recorded at 20, 500 and 600 ºC, additional bands at 255, 350, 477, 509 and 665 cm^{-1} were confirmed. These bands correlated with those published in the literature.[1, 2.] Differences between the prepared and in situ spectra can be ascribed to either quenching phenomena or the fact that only a single crystal is focussed under the microscope in both cases, and this may not be representative. Samples prepared above the melting point cooled to a homogenous glass and spectra collected from samples that were reacted between 950 and 1150 ºC in Figure 5.1, show bands at 515, 783, 980 and 1663 cm^{-1}. No published spectra were found for $Li_2O.2B_2O_3$, but these features compare well

with published spectra of $Na_2O.2B_2O_3$ and $K_2O.2B_2O_3$ glasses[1]. Only the bands at 509-515 and 783 cm^{-1} were observed in both the glass and crystalline phases, but a band shift is observed for the transition from crystalline to glass and the shape of the band changes from a sharp symmetric band to a broad band.

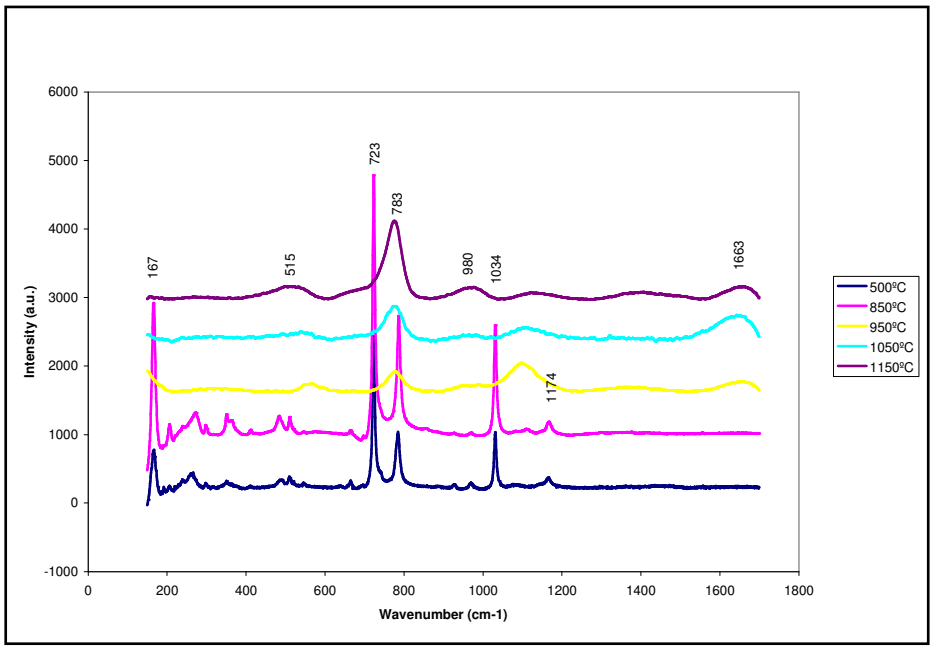

Figure 5.1 Raman spectra of lithium tetraborate reacted at different temperatures

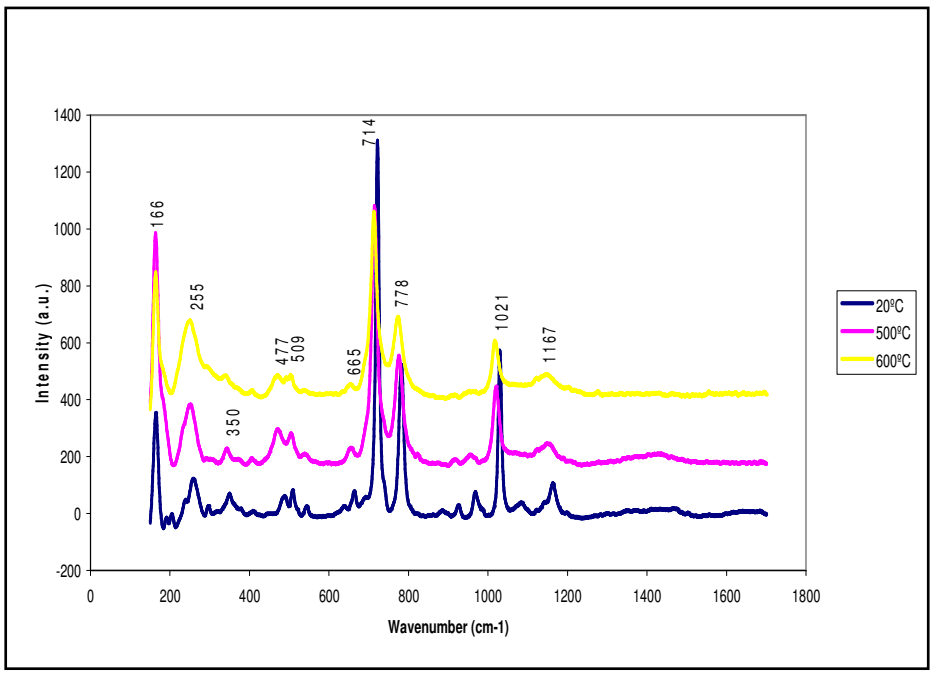

Figure 5.2 Raman spectra of lithium tetraborate. In situ heating

5.1.1.2 Lithium metaborate

The spectra of lithium metaborate, ($Li_2O.\ B_2O_3$) are presented in Figures 5.3 and 5.4. Samples of the ICPH FLUORE-X® AML 100 were reacted in a muffle furnace as selected from TGA data, (see Table 2.2), at 320, 440, 520, 720 and 1150 ºC (Figure 5.3). For the in situ measurements, the sample was once again heated from 20 to 600 ºC, the range of the Linkam® cell, and recorded at 20, 200, 300 and 500 ºC. In Figure 5.3 and 5.4 the spectra below the re-crystallisation temperature, ±520 ºC, show amorphous characteristics, i.e. broad flat bands. (The scales are different showing more detail in Figure 5.4 where intense signals do not have an influence). Above the re-crystallisation temperature sharper more intense bands are seen as in the 720 ºC spectrum, and above the melting temperature of lithium metaborate, 845 ºC, sharp, intense bands are observed, as the sample re-crystallised on cooling and did not form a stable glass like lithium tetraborate. The 500 ºC spectrum of the in situ heated lithium metaborate, Figure 5.4, was the only case where a difference was observed between the previously prepared sample and in situ recordings. Figure 5.4 provides the clearest representation of the glass phase features which are Raman bands between 545-582, 765, 955, 1108-1128 and 1467 cm^{-1}. These bands were also reported by Kamitsos et al.[3, 4], and Chryssikos et al.[5]

The sample that was heated above the melting temperature, recrystallised on cooling (Figure 5.3: 1150 ºC), and showed major bands at 640, 671, 724 and two less resolved bands in the 1475 -1495 cm^{-1} region. These features compare well with those described in the literature[1, 3, 6, 7]. Weaker bands were observed at 237,

299, 353, 413, 842, 1140 and 1225 cm^{-1}.

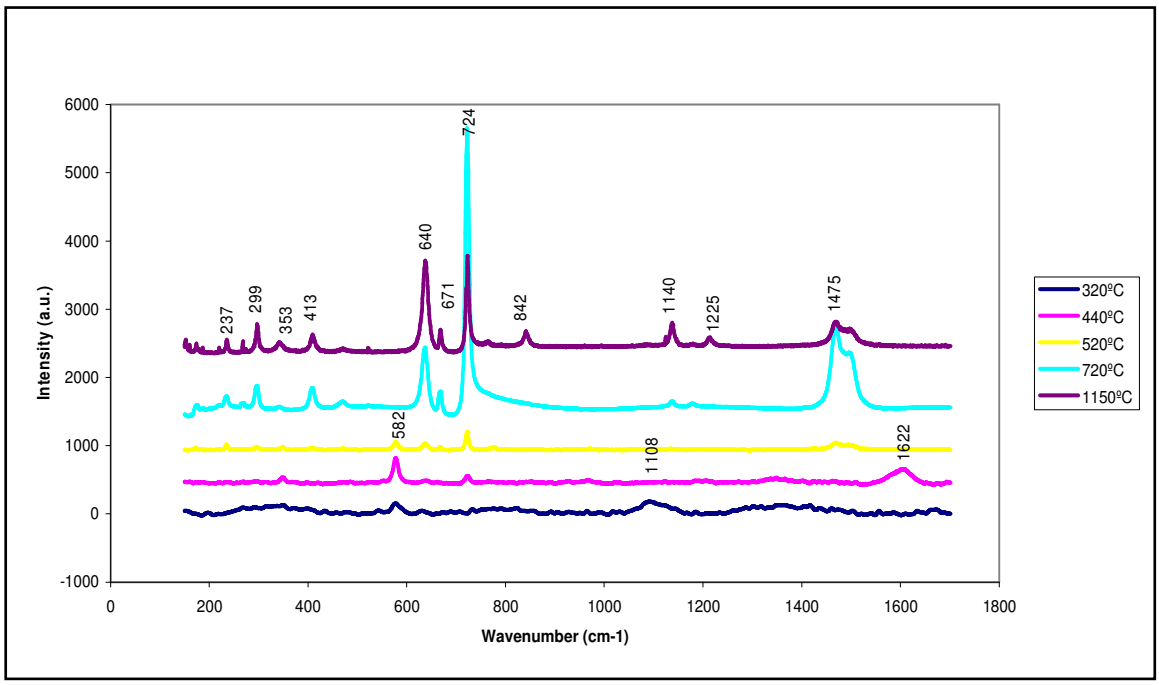

Figure 5.3 **Raman spectra of lithium metaborate reacted at different temperatures**

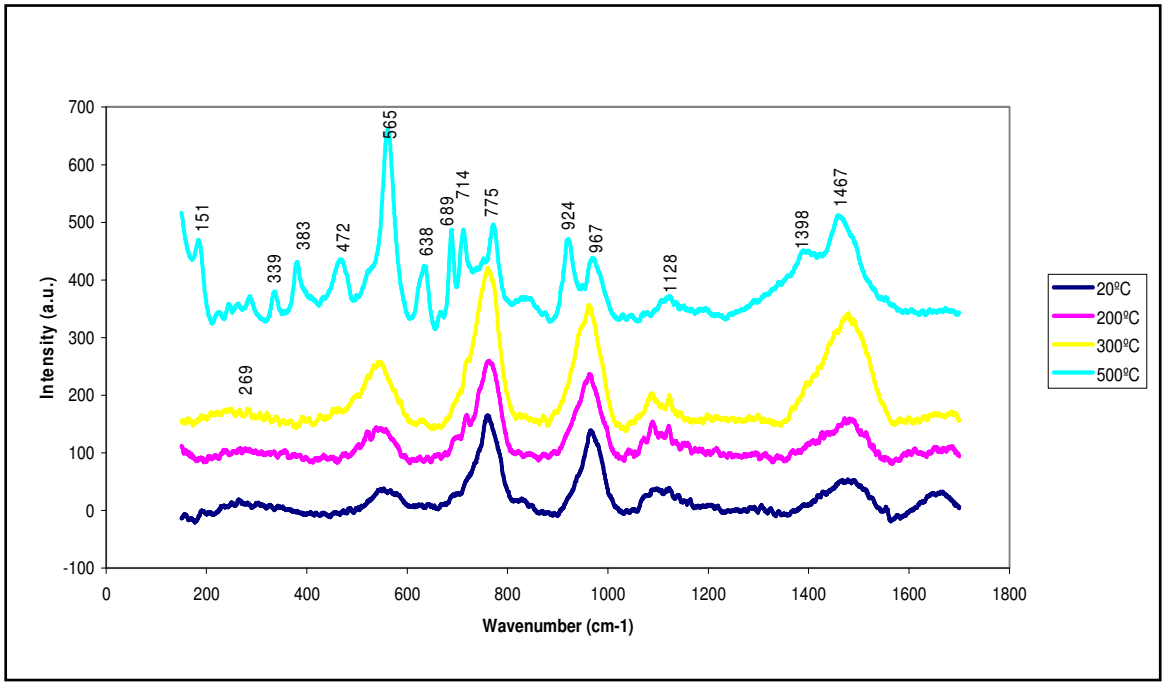

Figure 5.4 **Raman spectra of lithium metaborate. In situ heating**

Only the region between 1475 -1495 cm^{-1} is present in both the glassy and crystalline form, but this is not well observed in Figure 5.3: 320 and 440 ºC due to low intensities, but better observed in Figure 5.4. The spectrum of the in situ heated lithium metaborate, at 500 ºC, Figure 5.4, appears to capture the recrystallisation reaction in situ. It shows features of the crystalline structure as well as the glass phase.

5.1.1.3 Lithium metaborate tetraborate mixture

ICPH FLUORE-X® 20 was the third flux investigated (Figures 5.5 and 5.6.) This is a mixture of 80% lithium metaborate and 20% lithium tetraborate, thus 0.45 Li_2O.0.55 B_2O_3, or expressed in weight percentages 26.3% Li_2O and 73.7% B_2O_3. These proportions position this flux mixture between the previous two with regard to the Li_2O to B_2O_3 ratio. This flux mixture was selected, because it has an eutectic melting point at 840 ºC[1], see Figure 1.1. Preparations were reacted in a muffle furnace as selected from TGA data, (see table 2.2), and recorded at 540, 880 and 1040 ºC (Figure 5.5). The in situ measurement was made as before and recordings made at 20, 500 and 600 ºC (Figure 5.6).

Because of the fact that the Raman spectra were collected using a microscope, the orientation of a crystal or glass particle under the microscope played an important role in the quality of the final spectrum, and the quality of spectra differed, thus the use of a specific spectrum in either pre-reacted or in situ measurements to investigate a sample due to its quality intense bands.

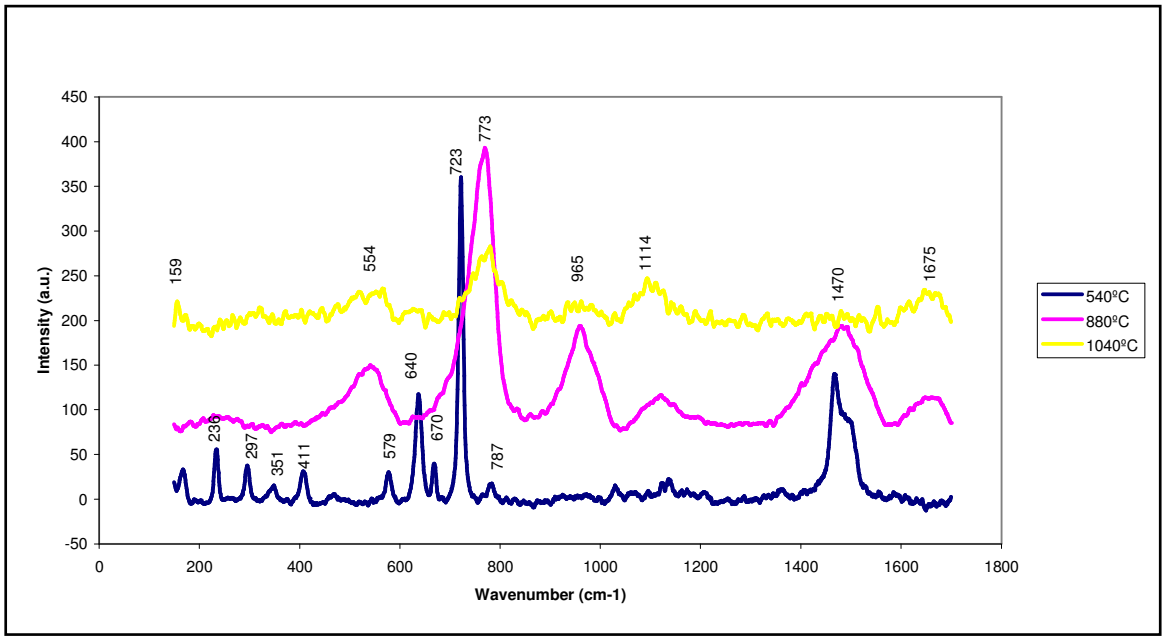

Figure 5.5 **Raman spectra of lithium metaborate-tetraborate mixture reacted at different temperatures**

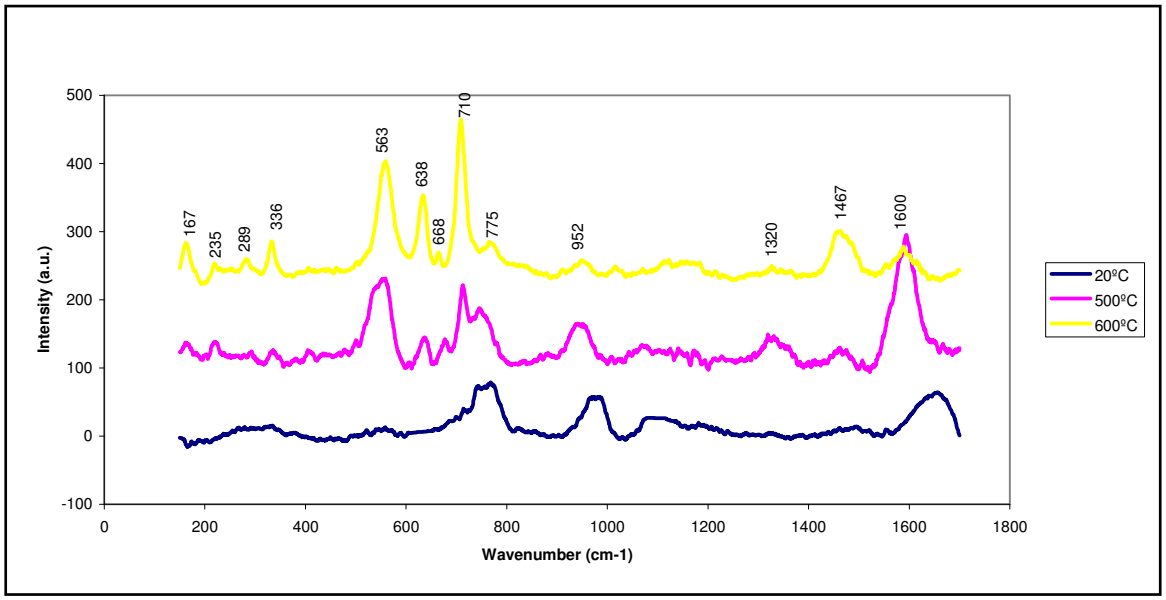

Figure 5.6 **Raman spectra of lithium metaborate - tetraborate mixture. In situ heating**

A study of the glass phase spectra, which is best typified in the 880 ºC spectrum, (Figure 5.5) shows bands at 236, 554, 773, 965, 1114, 1470 and 1675 cm^{-1}. These correspond to both the pure lithium tetraborate and lithium metaborate glass phase spectra. Some shift is observed between the three compositions, this can be clearly seen if the highest intensity band at 773 cm^{-1} in Figure 5.5 is considered. This band lies at 783 cm^{-1} for the lithium tetraborate glass phase (Figure 5.1: 950, 1050 and 1150 ºC spectra) and at 765 cm^{-1} for the lithium metaborate glass phase (Figure 5.4: 20, 200, 300 ºC spectra and Figure 5.3: 320, 440 and 520 ºC spectra). This systematic shift in the various regions is consistent with the change in Li_2O: B_2O_3 ratio, which is 1:1 for lithium metaborate, 1:2 for lithium tetraborate and 0.45:0.55 for the present mixture. These observations agree with those reported by Kamitsos et al.[4] who prepared glasses in the system $xLi_2O,(1-x)B_2O_3$, and recorded the Raman spectra (Figure 5.7). The x = 0.36 spectrum closely resembles lithium tetraborate with x = 0.33. The x = 0.46 spectrum closely resembles the 80% lithium metaborate and 20% lithium tetraborate mixture where x = 0.45, and the spectrum with x = 0.49 corresponds to lithium metaborate with x = 0.5.

In the crystalline phases, best typified by the 540 ºC spectrum in Figure 5.5, bands corresponding to both lithium metaborate, 236, 297, 411, 579, 640, 670, 723, and 1470 cm-1, and lithium tetraborate, 166 and 787 cm-1 were observed. The band observed at 351 cm^{-1} is characteristic of both lithium tetraborate and metaborate.

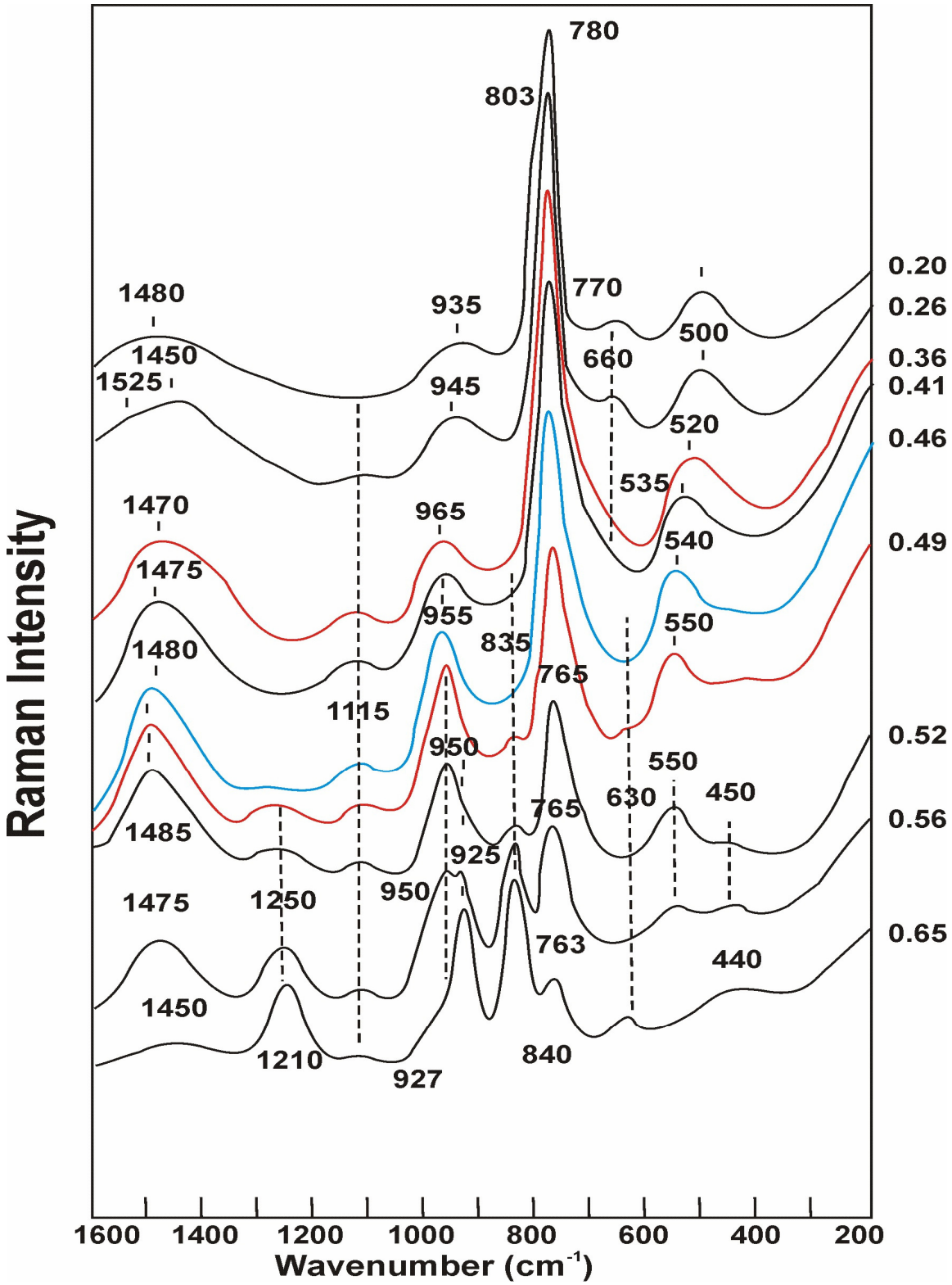

Figure 5.7 Raman Spectra of glasses in the system $xLi_2O,(1-x)B_2O_3$ after Kamitsos et.al.[14]

5.1.2 New flux prototype

The data for new experimental flux prototypes were obtained as part of this study (Figures 5.8 and 5.9).

PR0301A (Figure 5.8) is a pre-fused flux, implying that after the calcination process, the prepared flux was fused in a platinum reactor, and the glass formed was ground and packed for distribution. This is done to remove adsorbed water and reduce hygroscopy by minimising the surface area. The resultant flux is an amorphous mixture as can be observed in the room temperature spectrum in Figure 5.8. The main features in the glass phase spectra i.e. 20 and 400 ºC is an intense band at 776 cm^{-1}, with additional bands around 474-515, at 980, 1115 and 1657 cm^{-1}, which corresponds with the lithium tetraborate glass phase spectra previously collected. The crystalline phase obtained after heating to 600 ºC also corresponds to the tetraborate spectra obtained previously, namely bands at 164, 252, 350, 474, 509, 713, 776, 1019 and 1163 cm^{-1}. This is clearly seen when Figures 5.1 and 5.2 are compared. Together with the melting temperature determined by TGA (section 3.1.2), and XRD (section 4.1.2), this confirms PR0301A to be pure lithium tetraborate. PR0301B was not as clearly identifiable. In Figure 5.9, bands were observed at 166, 254, 480, 639, 713, 773, 964, 1022 cm-1, 1158 and 1474 cm^{-1} at all temperatures. These correspond to lithium tetraborate with the exception of the bands at 639 cm^{-1}, and 1474 cm^{-1}, which appears in the lithium metaborate spectra.

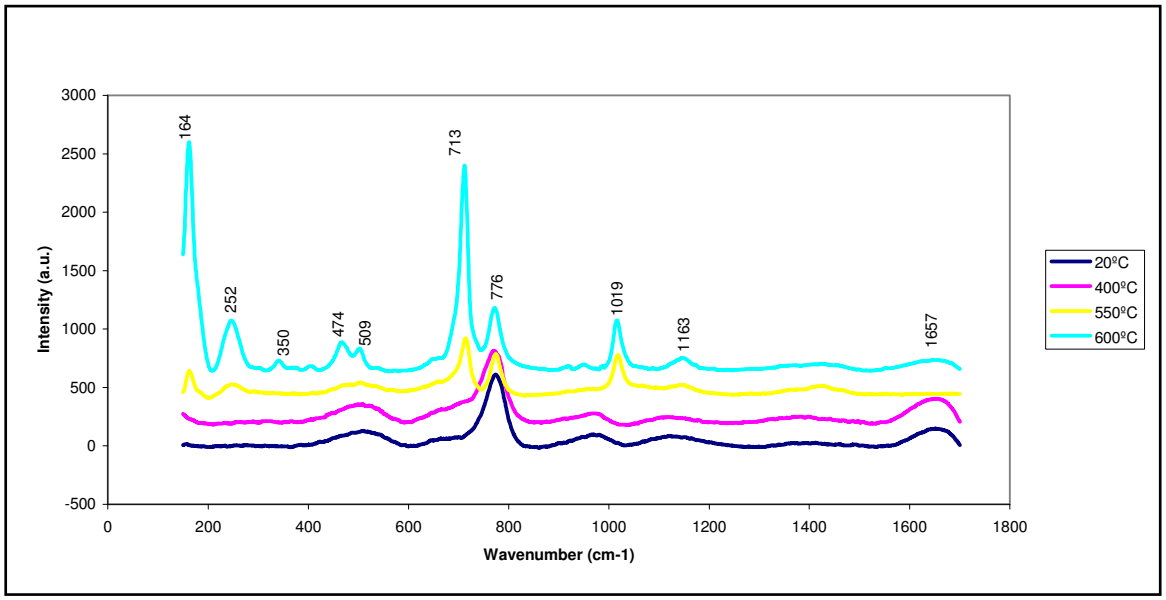

Figure 5.8 **Raman spectra of PR0301A. In situ heating**

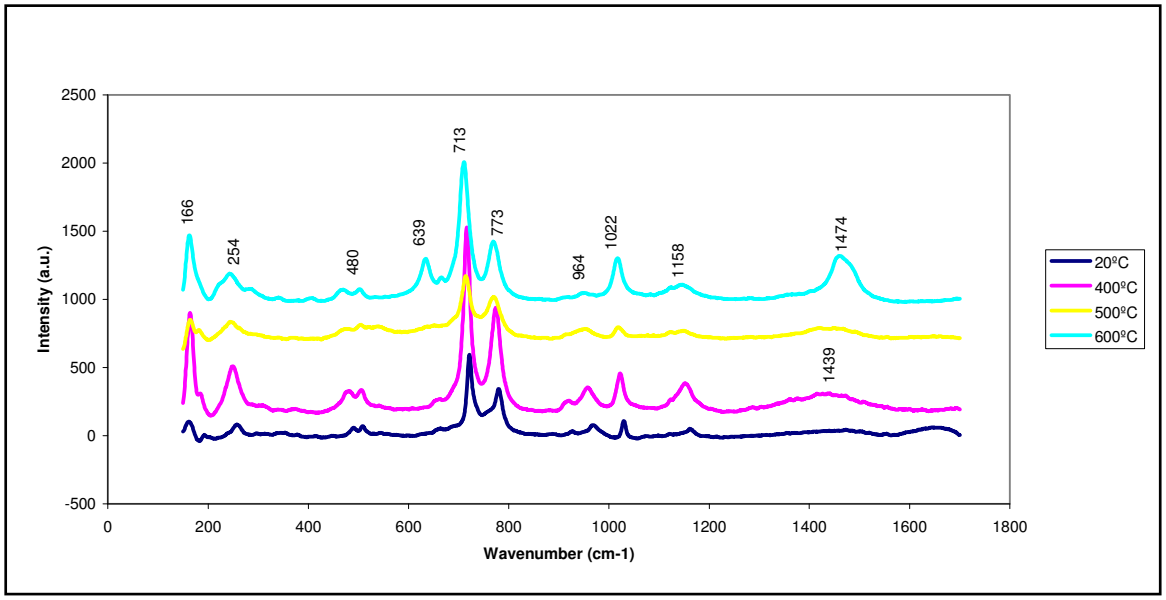

Figure 5.9 **Raman spectra of PR0301B. In situ heating**

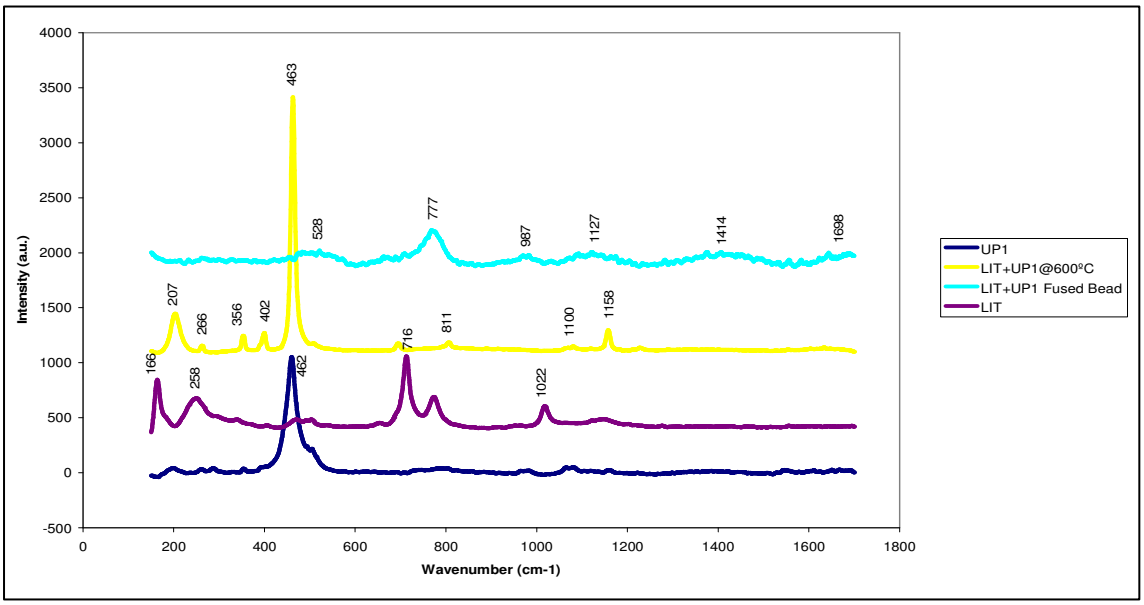

Figure 5.10 Raman spectra of sample (UP1) flux mixture

No new bands were observed which annuls the claim of the manufacturer that a bi-borate phase was formed in the manufacturing process. The Raman spectral results, as well as the dual melting points observed in the DSC and the presence of lithium tetraborate and lithium metaborate determined in the XRD confirms that this sample is probably a mixture of two phases and not a new compound.

The manufacturer claimed the presence of microcrystalline particles included in the amorphous flux, with the purpose of quenching possible micro fissure propagation during heating of the flux. These micro fissures arise due to strain in the glass structure, and lead to explosive behaviour when the flux is heated, with resultant loss of material and quantitative inaccuracy. In the PR0301A spectra (Figure 5.8: 20 and 400 ºC) no crystallinity was observed but the Raman spectra of PR0301B

(Figure 5.9), displayed a greater degree of crystallinity although the XRD (Figure 4.11) was largely amorphous. This could be ascribed to the fact that the Raman was measured using a microscope and depending on which particle the laser was focussed, either a glassy or a crystalline particle could be analysed. Crystallinity did intensify as the temperature was increased to 600 ºC.

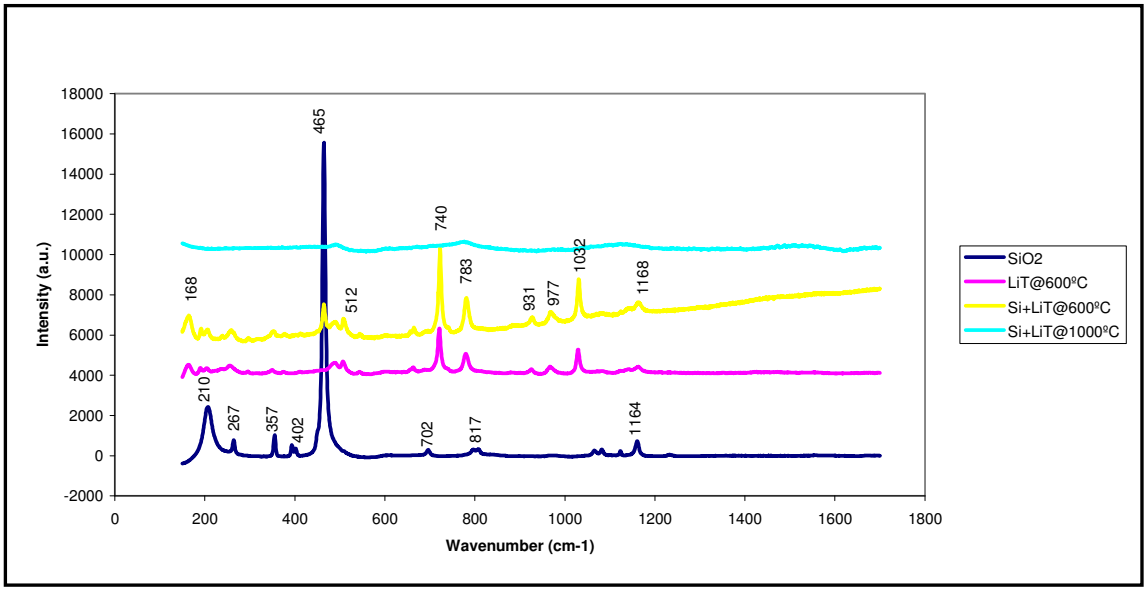

Figure 5.11 Raman spectra of SiO_2 and flux mixture. Macro Raman

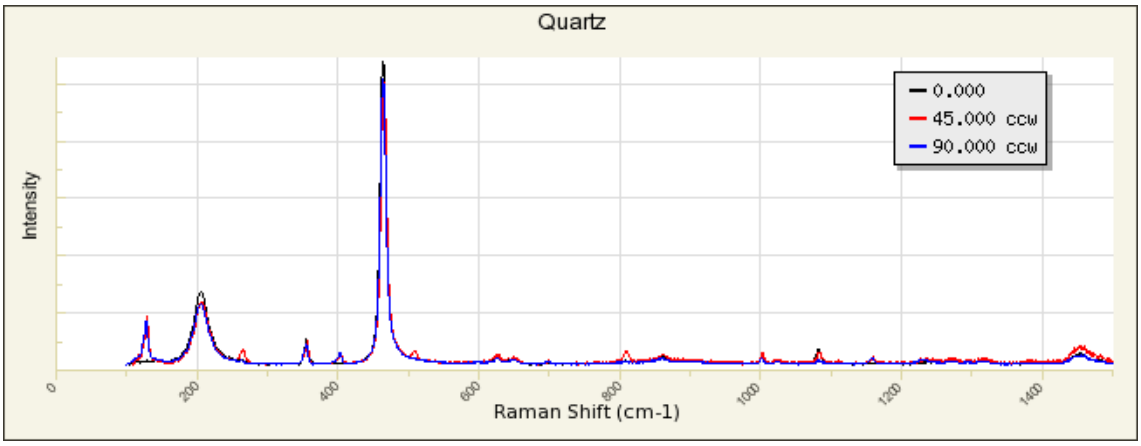

Figure 5.12 Published Raman spectrum of SiO_2. RUFF™ [8]

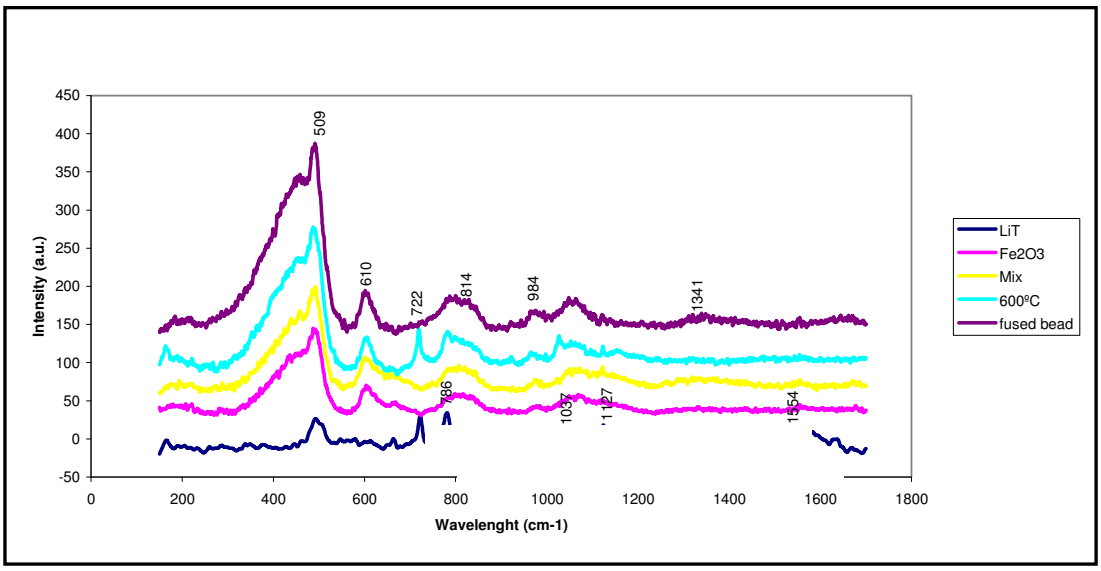

Figure 5.13 Raman spectra of Fe_2O_3 and flux mixture. Macro Raman

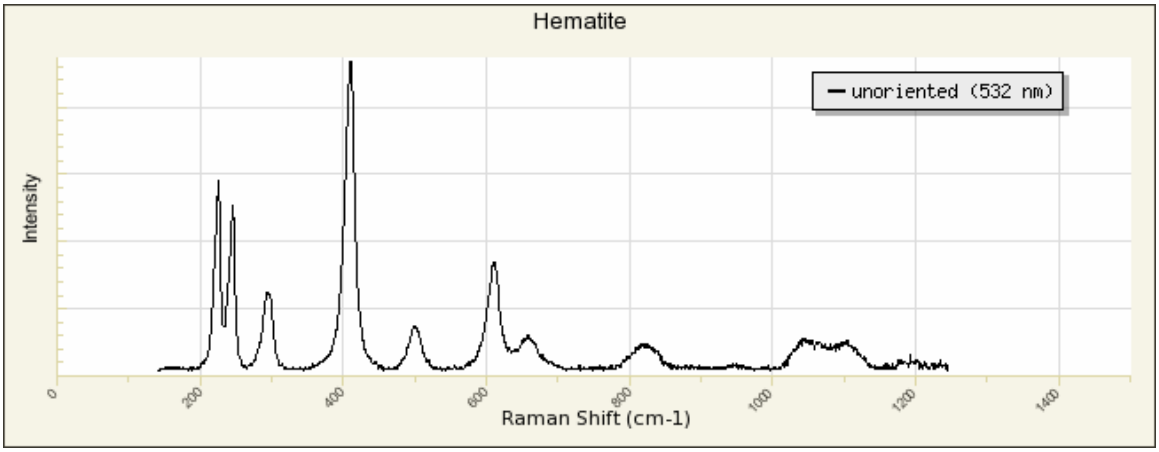

Figure 5.14 Published Raman spectrum of Fe_2O_3. RUFF™ [8]

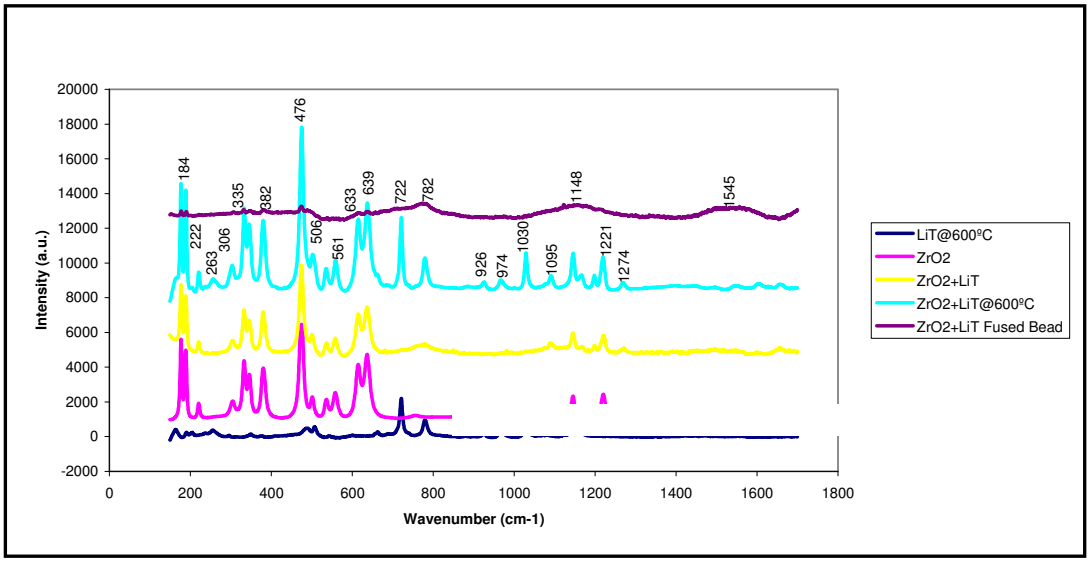

Figure 5.15 Raman spectra of ZrO_2 and flux mixture. Macro Raman

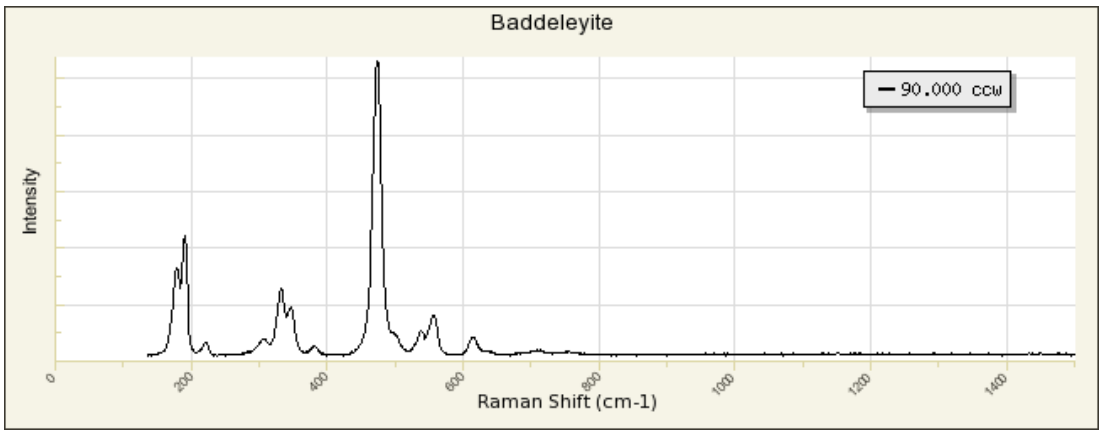

Figure 5.16 Published Raman spectrum of ZrO_2. RUFF™ [8]

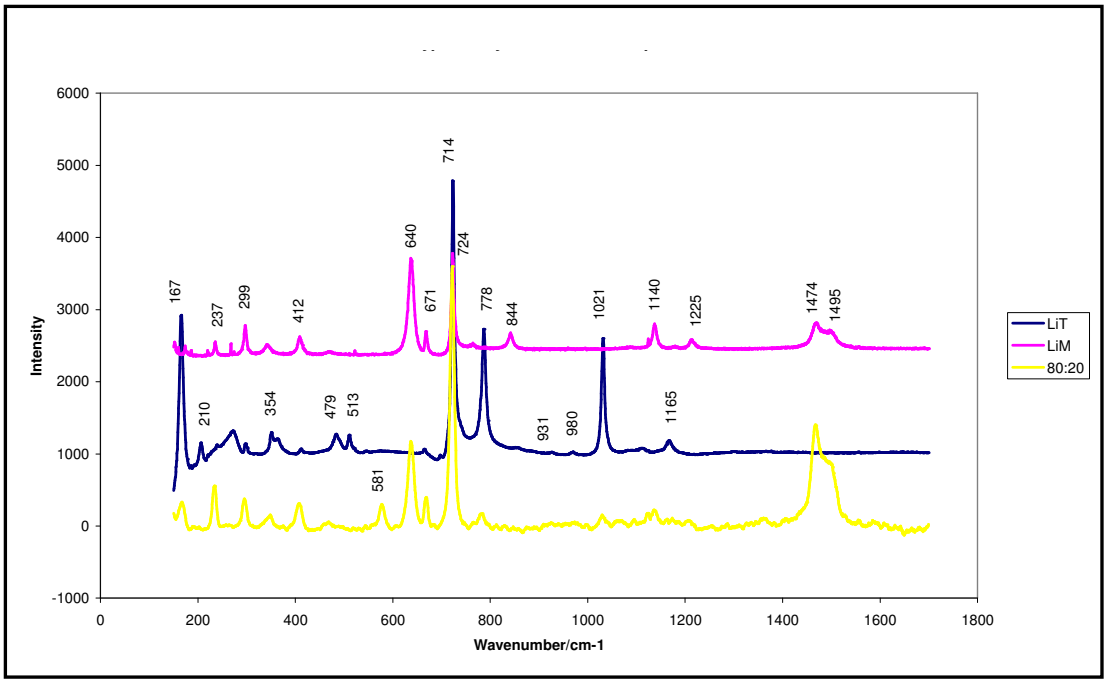

Figure 5.17 Typical Raman Spectra of crystalline lithium borates

5.1.3 Sample/flux mixtures

To evaluate any possible reactions between sample and flux below melting temperatures, a sample-flux mixture was prepared at different temperatures in a muffle furnace and analysed. Lithium tetraborate was used for these experiments as it is the most stable flux. Figure 5.10 is a representation of a granite sample, UP1, containing quartz (SiO_2), orthoclase ($KAlSi_3O_8$), plagioclase ((Ca, Na) Al $_{1-2}$ Si $_{2-3}$ O_8), orthopyroxene ((Mg, Fe) SiO_3), ilmenite ($FeTiO_3$) and apatite ($Ca_5(PO_4)_3(F, Cl, OH)$). 1g was mixed with 6g lithium tetraborate. The Raman spectra of four different data sets were plotted; the sample UP1, lithium tetraborate (LIT), the UP1- LIT mixture as prepared for fusion, at 600 ºC and finally the fused bead. The lithium tetraborate spectrum was identical to those previously collected (Figure 5.1, 5.2).

The UP1 spectrum had a strong signal at 463 cm^{-1}, due to SiO_2. Weaker signals were observed at 207, 266, 356, 402, 1100 and 1158 cm^{-1}.

5.1.3.1 UP1 and flux

In the 600 ºC spectrum of the sample flux mixture (Figure 5.10), stronger signals of the bands observed in the UP1 spectrum at 207, 266, 356, 402, 463, 1100 and 1158 cm^{-1} are seen. The lithium tetraborate bands were absent in this mixture showing an inherent problem with using the micro Raman technique – depending on where the laser focuses, different particles will be analysed. The only two bands in the mixture not present in the UP1 or LIT spectra, were those at 699 and 811 cm^{-1}. These bands are in close proximity to lithium tetraborate bands at 716 and 777 cm^{-1}, and could be interpreted as a change in the structure of the flux/sample mixture before actual fusion occurs. The fused bead spectrum showed only bands associated with lithium tetraborate glass i.e. 166, 528, 777, 987, 1127, 1414 and 1698 cm^{-1}.

Concern arose regarding the nature of the possible reactions seen as the granite sample used contained some mineral phases that could melt at lower temperatures than the flux. There is also doubt whether the sample analysed under the microscope was representative. The experiment was repeated with three inherently stable refractory materials and flux, this time using a macro Raman setup where a sample is placed in a capillary and then introduced to the laser beam. The Figures 5.11, 5.13 and 5.15 represent the results of these analyses.

5.1.3.2 SiO_2 and flux

Figure 5.11 represents spectra of a mixture of 1g SiO_2 and 6g lithium tetraborate reacted at 600 ºC and 1000 ºC, as well as the pure SiO_2 and lithium tetraborate. The lithium tetraborate spectrum shows bands at 168, 210, 265, 496, 669, 740, 783, 931, 997, 1032 and 1168 cm^{-1}. This corresponds well with previous lithium tetraborate spectra (Figures 5.1, 5.2 and 5.8). The SiO_2 spectrum has bands at 210, 267,357,402, 465, 702, 817 and 1164 cm^{-1}. These bands are identical to those obtained from the RRUFF™ [21] database (Figure 5.12). The spectrum of the mixture at 600 ºC exhibits bands from both SiO_2 and lithium tetraborate. The band at 465 cm^{-1} corresponds to the strongest band in the SiO_2 sample. Bands at 168, 512, 669, 740, 783, 931, 977 and 1032 cm^{-1} originate from the flux only and bands at 210, 265, 357and 1168 cm^{-1}, were observed in both flux and SiO_2. The 1000 ºC, fused bead sample is an amorphous glass and shows only very weak bands around 499, 786, 1160 and 1534 cm^{-1}. No bands observed in the 600 ºC mixed spectrum could be ascribed to something other than the flux or original sample.

5.1.3.3 Fe_2O_3 and flux

Figure 5.13 represents a mixture of Fe_2O_3 (1g) and lithium tetraborate (6g), reacted at 600 ºC and 1000 ºC, as well as the pure Fe_2O_3 and lithium tetraborate. The lithium tetraborate spectrum shows bands at 170, 503, 669, 722, 786, 1037, 1127 and 1554 cm^{-1}. This corresponds well with previous lithium tetraborate spectral data (Figures 5.1, 5.2 and 5.8). The Fe_2O_3 spectrum has a strong broad band between 400 and 500 cm^{-1} with a sharp band at 509 cm^{-1}, broad bands at 610, 814, 984 and

1067 cm^{-1}. This spectrum has the characteristics of an amorphous material with the weak broad bands. There is reasonable agreement between the position of the bands in the collected Fe_2O_3 spectrum and the spectrum obtained from the RRUFF™ [166] database where bands at 220, 250, 300, 410, 509, 610, 650, 815, 980, 1050 and 1100 cm^{-1} were the characteristic features (Figure 5.14). The published spectrum was collected using the micro Raman and at a slightly different wavelength (532nm) than Figure 5.13 collected in macro configuration using a 514.5nm laser line, thus the difference in intensities. The mixed spectrum is identical to the previous Fe_2O_3 spectrum with only a weak band at 1127 cm^{-1} indicative of the presence of lithium tetraborate. A spectrum after reaction at 600 ºC shows, in addition to all the bands observed in the Fe_2O_3 spectrum, lithium tetraborate bands at 170, 722, 786, 1037 and 1127 cm^{-1}. The fused bead spectrum is again identical to the Fe_2O_3 spectrum with the exception of a weak broad band at 1341 cm^{-1} not present in any of the previous spectra that could be indicative of structural change.

5.1.3.4 ZrO_2 and flux

The last sample flux mixture investigated was a mixture of ZrO_2 (1g) and lithium tetraborate (9g). The higher dilution is identical to that used in routine XRF sample preparation as ZrO_2 is a difficult material to fuse. In Figure 5.15 spectra are plotted for pure lithium tetraborate, pure ZrO_2, the cold mixture, mixture after reaction at 600 ºC and the final fused bead. The lithium tetraborate spectrum is identical to the previous with bands observed at 170, 506, 722, 782, 926, 974, 1030 and 1170 cm^{-1}.

The ZrO_2 spectrum shows a crystalline sample with sharp bands at 184, 190, 222, 306, 335, 347, 382, 476, 506, 538, 561, 633, 639, 750, 1095, 1148, 1221 and 1274 cm^{-1}. This correlates perfectly with the published spectrum from the RRUFF™ [8] database except that the bands above1000 cm^{-1} is not clearly visible in the 532nm laser spectrum (Figure 5.16).

The lithium tetraborate/ZrO_2 mixture is identical to the pure ZrO_2 spectrum and, only after heating to 600 ºC, are some lithium tetraborate bands observed in addition to the bands associated with ZrO_2, namely bands at 722, 782, 926, 974, 1030 and 1148 cm^{-1}. The spectrum of the fused glass bead has broad weak bands at 476, 635, 782, 1148 and 1545 cm^{-1}. This would seem that the ZrO_2 structure remains unchanged in the fusion but the broadening of bands indicate the transition from crystal to glass.

5.2 Discussion of results with relation to published literature

To simplify discussions the most characteristic crystalline and glassy spectra for lithium tetraborate, lithium metaborate and the 80:20 mixture (80 wt% lithium metaborate, 20 wt% lithium tetraborate), were selected from Figures 5.1-5.6 and represented in Figures 5.17 and 5.18.

First, consider the polycrystalline lithium metaborate (Figure 5.17 (LiM)). This is one of the compounds investigated by Konijnendijk[1] as a fingerprint to reveal the

presence of certain structural units in the corresponding glasses. In his thesis he distinguishes between metaborate compounds consisting of ring type planar $B_3O_6^{3-}$ groups, such as $Na_2O.B_2O_3$ and $K_2O.B_2O_3$, and those metaborate compounds that consist of long chains of BO^{2-} ions, such as $Li_2O.B_2O_3$ and $CaO.B_2O_3$, by the presence or absence of certain bands. He concluded the absence of a strong peak in the range 610-630 cm^{-1} as being indicative of an endless chain structure, and assigns the bands in the region of 1500 cm^{-1} to symmetric vibrations of the three non-bridging oxygen ions. Figure 5.19 depicts the ring type lithium metaborate structure.

The data for the polycrystalline lithium tetraborate is shown in Figure 5.17 (LiT). As previously reported by Krogh-Moe[9-12], this compound is built up of diborate groups in which all oxygen ions are bridging and two BO_4 tetrahedra are connected to each other (Figure 5.20). Konijnendijk[1], suggests the strong band around 770 cm^{-1} is due to a vibration in which all oxygens of the six membered ring, of a borate group with one or two BO_4 units in the ring, take part. This strong band in the region of 770 cm^{-1} (778 $cm^{-1,}$ Figure 5.17, also 783 cm^{-1}, Figure 5.1, 778 cm^{-1}, Figure 5.2, 776 cm^{-1}, Figure 5.8) was observed in the lithium tetraborate spectra collected during the present study. It was not the strongest band present, but when one refers to Konijnendijk's spectra, it is observed that this was not the strongest band in his either.

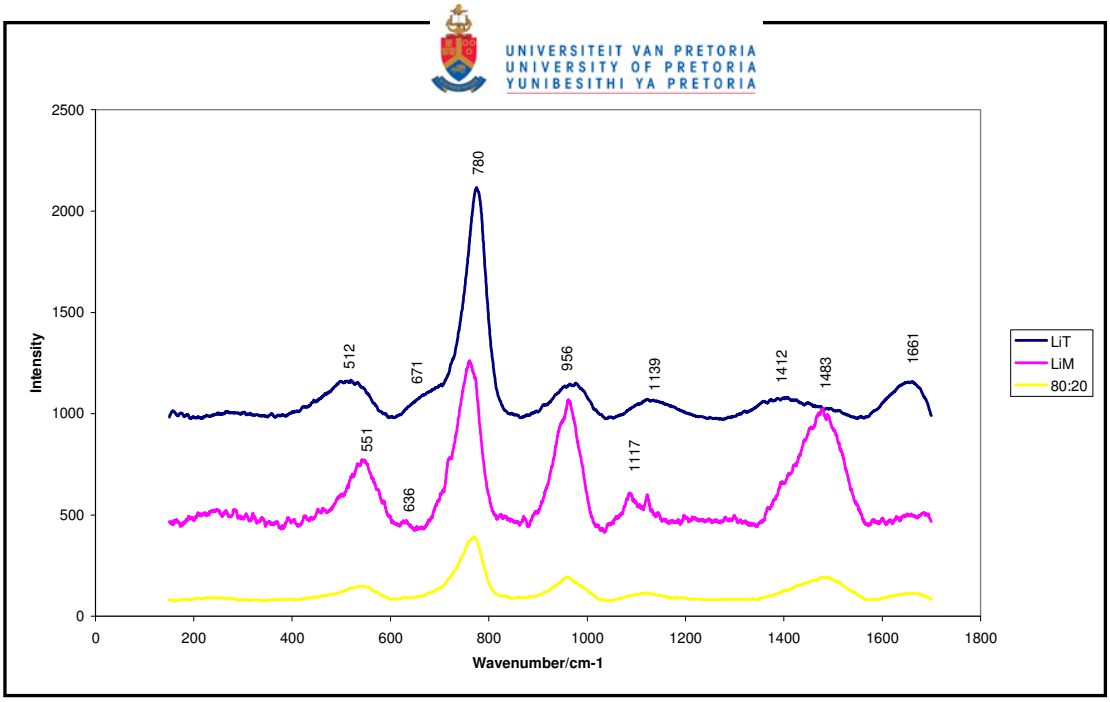

Figure 5.18 Typical Raman Spectra of lithium borate glasses

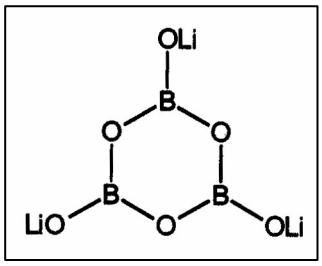

Figure 5.19 Structural drawing of lithium metaborate

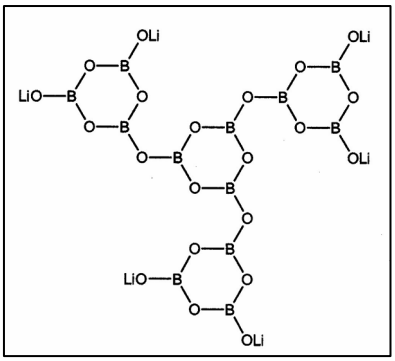

Figure 5.20 Structural drawing of lithium tetraborate

When the glass spectra in Figure 5.18 is considered, more similarities are observed between the lithium tetraborate (LIT), lithium metaborate (LIM) and the 80 wt% lithium metaborate, 20 wt% lithium tetraborate mixture (80:20). Broad bands in the region 510-550, 780, 950, 1120-1140, 1410-1490, and 1660 cm^{-1} are observed in all three flux compositions, indication of the fact that when long range order is destroyed as in the case of a glass, the short range bonds of lithium tetraborate and lithium metaborate are similar.

A glass network is built up from structural groups, consisting of several atoms, not unlike the unit cells in a crystal [5,12,13]. Disorder in this case indicates deviation from strict translational repetition of the groups, which would convert the glass to its crystalline state. The randomness associated with the oxygen bridges connecting these units was thought to account for the excess entropy in glass and its expanded network. Brawer[13] published a more fundamental description of the vibration spectra of glasses and concluded that the spectra of glass and crystal with the same composition show considerable agreement as long as the same groups occur in both glass and crystal and little coupling occurs between the structural groups. He continued to state that the disorder in the glass could enhance polarisability and this could lead to the enhancement of certain groups in the glass spectrum that were hardly visible in the corresponding crystalline spectrum. He also showed with calculations that the width of the modes generally increases considerably.

Konijnendijk[1] stated that up to addition of about 20% alkali oxide to boron-oxide

glass, mainly tetraborate groups are formed. Above this concentration, the structure of a borate glass is mainly build up of tetraborate groups, a minor number of boroxol groups, a minor number of loose BO_3 triangles and BO_4 tetrahedra. With increasing alkali oxide (20 to 35 mol%), evidence suggests that the diborate group is the predominant group in sodium-borate glasses at about 33 mol% Na_2O. A minor number of "loose" BO_3 triangles and BO_4 tetrahedra is probable. This is approximately the same composition as the lithium tetraborate flux investigated in the present study, and these conclusions could be applied to the material. Konijnendijk did actually include one lithium borate glass at 33 mol% Li_2O (Figure 5.21), and the spectrum is almost identical to those obtained in the present study (Figure 5.18), with the exception that the range was wider in the present case.

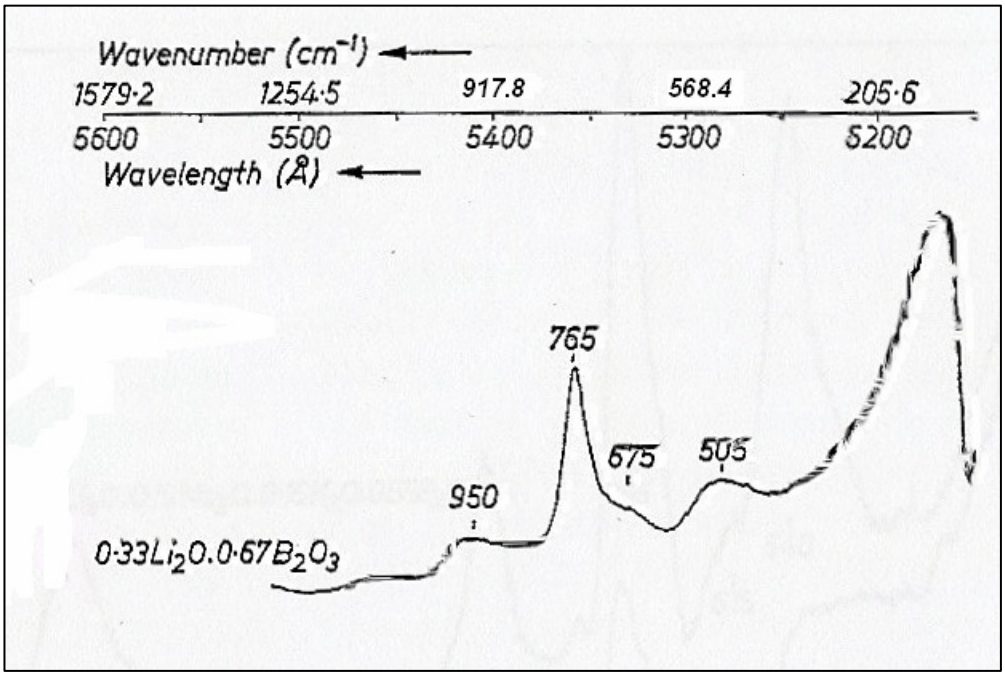

Figure 5.21 Raman spectrum of lithium tetraborate glass from Konijnendijk[8]

Konijnendijk reported that at x=0.5 the structure is built up of diborate groups, some orthoborate units, pyroborate groups and "loose" BO_3 triangles with or without a non-bridging oxygen ion. The presence of a small number of ring type metaborate groups are indicated. This composition of 50 mol% alkali oxide, corresponds with the lithium metaborate investigated in the present study.

For a more detailed discussion of Figure 5.18, a paper published in 1987 by Kamitsos, Karakassides and Chryssikos[4], is useful. The paper included the [x Li_2O**.** (1-x) B_2O_3] composition of the lithium tetraborate, x = 0.33, lithium metaborate, x = 0.5, and the 80:20 lithium metaborate, tetraborate mixture, x = 0.45, that was considered in this present study (Figure 5.7). The shift of the band around 765 – 780 cm^{-1} to lower frequencies with increase in Li_2O content, as reported, was clearly seen in the present Raman spectra (Figure 5.18). In this paper of Kamitsos et al. the spectra of glassy and crystalline lithium borates were compared and the band at 1115 cm^{-1} in the glass and those at 1170 and 1035 cm^{-1} in crystalline $Li_2O.B_2O_3$ were assigned to a characteristic vibration of diborate groups. These correspond to the bands at 1117 cm^{-1} in Figure 5.18 (LiM) and 1140 cm^{-1} in Figure 5.17 (LiM). The authors also conclude that the decrease in intensity of the 1300-1500 cm^{-1} region at high lithium content (Figure 5.7), previously assigned to stretching of $B\text{-}O^-$ bonds attached to larger borate groups, does not imply a reduction in the non-bridging oxygen concentration of the glass, but rather indicates that large interconnected borate network structures containing $B\text{-}O^-$ bonds, are dismantled in favour of smaller units containing non-bridging oxygens with well defined Raman peaks. This

was clearly seen in Figure 5.18 where the band in the 1400-1500 cm^{-1} region in LiT, x = 0.33, became more intense in the 80:20 mixture where x=0.45. In the LiM x=0.5 the band was strong and sharp. The presence of a weak shoulder at 670 cm^{-1} (Figure 5.18) in the LiT glass spectrum was observed, and confirmed in this paper by Kamitsos et al.[4], although he stated that diborate groups do not scatter in this region, a band around 500 cm^{-1}, (Figure 5.17(LiT)) indicates the presence of diborate groups[4].

Considering Figure 5.17, (LiM), the band at 724 cm^{-1}, was confirmed by Kamitsos et al.[3,14] to be associated with the presence of chain metaborate groups as the strongest feature, accompanied by two characteristic peaks at 671 and 640 cm^{-1}, a broad feature centred at 1480 cm^{-1}, and a number of bands below 400 cm^{-1} . On these grounds the presence of non-bridging oxygen atoms could be concluded. Considering Figure 5.17, (LiT), the strong band at 714 cm^{-1}, was confirmed by these authors, and they assigned bands observed at 513, 930 and 1165 cm^{-1} to the presence of BO_4 tetrahedra, although, according to them, the complexity of these spectra make assignment to specific vibrational modes almost impossible.

5.3 Conclusion

Using Raman spectroscopy important information could be obtained from the lithium borate flux mixtures. In all three pure fluxes the difference between glass and crystalline phases were clearly distinguishable by the characteristic spectra. Spectra

collected from crystalline materials had sharp well defined bands with a flat background, and as the sample moved towards the melting point broadening of the bands was observed (e.g. 720 ºC spectrum of lithium metaborate in Figure 5.3). The glassy phases were characterised by broad bands.

Structure could be distinguished as glassy lithium metaborate and tetraborate consists of large fractions of boron-oxygen , scattering mainly between 500-600 cm^{-1} and 800-1100 cm^{-1} in the Raman spectrum. These bands are absent in the crystalline lithium metaborate and tetraborate. From all the abovementioned data it can be concluded that glassy lithium borates do not only consist of the same local units as their devitrification products, but seem to preserve in its network domains with some longer range ordering inherent to the crystalline products. These enabled the estimation of composition by comparing glass spectra with published spectra of the crystalline compounds and recognise functional units present in both.

REFERENCES:

1. Konijnendijk, W.L. The Structure of Borosilicate Glasses. *Philips Res. Suppl*. 1975. No.1.
2. Brill, T.W. Raman Spectroscopy of Crystalline and Vitreous Borates. *Philips Research Report Supplement.* 1976. No.2.
3. Kamitsos, E.I., Karakassides, M.A.,Chryssikos, G.D. Structure of Borate glasses. Part1. Raman study of caesuim, rubidium, and potassium borate glasses. *Phys. Chem. Glasses*. **30 (6)**, 229 (1989)
4. Kamitsos, E.I., Karakassides, M.A.,Chryssikos, G.D. A vibrational study of lithium borate glasses with high Li_2O content. *J. Phys. Chem*. **91,** 1073-1079 (1987).
5. Chryssikos, G.D., Kamitsos, E.I., Patsis, A.P., Bitsis, M.S., Karakassides, M.A. The devitrification of lithium metaborate: polymorphism and glass formation. *J.Non-Cryst. Solids*. **126,** 42-51 (1990).
6. Chryssikos, G.D., Kapoutsis, J.A., Patsis, A.P., Kamitsos, E.I. A classification of metaborate crystals based on Raman spectroscopy. *Spectrochim. Acta*, Part A. **47A. No.8,** pp.1117-1126 (1991).
7. Chryssikos, G.D. Bond Length-Raman Frequency Correlations in Borate Crystals. *Journal of Raman Spectroscopy*. **22,** 645-650 (1991).
8. RUFF™ Web: http://minerals.gps.caltech.edu/FILES/raman/Index.htm
   Raman spectra acquired at Caltech (the original on-line database of Raman

spectra of minerals). (2005)

9. Krog-Moe, J. Borate glass structure. *Ark.Kemi.* **12,** 451 (1958).
10. Krog-Moe, J. The crystal structure of lithium diborate, $Li_2O.2B_2O_3$. *Acta Cryst.* **15,** 190 (1962).
11. Krog-Moe, J. The crystal structure of silver tetraborate $Ag_2O.4B_2O_3$. *Acta Cryst*. **18,** 77 (1965).
12. Krogh-Moe, J. Structural interpretation of melting point depression in the sodium borate system. *Phys. Chem. Glasses*. **3,** 101 (1962).
13. Brawer, S. Theory of the vibrational spectra of some network and molecular glasses. *Phys. Rev*. **B11,** 3173 (1975).
14. Chryssikos, G.D., Kamitsos, E.I., Karakassides, M.A. Structure of borate glasses. Part 2: The alkali-induced network modification schemes in terms of structure and properties. *Phys. Chem. Glasses*. **31,** 109 (1990).
15. Rulmont, A., and Almou, M. Vibrational spectra of metaborates with infinite chain structure: $LiBO_2$, CaB_2O_4, SrB_2O_4. *Spectrochim. Acta*, Part A. **45,** 603 (1989).

CHAPTER 6: ELECTRON MICROPROBE ANALYSIS (EPMA) AND MICROSCOPIC WORK

The study of fluxes and flux sample mixtures using TGA/DSC, Raman Spectroscopy and XRD each contributed new insights on the mechanism of borate fusion, but none of the techniques provided a clear solution to the problem of identifying the mechanism and supplied a way of predicting the solubility of oxides in a flux.

To obtain an additional insight on this problem electron microprobe analysis was done on two oxide/flux specimens prepared by fusion. ZrO_2 and Cr_2O_3 were selected for this exercise as these are notoriously difficult oxides to dissolve in a lithium borate flux. Hematite, quartz and UP1, used in other test work would have fused without undissolved particles to study.

6.1 Experimental results of EPMA

Specimens of an excess pure oxide (low solubility) were prepared in lithium borate flux. Once homogenised, the specimens were mapped with the CAMECA SX 100 Electron Probe Micro Analyser (EPMA). This state of the art instrument, equipped with four wavelength dispersive spectrometers as well as the latest energy dispersive system from Röntec, facilitates analysis of major and trace elements on a microscopic scale.

If maximum concentration of the analyte is assumed on an undissolved particle, the area next to it should theoretically have the maximum concentration of the specific oxide soluble in the flux.

Two samples were prepared: 0.25g chromite ($Fe^{2+}Cr_2O_4$), with 6g $Li_2B_4O_7$ was fused for an hour at 1050 ºC while mixing continuously to homogenise the fused glass. After the prepared glass bead was annealed, a cross section was cut using a diamond saw and mounted and carbon coated for EPMA analysis. A second specimen consisting of 1g Zircon ($ZrSiO_4$), with 6g $Li_2B_4O_7$ was prepared according to the same method.

6.1.1. Chromite dissolved in lithium tetraborate glass bead analysed by EPMA

Figures 6.1 and 6.2 are two different enlargement reflected light images of the same chromite particle in the fused bead. Figure 6.3 is the back scatter electron image on the same scale as figure 6.2. Table 6.1 presents the analytical data determined by mapping over the undissolved particle. The measurement identified as “particle analysis” is the point on the undissolved/ recrystallised particle. The measurement identified as spot 1 in table 6.1 is closest to the particle, spot 3 is the furthest from the particle with equal distance between each spot. Only point five in table 6.1 gave an analytical total close to 100%. Due to the small grain size (BSE image figure 6.3) it is virtually impossible to have excitation volume only on the un-dissolved particle. Another factor is the depth of the particle in the flux, only when it is on the

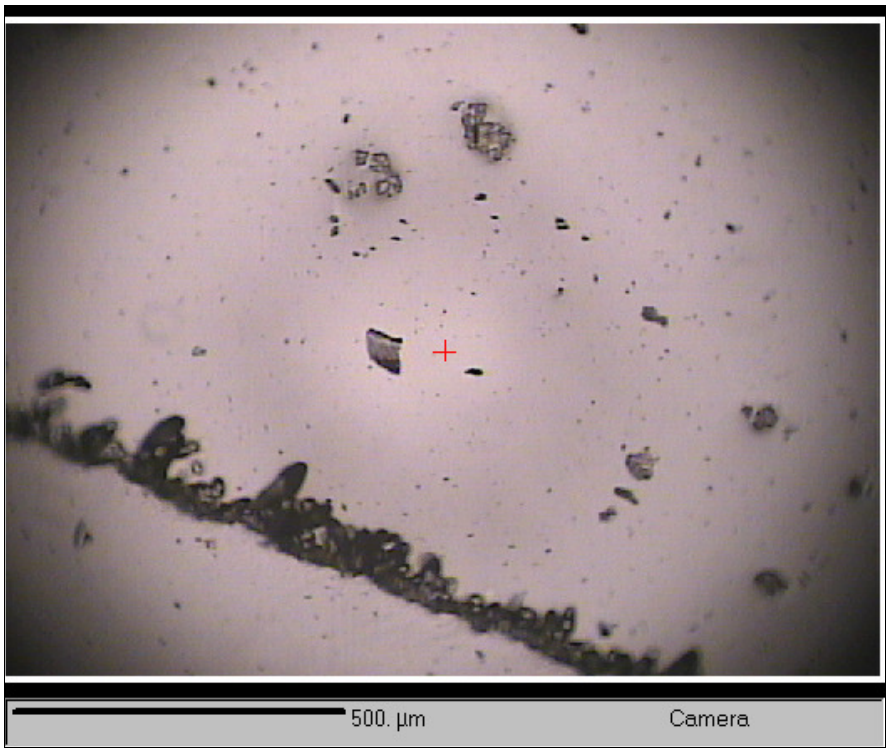

Figure 6.1 **Chromite particles - reflected light TV image**

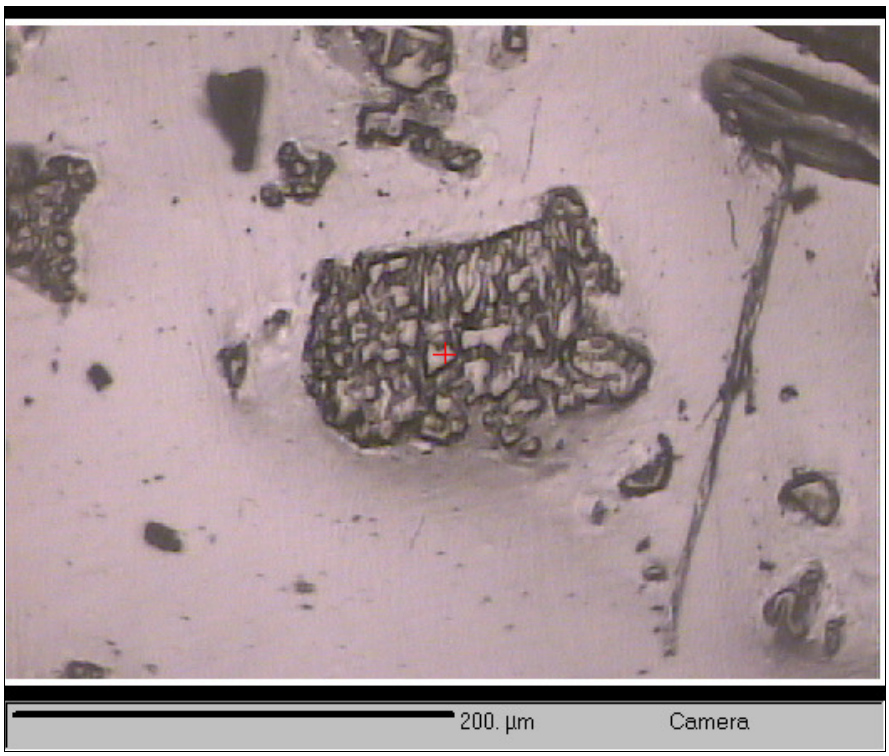

Figure 6.2 **Chromite particles - reflected light TV image**

surface and exposed will the total reflect the elemental concentration of the particle only. EPMA cannot analyse for boron and lithium so the flux makes up the difference and analysis and totals represents only the concentration of the measured elements.

When considering the analysis in table 6.1 point 1, 5 and 9 represents particles, and from the Cr_2O_3 concentration we can see that point 5 was closest to the surface whereas the others were imbedded deeper in the flux. Consider the Cr_2O_3 concentration of points 2, 3, 4 and 6, 7, 8 and 10, 11 and 12 to calculate the maximum soluble Cr_2O_3 in the flux. The average Cr_2O_3 concentration in the flux surrounding the three undissolved particles is 1.34±0.06%, 1.39±0.06% and 1.41±0.03 % respectively. This gives an average of 1.38±0.05% Cr_2O_3 as the maximum solubility in lithium tetraborate flux. If we assume an average Cr_2O_3 concentration of around 48% in the original chromite specimen[1], this would equate to 35 times dilution which corresponds to the values of 40 x dilution published.[2, 3.]

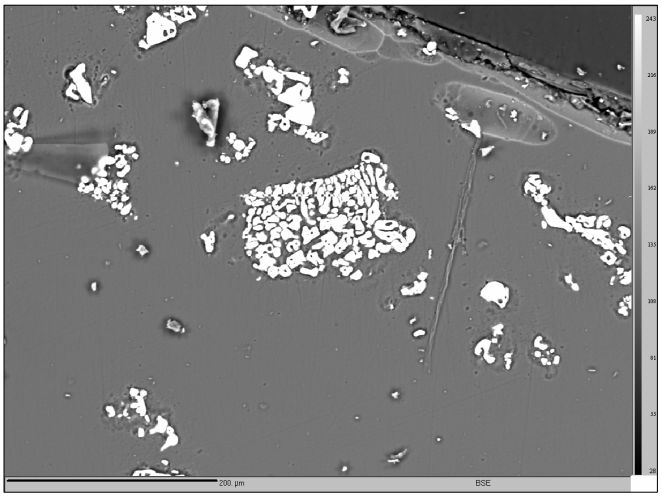

Figure 6.3 Chromite particles - BSE image

Table 6.1 EPMA analysis of chromite fused bead

Point	Al_2O_3	TiO_2	Cr_2O_3	FeO	ZrO_2	Total	X	Y	Z	Comment
1	1.18	0.1	68.55	2.56	0.01	72.41	-9470	21789	87	Particle_1
2	0.89	0	1.35	0.86	0	3.09	-9470	21708	87	Spot_1
3	0.95	0.02	1.4	0.83	0.01	3.2	-9470	21667	87	Spot_2
4	0.82	0.01	1.28	0.85	0.03	2.98	-9470	21619	87	Spot_3
5	0.3	0.32	95.76	2.49	0	98.87	-8897	21682	87	Particle_2
6	0.87	0.02	1.44	0.78	0.02	3.13	-8950	21682	87	Spot_1
7	0.83	0.04	1.41	0.86	0.03	3.17	-9030	21682	87	Spot_2
8	0.82	0.01	1.32	0.88	0.06	3.09	-9072	21682	87	Spot_3
9	0.56	0.19	52.37	2.05	0	55.17	-7941	21260	87	Particle_3
10	0.89	0	1.39	0.84	0.02	3.14	-7942	21205	87	Spot_1
11	0.86	0	1.44	0.85	0.04	3.19	-7942	21159	87	Spot_2
12	0.79	0.01	1.4	0.83	0	3.03	-7942	21127	87	Spot_3

6.1.2. Zircon dissolved in lithium tetraborate glass bead analysed by EPMA

Figures 6.4 and 6.5 are two different enlargement reflected light images of the same zircon particle in the fused bead. Figure 6.6 is the back scatter electron image on the same scale as figure 6.4. Table 6.2 presents the analytical data determined by mapping over the undissolved particle. The measurement identified as “particle analysis” is the point on the undissolved/ recrystallised particle. The measurement identified as spot 1 in table 6.2 is closest to the particle, spot 3 is the furthest from the particle with equal distance between each spot. Apart from the problems due to the small grain size (BSE image figure 6.6) as described before, the zircon particle has an additional problem in that secondary fluorescence occurs on Zr which

impedes accuracy. When we treat the data in a similar way as the chromite data under the previous heading, points 13, 17 and 21 in table 6.2 represent the undissolved particles and points 14-16, 18-20 and 22-24 the maximum solubility of ZrO_2 in lithium tetraborate flux.

The values for this are 13.8±0.6%, 13.0±0.9% and 13.5±0.1% respectively that gives the average solubility of ZrO_2 from a zircon, in lithium tetraborate flux as 13.4±0.6%. This would account for a five time dilution if a 66% ZrO_2 concentration is taken as the average ZrO_2 in zircon.

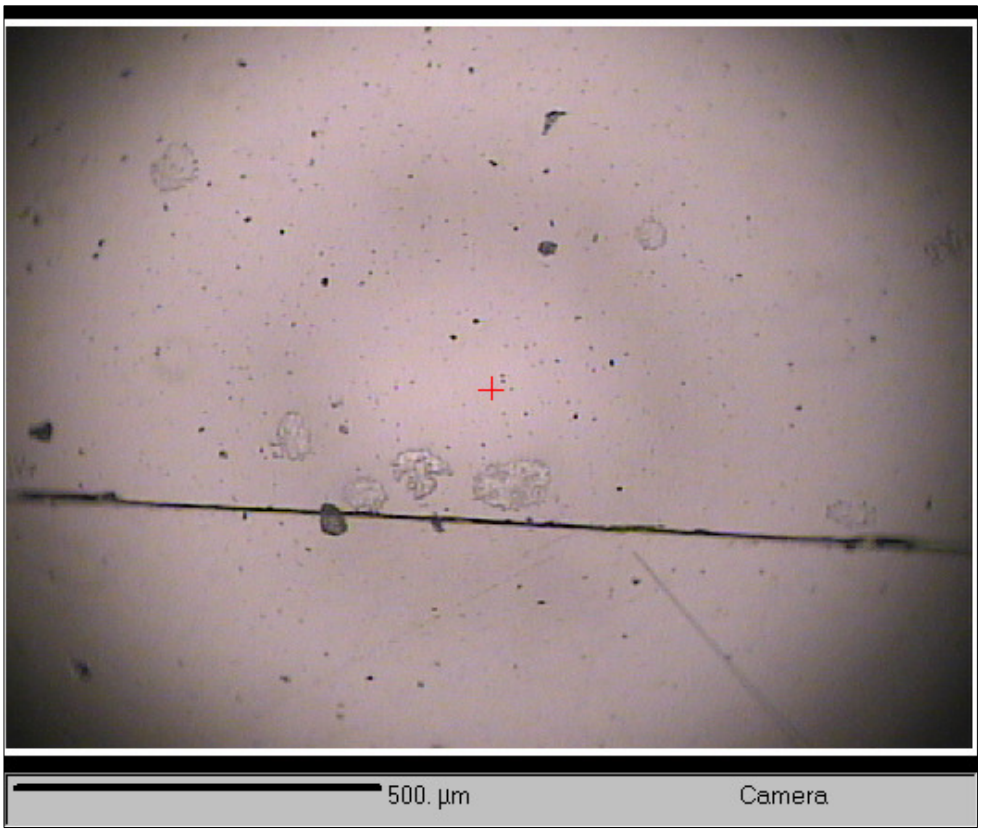

Figure 6.4 Zircon particles - reflected light TV image

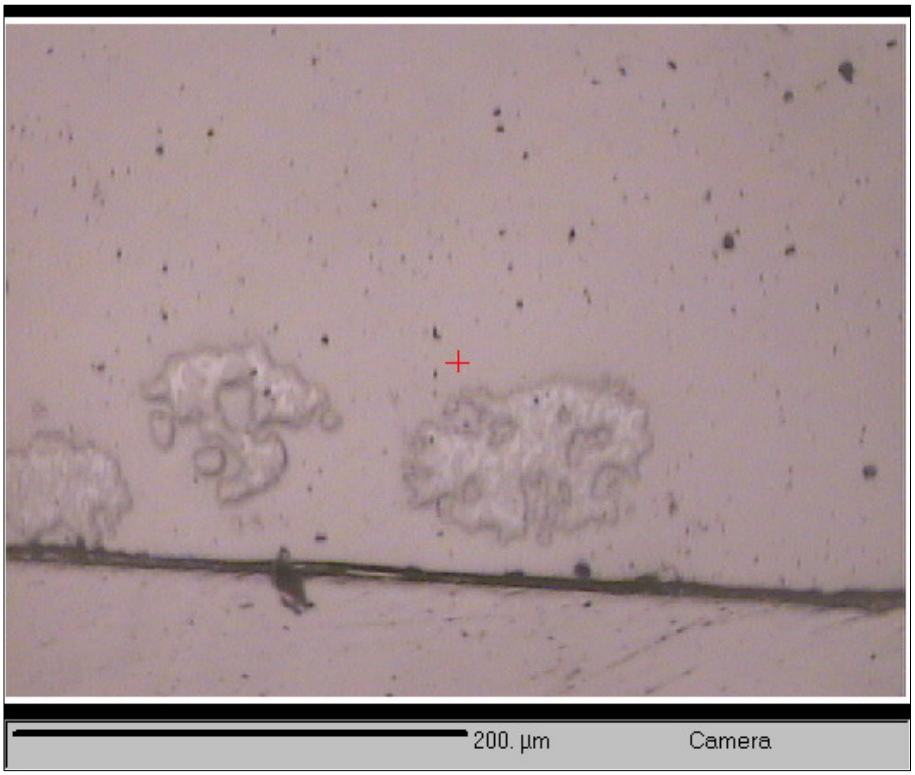

Figure 6.5 Zircon particles - reflected light TV image

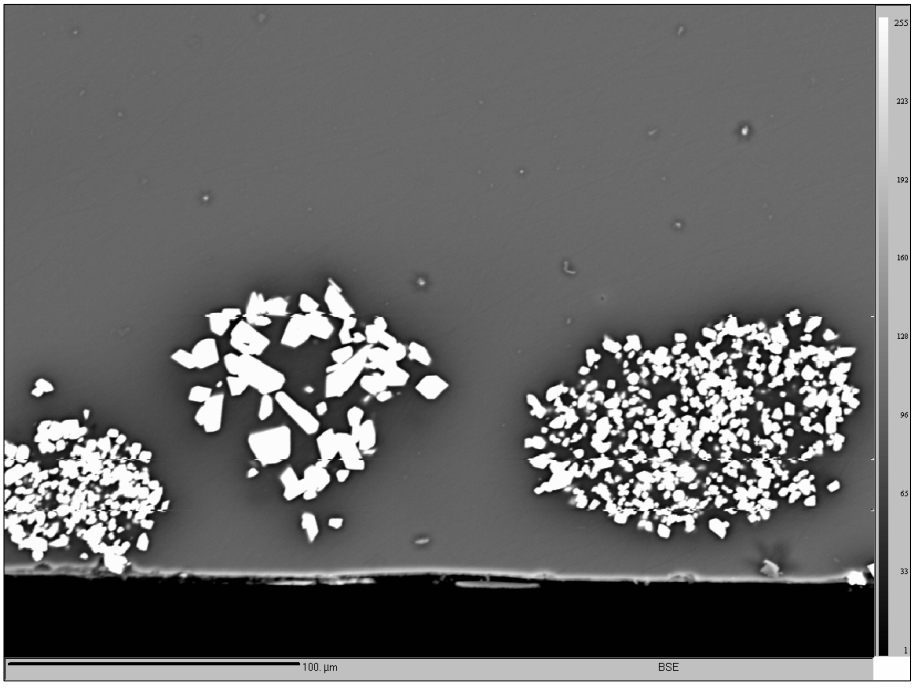

Figure 6.6 Zircon particles - BSE image

Table 6.2 EPMA analysis of zircon fused bead

Point	Al2O3	TiO2	Cr2O3	FeO	ZrO2	Total	X	Y	Z	Comment
13	0.02	0.02	0	0.01	66.52	66.56	5182	-21546	92	Particle_1
14	0.03	0	0.02	0.01	13.15	13.21	5182	-21492	92	Spot_1
15	0.03	0.06	0.03	0.03	14.13	14.28	5182	-21456	92	Spot_2
16	0.03	0.06	0.01	0.02	14.09	14.23	5182	-21415	92	Spot_3
17	0.02	0.04	0	0	25.06	25.12	5021	-21500	92	Particle_2
18	0.03	0.06	0.01	0.02	11.96	12.08	5021	-21448	92	Spot_1
19	0.03	0.03	0	0.02	13.29	13.37	5021	-21405	92	Spot_2
20	0.02	0.06	0.03	0.01	13.71	13.83	5021	-21372	92	Spot_3
21	0.04	0.06	0.04	0.02	55.42	55.58	4382	-21540	92	Particle_3
22	0.02	0.04	0.02	0.01	13.41	13.5	4382	-21475	92	Spot_1
23	0.02	0.01	0	0	13.42	13.46	4382	-21437	92	Spot_2
24	0.04	0.04	0	0.02	13.52	13.63	4382	-21388	92	Spot_3

6.2 Experimental results Microscopy

The sample preparation was repeated with coarser starting material to obtain larger particle sizes (larger than beam size of EPMA), which will enable accurate analysis. This proved problematic as the same problems were encountered time and time again. To elucidate this problem the samples were investigated under a Nikon Eclipse E200 microscope with 50x10 enlargement in focussed mode.

6.2.1 Microscopy: Zircon dissolved in lithium tetraborate glass bead

Figures 6.7, 6.8 and 6.9 represent different particles in the zircon ($ZrSiO_4$) specimen.

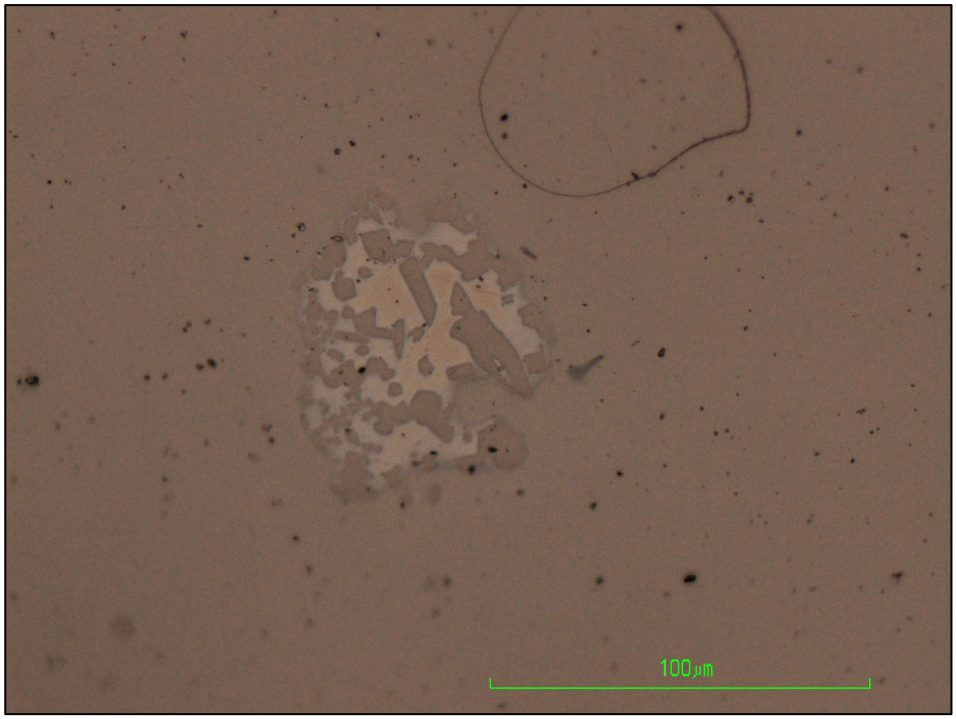

Figure 6.7 Nikon Eclipse E200 microscope image of a zircon particle

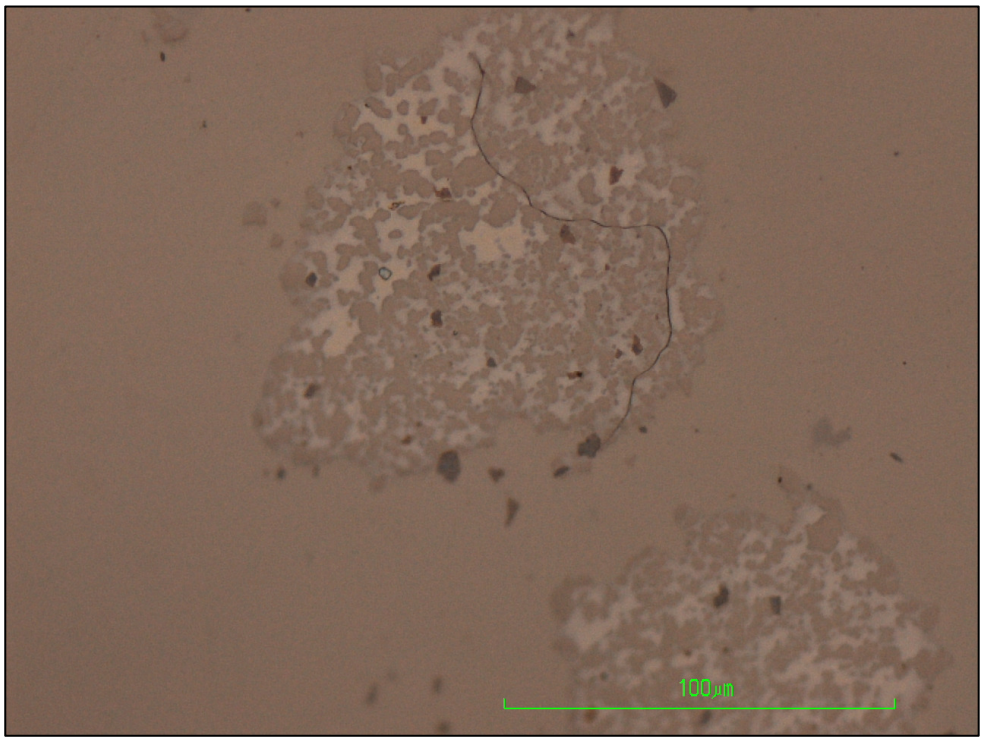

Figure 6.8 **Nikon Eclipse E200 microscope image of a zircon particle**

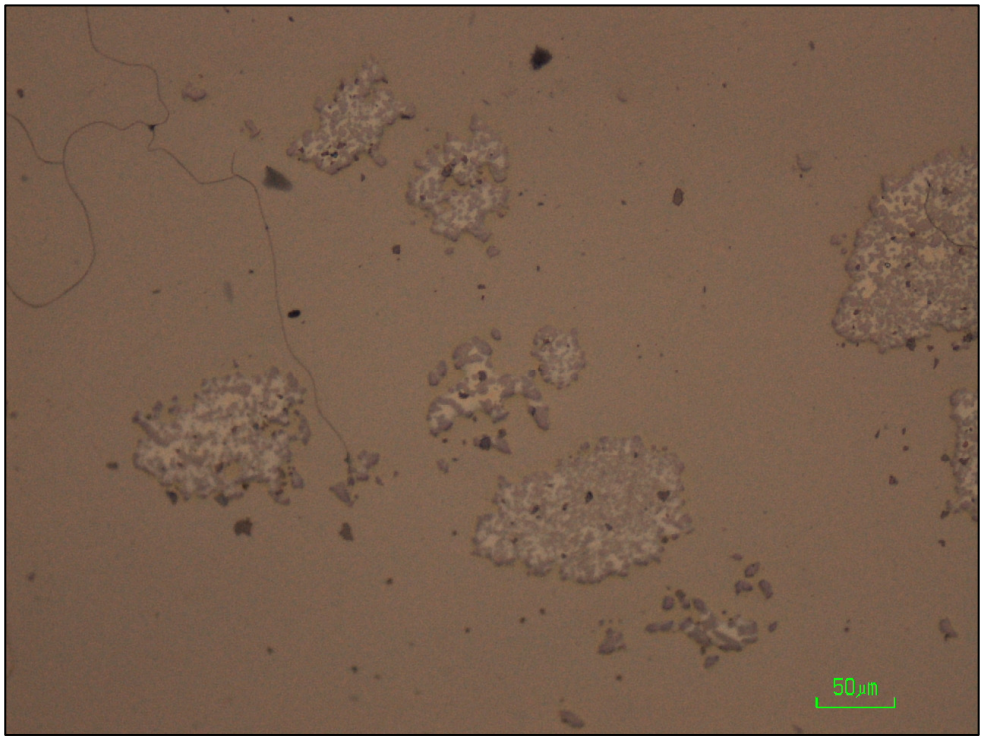

Figure 6.9 **Nikon Eclipse E200 microscope image of a zircon particle**

From these images of the zircon particles it is clear that the crystals actually dissolved and re-precipitated as two separate phases, ZrO_2 and SiO_2 as two colours can be distinguished. From this it can be deduced that the flux was thus saturated and then re-precipitated as a different phase on the original particle site. The particles are crystals because they are elongated with sharp edges. The particles were localised on the bottom surface of the glass bead, probably due to density effects.

6.2.2 Microscopy: Chromite dissolved in lithium tetraborate glass bead

Figures 6.10, 6.11 and 6.12 represent different particles in the chromite ($Fe^{2+}Cr_2O_4$) specimen.

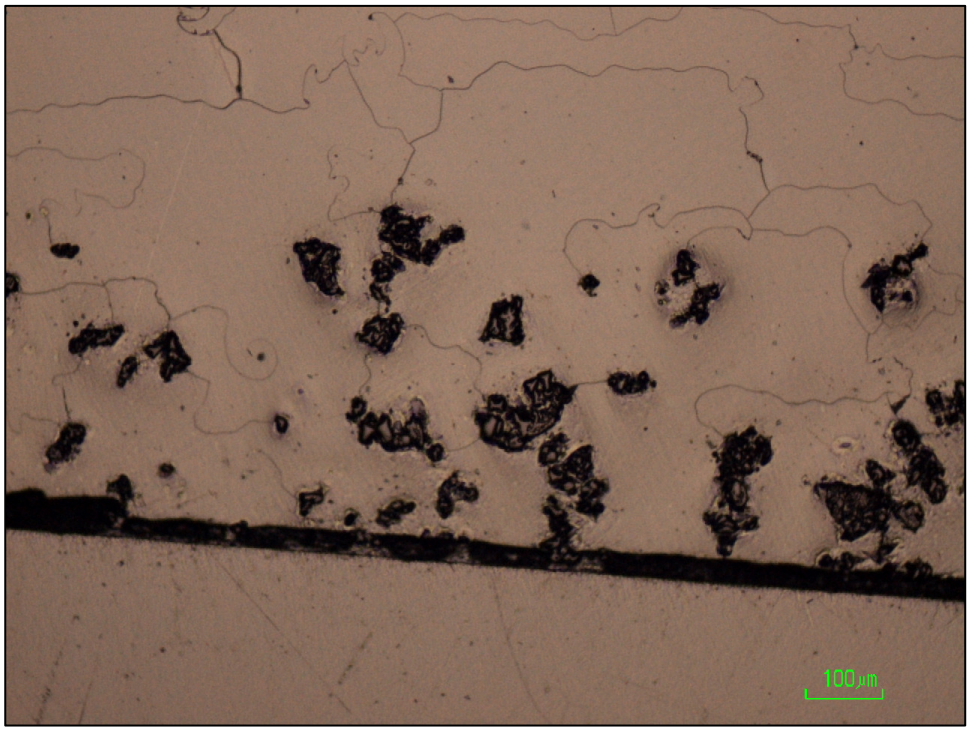

Figure 6.10 Nikon Eclipse E200 microscope image of a chromite particle

The chromite particle is totally dissociated and also concentrated on the bottom surface of the glass bead. This can be deduced from the two different coloured phases, dark and light that can be distinguished in Figures 6.10-6.12. The composition is possibly an ionic complex. The white spots observed are due to the carbon coating.

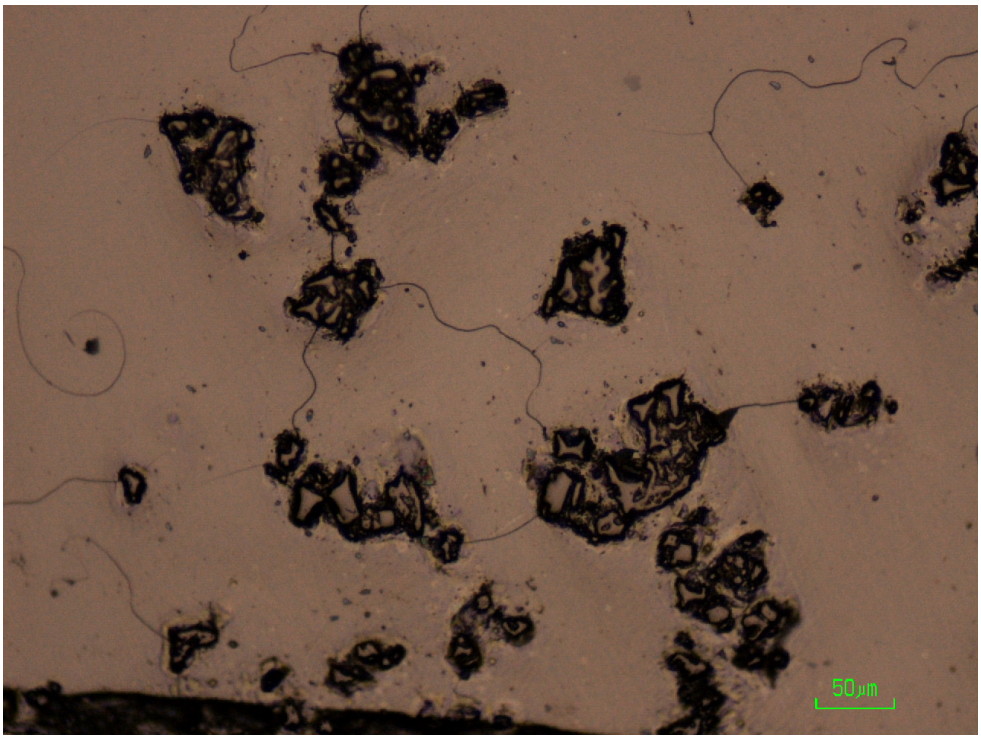

Figure 6.11 Nikon Eclipse E200 microscope image of a chromite particle

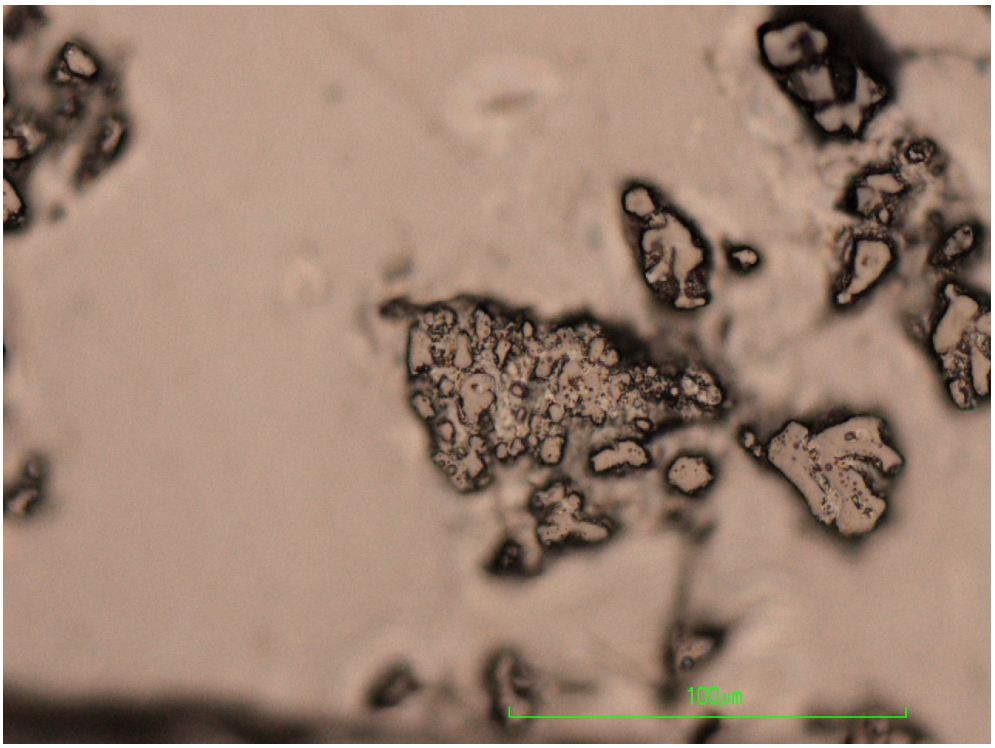

Figure 6.12 Nikon Eclipse E200 microscope image of a chromite particle

6.3 Conclusion

From the microscope images it is clear that dissociation occurred, the flux oxide mixture devitrify when oversaturated. The concentration next to the particle in the EPMA analysis reflects the maximum ZrO_2 to flux ratio. This exercise proves one of the stated advantages of fused beads, namely the destruction of mineralogical effects very effectively: In the flux, even when crystallised, the zircon exists as ZrO_2 and SiO_2 therefore no mineralogical effect remains when the minerals are completely dissolved.

In the case of the chromite specimens there was again an excess oxide in the flux that recrystallised out of the melt. The Cr remaining in the flux is the equilibrium concentration. Directly next to the particle the concentration would thus be depleted, so to measure the equilibrium concentration one would have to measure further away.

Using the EPMA data a maximum solubility for ZrO_2 from a zircon sample was calculated at 13.4±0.6% and the maximum solubility of Cr_2O_3 from a chromite in lithium tetraborate as 1.38±0.05% Cr_2O_3. This proved to be a very informative exercise and should be expanded to get maximum solubilities for more oxides that could be compared to solubilities obtained experimentally and calculated theoretically.

REFERENCES:

1. Deer W.A., Howie R.A. and Zussman J. *An Introduction to The Rock Forming Minerals.* Pearson Education Limited (United Kingdom) (1992) **2 Rev Ed.** pp712
2. S. S'anchez Ramos M. D. Jorge Cubillos, J. V. Gimeno Adelantado. Quantitative analysis of chromite ores using glass discs in moderate dilutions of lithium tetraborate by x-ray fluorescence spectrometry. *X-Ray Spectrom.* 2006. **35**: 243–248.
3. Gazulla, M.F., Barba, A., Gómez, M.P. and Orduña, M. Chemical Characterisation of Chromites. *Geostandards and Geoanalytical Research.* 2006. **30**: 237-243.

CHAPTER 7: CONCLUSION

The objective of this project was to obtain a better understanding of the reactions occurring during a fusion reaction in both pure lithium borate flux as well as flux sample mixtures. It was anticipated that this work can be extrapolated to the design of fused bead recipes for new or difficult matrices that needs to be dissolved in lithium borate flux for the purpose of XRF or ICP sample preparation.

As a starting point TGA/DSC analyses were executed. This provided some unexpected results: Most importantly the hygroscopic nature of fluxes could be demonstrated by the loss of water above 120 ºC in the TGA curve. It was observed that pre-fused fluxes showed a much lower tendency for H_2O absorption, demonstrated by smaller weight losses above 120 ºC. Also observed was the exothermic reaction at ±500 ºC in the DSC curves, associated with the re-crystallisation of pre-fused flux mixtures. This large exothermic reaction could be the explanation for spluttering observed in automated fluxers when flux explodes out of the crucible. A new submitted prototype with microcrystalline inclusions was proposed as a solution for this problem, and in this study the amorphous and crystalline nature of this prototype was confirmed.

From the DSC curves, the melting point for different fluxes could be accurately determined and interestingly, dual melting points were observed for certain flux mixtures indicating the presence of two separate components, even in pre-fused

fluxes. It can thus be deduced that the pre-fusion step does not cause a reaction that forms a new compound, but only melts the different phases together.

The most enlightening result from the TA/DSC results was the large mass loss above 1050 ºC. Literature often prescribes prolonged fusions at elevated temperatures (1100 - 1200 ºC) for certain fusions. The observed loss was qualified by ICP analysis as a volatilisation reaction of lithium tetraborate or lithium metaborate. The hypothesis that added oxides might change this scenario was tested with SiO_2 added to a flux, but the mass loss still occurred.

Recommendation: Fuse longer at lower temperatures to prevent loss of flux. The maximum temperature needed for a fusion is the melting temperature of the flux. It was illustrated by the DSC curves of flux-oxide mixtures that a mixture always melts at a temperature lower than its constituents.

The next analytical technique applied to the flux samples was XRD. As XRD relies on the diffraction of monochromatic x-rays by a crystalline material, the results were mostly limited to crystalline flux material. Where pre-fused fluxes were investigated, the XRD data served as confirmation of the glassy state of the pre-fused flux as seen from an amorphous scan instead of a diffractogram. After heating to above the temperature of re-crystallisation, the phases present could be identified from the diffractogram.

XRD also confirmed the reported presence of microcrystalline particles in the prototype flux PR0301A and PR0301B. The composition of PR0301A was confirmed as lithium tetraborate. The reported composition of PR0301B as “biborate” was refuted and a lithium tetraborate, lithium metaborate mixture deduced, although a peak shift, possibly along one axis, was observed, which could be a result of the fusion step.

Provisional results using the in situ temperature stage point towards the possibility of using this technique to great effect. When a lithium tetraborate sample was heated from 25 to 950 ºC and cooled again, recrystallisation was seen as well as the amorphous glass above the melting temperature. On cooling some peaks were observed at different positions than the original structure. Unfortunately the instrumental setup was not ideal as molten flux ran off the platinum strip and damaged the electrodes. Subsequently the flux-oxide mixtures were ran below melting temperature, but in the case of a flux-Cr_2O_3 mixture, after cooling a Cr-Li phase was observed indicating the new phases formed during a fusion reaction. As the heating stage is slow-cooled, the chance of crystallisation in the glass is great providing the possibility for investigating this further with a more suitable heating element.

Raman spectroscopy was subsequently used to gain information about the bonds within the flux. Pure lithium tetraborate and lithium metaborate fluxes were analysed. The vibrations could not be predicted from first principles as band

broadening occurs in glasses that makes theoretical predictions very difficult. The data obtained was compared to similar studies in literature and good agreement was found.

The difference between glass and crystalline phases were easily observed as crystalline samples gave sharper narrow bands than the broad bands from glasses. Raman spectroscopy was implemented to determine the crystallinity of a flux. Most of the original Raman studies were done using a micro-Raman configuration. One of the problems encountered on the microscope stage was that results were dependent on which exact particle the laser was focussed on. Reproducibility remained a problem and the configuration was switched to a macro – Raman mode.

In oxide-flux mixtures definite new bands were observed that was not part of the flux or oxide spectrum. Identifying such bands was difficult due to broadening of the bands in the glassy phase.

At the outset it was envisaged to be able to prove or disprove that bonds formed between flux and oxide samples and from that information deduce the actual mechanism used during the production of a fused bead. This turned out to be more complicated than originally foreseen due to the difficulty in identifying the bands in Raman and the problems encountered with the in situ XRD.

From the information gained though, a very clear set of data was collected for a

baseline of pure fluxes and the possibility of actually being able to identify bonds formed between flux and oxide samples seems promising and would be a worthwhile project to undertake. Such a project would include repeating the XRD on oxide flux mixtures with a suitable heating stage that would not be damaged in the process, and revisiting the Raman data.

With the baseline study on the fluxes executed by the TGA/DSC, it is clear that this technique by far provided the most promising results in furthering the understanding of reactions between flux and sample. It would be ideal to systematically run high temperature DSC scans on common geological oxide/flux mixtures and also use this technique to elucidate advanced fusion procedures where oxidants or other additives are added to sample/flux mixtures.

Originally the EPMA did not seem promising due to the difficulties with obtaining accurate results, but when combining the data obtained with the microscope images some new insights were revealed. It could clearly be seen that dissociation occurred, the flux oxide mixture devitrify when over saturated. This exercise proved one of the stated advantages of fused beads, namely the destruction of mineralogical effects: In the flux, even when crystallised, the zircon existed as ZrO_2 and SiO_2 therefore no mineralogical effect remained. In the case of the chromite specimens there was again an excess oxide in the flux that recrystallised out of the melt in two distinguishable phases. This may tie in with the $LiCrO_2$ phase identified in the high temperature XRD (section 4.1.4.4).

Although the beam size influences the accuracy of the undissolved particle analysis, measurement of the flux surrounding the recrystallised particles give a true reflection of the equilibrium concentration of an oxide in the flux. Using the EPMA data a maximum solubility for ZrO_2 from a zircon sample was calculated at 13.4±0.6% and the maximum solubility of Cr_2O_3 from a chromite in lithium tetraborate as 1.38±0.05% Cr_2O_3. This proved to be a very informative exercise and should be expanded to get maximum solubilities for more oxides that could be compared to solubilities obtained experimentally and calculated theoretically. Homogenous lithium borate fused beads prepared from certified reference materials could be used to calibrate the EPMA for this.

This study did not supply all the answers; at most it opened some windows and provided a peep into the possibilities that could be achieved when a very old problem is addressed using new techniques and a systematic approach.

Acknowledgements

When you hand in a thesis, you sign a declaration stating that all the work described in the report is your own – and so it should be, but a project of this size and duration cannot be done without the involvement and support of many others.

I believe in a Higher Hand that guides our lives and gives us the abilities to undertake projects like this, and I am thankful.

I dedicated this work to Fernand Claisse. When I showed him what I was busy with early in 2004 he got extremely excited and has been supportive ever since.

I owe a huge amount of gratitude to James Willis, who "lit my XRF candle" and has taught me everything I know about the subject.

Bruno Vrebos from PANalytical Netherlands could always find me an obscure Philips technical report and continuously gave constructive criticism and encouraged me to go ahead when I was ready to throw in the towel.

I am very fortunate to have been in the employ of the University of Pretoria for fifteen years, where I had the opportunity to get access to excellent analytical facilities to conduct this research. A special word of thanks to all the spectroscopists and colleagues, who allowed me to invade their laboratories over the years and encouraged and supported me otherwise;

- Linda Prinsloo and Werner Barnard for the Raman assistance.
- Christien Strydom and Liezel van der Merwe for the thermal analysis support.
- Sabine Verryn for the XRD and
- Peter Graser for the Electron Microprobe analysis.
- Wikus Jordaan from the Council for Geoscience for the ICP analysis.

To Chrisna Nel, who did the editing and formatting, I would never have completed it in time without her help.

My supervisors deserve a medal for their support, both Peet van Rooyen and Johan de Villiers took over as supervisors when my original project leader withdrew and really helped me to shape mountains of data into a concise document. They encouraged and believed in me when I was giving up on myself, and kicked butt when that was necessary too.

The examiners have to be thanked for their time and dedication, especially the external examiner who saw this for the first time and gave a fresh perspective and contributed to improving the study with his constructive criticism.

Thank you to my original supervisor, Danita de Waal – who taught me a lot more than just Chemistry.

Thank you to Prof. Cukrowski, who did not know me at all in 2005 when he suddenly landed with a student without a supervisor and assisted me in good faith.

I am deeply thankful to my PPC colleagues for their support and for giving me the time off to complete and hand in.

Lastly but not the least – Geoff for reading this a hundred times and patiently correcting my Afri-English time and time again, and my three sons, Duane, Francois and Alex that inspired me to get this degree before they all have post graduate qualifications. Francois, fortunately handed in his 4th year Engineering project a few weeks ago, so he was very well qualified to do the final printing and handing in on his mother's behalf when I had to rush off to Lime Acres for work. Thanks my son!